PHYSIK

AG MAGNETISMUS

Annual Report 2015

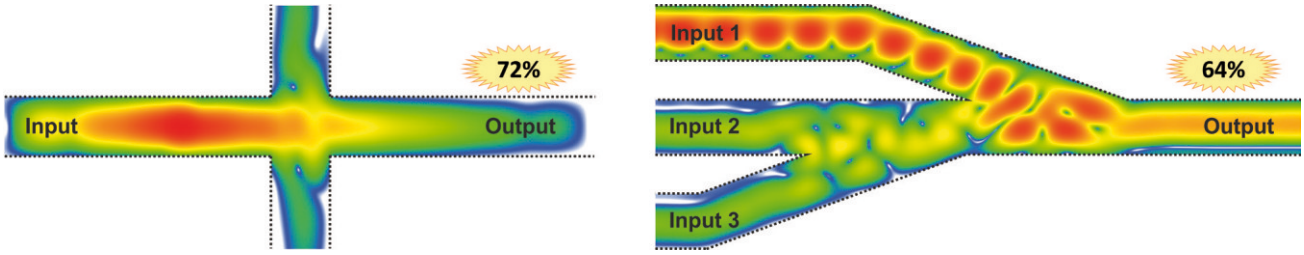

AG MAGNETISMUS TU KAISERSLAUTERN

OPTIMAS

TECHNISCHE UNIVERSITÄT KAISERSLAUTERN

Cover page: Shown are micromagnetic simulations of out-of-plane magnetized magnonic circuits. The diagrams present the flow of forward volume spin waves, with the efficiency of spin-wave energy transmission indicated in each panel. For more details see Section 4.5 and Appl. Phys. Lett. **106**, 212406 (2015). Left: Crossing of two data-carrying magnonic conduits. The waveguide crossing structure is planar, no three-dimensional geometry of vias is needed. The spin-wave signal is applied to the left arm. Right: Asymmetric majority gate design optimized for isotropic forward volume spin waves. The spin-wave signal is applied only to Input 1. The majority gate is used to perform majority logic operations with binary data coded into spin-wave phases.

Annual Report 2015

Address:	Prof. Dr. Burkard Hillebrands Fachbereich Physik Landesforschungszentrum OPTIMAS Technische Universität Kaiserslautern Erwin-Schrödinger-Straße 56 67663 Kaiserslautern, Germany Tel.: +49-(0)631-205-4228 Fax.: +49-(0)631-205-4095
Postal address:	Postfach 3049 67653 Kaiserslautern, Germany
Internet:	http://www.physik.uni-kl.de/hillebrands/
E-Mail:	hilleb@physik.uni-kl.de

This Annual Report can be downloaded from:
http://www.physik.uni-kl.de/hillebrands/publications/annual-reports/

Our Group

From left to right:

Jun. Prof. Dr. Evangelos Papaioannou, Dr. Philipp Pirro, Viktor Lauer, Dr. Britta Leven, Tobias Fischer, Thomas Langner, Donata Passarello, Martin Kewenig, Philipp Jaeger, Laura Mihalceanu, Timo Noack, Hauke Schäfer, Björn Heinz, Dmytro Bozhko, Dr. Peter Clausen, Michael Schneider, Moritz Geilen, Dr. Alexander Serga, Sascha Keller, Matthias Schweizer, Dr. Vitaliy Vasyuchka, Prof. Dr. Burkard Hillebrands, Thomas Meyer, Dr. Andrés Conca Parra, Frank Heussner

(The picture was taken at our group retreat in Annweiler in October 2015.)

Not on the picture: Dr. Andrii Chumak, Jochen Greser, Sibylle Müller, Dr. Isabel Sattler, Dieter Weller

Contents

Chapter 1: Preface

Dear Colleagues and Friends,

we are happy to present once again our Annual Report. This time it is covering the period November 2014 to October 2015. We tried to cut back the length of the Report to four pages per project to provide you with more clear and concise information.

This was a year with a very dense sequence of events. I am particularly glad, that we could celebrate last April the 20th anniversary of my research group, the *AG Magnetismus*. We had several important events regarding funding: In February our Collaborative Research Center TR49 *Condensed matter systems with variable many-body interactions*, jointly conducted by groups from the universities of Frankfurt, Mainz and Kaiserslautern, was extended for a final four-year funding period, thus securing funds for our research on magnon gases. In September our new initiative for a Collaborative Research Center *Spin + X: Spin in its collective environment*, jointly with groups at the Johannes Gutenberg University in Mainz, was evaluated, and we now wait for the final decision of the funding board. And, on top, Andrii Chumak received notification that his European Research Council Starting Grant proposal on *Nano-Scale Magnonic Circuits for Novel Computing Systems* (*MagnonCircuits*) was positively evaluated and recommended for funding, and he is now in the contract negotiations. Furthermore we received an equipment grant to establish a setup for broadband microwave analysis up to 70 GHz.

New research highlights are: We identified in detail the thermalization channels for Bose-Einstein magnon condensation with regard to dipolar and exchange channels including a new stimulation mechanism. Our first steps into magnonic macroscopic quantum states made progress. More evidence was found for magnonic supercurrents by better data and a new model based on rate equations. By employing parallel parametric pumping in the non-adiabatic regime, we realized phase-dependent amplification of a coherent spin wave propagating in a micro-structured Permalloy waveguide. This technique can be used for converting phase-coded information into amplitude information in future magnonic devices. We continued our work on majority gates showing by numerical simulations, that these gates can be favorably implemented in perpendicularly magnetized films. Spin pumping and spin transfer torque were other phenomena where we pushed our frontiers, in particular regarding damping control and spin wave excitation in Yttrium Iron Garnet/Pt structures. Using the spin-transfer torque effect, we were able to realize efficient spin-wave damping control in a Heusler system, and we showed damping compensation in spatially extended Heusler-Platinum waveguides. This is a further step towards the implementation of Heusler materials into spintronic devices. We also investigated epitaxial metallic systems with regard to spin pumping. As a model system we have used fully epitaxial Fe/Pt bilayers with highly ordered interfaces. One focus was on epitaxial interfaces between Fe and Pt in order to better understand the microscopic origin of the spin-mixing conductance. In the field of spin caloric transport we have new findings on the impact of temperature and thermal gradients on parametric pumping processes in YIG/Pt bilayers in a wide wavevector range. Also a strong influence of the magnetic insulator thickness on the temporal dynamics of the longitudinal spin Seebeck effect was found.

With regard to outreach we published an invited Nature Physics review article on the state of the

art and main challenges in the fields of magnon spintronics and magnonics (*Magnon spintronics*, Nature Phys. **11**, 453 (2015)). We presented our magnon transistor work at several occasions, in particular at the CeBIT 2015 exhibition, the world's largest trade fair on information technology. Another field of outreach activities was the development of new spintronics demonstrators for automotive applications. Much of this work has been made in the frameworks of the Magnetism Network of the Greater Region (GRMN) and the Spintronics Technology Platform Rhineland-Palatinate (STeP), both having been concluded this year.

We concluded our very successful Japanese-German Research Unit *Advanced Spintronic Materials and Transport Phenomena* - ASPIMATT (FG 1464), conducted jointly between research groups in Sendai, Mainz/Dresden and Kaiserslautern, and funded jointly by the Japan Science and Technology Agency (JST) and the Deutsche Forschungsgemeinschaft (DFG). I would like to thank especially Profs. Yasuo Ando, Koki Takanashi and Claudia Felser for this very fruitful and stimulating, and very enjoyable collaboration. In my group we studied mostly linear and nonlinear spin-wave properties in Heusler systems.

Again, there have been several changes in our group. Philipp Pirro left us for a post-doc position at the Institut Jean Lamour, Université Lorraine, Nancy, France working with Stéphane Mangin. He acts as a linking person for collaborations bringing together the material science competences of the Nancy group with our competences in magnon physics. Ana Ruiz Calaforra, Thomas Brächer and Peter Clausen finished their Ph.D. Ana and Thomas left for post-doc positions at Spintec and CNRS in Grenoble. Milan Agrawal left for a position at Infineon Technologies, Munich.

Philipp Pirro received the *Preis des Freundeskreises der TU Kaiserslautern*, and Dmytro Bozhko two poster awards. Tobias Fischer, Frank Heussner, Stefan Klingler and Laura Mihalceanu finished successfully their Diploma theses, and Martin Hutzel, Manuela Kratz, Matthias Monzel and Oliver Nick their Master theses of education. We welcome Tobias Fischer, Frank Heussner and Laura Mihalceanu as new PhD students and Timo Noack as new Diploma student.

Our work would not have been possible without valuable collaborations with people all over the world. They are too many to list them here all. In particular we would like to thank, in alphabetical order, Christoph Adelmann, Adekunle Adeyeye, Johan Åkerman, Yasuo Ando, Antonio Azevedo, Christian Back, Matthieu Bailleul, Gerrit Bauer, Arne Brataas, Giovanni Carlotti, Florin Ciubotaru, Frederick Casper, Russell Cowburn, Sergej Demokritov, Thibaut Devolder, Bernard Dieny, Marco Doms, Rembert Duine, Carsten Dubs, Ursula Ebels, Hajo Elmers, Jürgen Fassbender, Gerhard Fecher, Claudia Felser, Albert Fert, Mark Freeman, Sebastian Goennenwein, John Gregg, Hubert Grimm, Dirk Grundler, Gianluca Gubbiotti, Konstantin Gusliyenko, Jaroslav Hamrle, Uwe Hartmann, Thomas Hauet, Michel Hehn, Jos Heremans, Atsufumi Hirohata, Axel Hoffmann, Koichiro Innomata, Gerhard Jakob, Xiaofeng Jin, Martin Jourdan, Gleb Kakazei, Boris Kalinikos, Alexy Karenowska, Sang-Koog Kim, Akihiro Kirihara, Olivier Klein, Mathias Kläui, Yuri Kobljanskyj, Peter Kopietz, Mikhail Kostylev, Tomohiro Koyama, Volodymyr Kruglyak, Takahide Kubota, Ronald Lehndorff, Joseph Losby, Jörg Lösch, Gregoire de Loubens, Sadamichi Maekawa, Stéphane Mangin, Gennadiy Melkov, Claudia and Tim Mewes, Shigemi Mizukami, Shuichi Murakami, Hiroshi Naganuma, Andrei Nikitin, Sergei Nikitov, Jean-Pierre Nozières, Kevin O'Grady, Hideo Ohno, Tereo Ono, Mikihiko Oogane, Yoshichika Otani, Stuart Parkin, Johannes Paul, Günter Reiss, Sergio Rezende, Caroline Ross, Manfred Rührig, Eiji Saitoh, John R. Sandercock, Rudi Schäfer, Gerd Schönhense, Helmut Schultheiss, Koji Sekiguchi, Jairo Sinova, Andrei Slavin, Rolf Slatter, Bob Stamps, Yoshishige Suzuki, Koki Takanashi, Vasyl Tiberkevich, Simon Trudel, Yaroslav Tserkovnyak, Ken-ichi Uchida, Alexey Ustinov, Bart van Wees, and Mingzhong Wu.

Collaborations within the Fachbereich Physik at the University of Kaiserslautern (in particular

Martin Aeschlimann, James Anglin, Sebastian Eggert, Michael Fleischhauer, Georg von Freymann, Jochen Kuhn, Herwig Ott, Hans-Christian Schneider, Volker Schünemann, and Arthur Widera and their groups), Michael Kopnarski and his team from the Institut für Oberflächen- und Schichtanalytik, as well as Sandra Wolff and her team from the Nano Structuring Center have been very stimulating. We are very grateful to be a member of the State Research Center for Optics and Material Sciences OPTIMAS.

I would also like to thank all our sponsors, which are the Deutsche Forschungsgemeinschaft (DFG), the Bundesministerium für Bildung und Forschung (BMBF), the Deutscher Akademischer Austauschdienst (DAAD), the European Community (EFRE, INTAS, INTERREG), the Carl Zeiss Foundation, the State of Rhineland Palatinate and the University of Kaiserslautern. Concerning our projects in applied research, I would like to express my gratitude to Sensitec GmbH and Singulus Technologies AG as our strong partners in R&D on spintronic sensors.

My special thanks go to Sascha Keller, Thomas Langner, Dieter Weller and Sibylle Müller for their help in preparing this report, and to the team from Photo-Repro-Druck, TU Kaiserslautern.

It is my special pleasure to greet all former group members. May this report help to stay in touch. If you are interested in our work I would be happy to hear from you.

With all my best wishes for Christmas, and a Happy New Year,

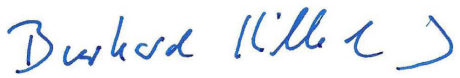

Kaiserslautern, November 2015

Vorwort

Liebe Kolleginnen und Kollegen, Freundinnen und Freunde unserer Arbeitsgruppe,

ich freue mich sehr, Ihnen wieder unseren Jahresbericht präsentieren zu dürfen. Diesmal deckt er den Zeitraum von November 2014 bis Oktober 2015 ab. Wir haben uns diesmal bemüht, den Umfang des Berichtes durch Beschränkung auf vier Seiten pro Beitrag zu reduzieren, um Ihnen ein einfacheres Lesen zu ermöglichen.

Dieses Jahr war erfüllt von vielen dicht aufeinanderfolgen Ereignissen. Ich freute mich, dass wir im April das zwanzigste Jubiläum meiner Arbeitsgruppe, der *AG Magnetismus*, feiern konnten. Wir hatten mehrere wichtige Ereignisse bezüglich der Förderung: Im Februar wurde unser Sonderforschungsbereich/ Transregio TR49, *Condensed matter systems with variable many-body interactions*, welchen wir gemeinsam mit Arbeitsgruppen der Universitäten von Frankfurt, Mainz und Kaiserslautern durchführen, um eine abschließende vierjährige Förderungsperiode verlängert. Dies sichert uns nun die Mittel für die weitere Forschung an den Magnonengasen. Im September wurde unsere neue Initiative für einen Sonderforschungsbereich/Transregio *Spin + X: Spin in its collective environment*, gemeinsam mit Arbeitsgruppen der Johannes Gutenberg Universität in Mainz, evaluiert und wir erwarten nun die endgültige Entscheidung des Förderungsausschusses. Ein weiteres wichtiges Ereignis: Andrii Chumak erhielt die Nachricht, dass sein European Research Council Starting Grant-Antrag für *Nano-Scale Magnonic Circuits for Novel Computing Systems* (*MagnonCircuits*) positiv evaluiert und zur Förderung empfohlen wurde. Er befindet sich derzeit in den Vertragsverhandlungen. Weiterhin erhielten wir eine Ausstattungsbewilligung für die Errichtung eines Aufbaus zur breitbandigen Mikrowellen-Analyse bis hin zu 70 GHz.

Unsere diesjährigen Forschungs-Highlights: Wir identifizierten die Thermalisierungskanäle für Bose-Einstein-Magnonenkondensation im besonderen Hinblick auf die Dipol- und Austauschkanäle und fanden einen neuen Stimulationsmechanismus. Unsere ersten Schritte in magnonische makroskopische Quantenzustände machten Fortschritte. Wir fanden neue Hinweise auf magnonische Supraströme durch bessere Messdaten und durch ein neues, auf Ratengleichungen basierendes Modell. Durch die Anwendung parallelen parametrischen Pumpens im nichtadiabatischen Regime realisierten wir eine phasenabhängige Verstärkung einer kohärenten Spinwelle, die sich in einem mikrostrukturierten Permalloy-Wellenleiter ausbreitete. Diese Technik kann für die Konvertierung phasenkodierter Informationen in amplitudenkodierte Informationen in zukünftigen magnonischen Geräten verwendet werden. Wir setzten unsere Arbeit an den Majoritätsgattern fort, indem wir anhand numerischer Simulationen zeigten, dass diese Gatter besonders gut in senkrecht magnetisierten Schichten implementiert werden können. Der Spinpump- und der *Spin Transfer Torque*-Effekt waren weitere Phänomene, deren Anwendungen wir weiter vorangetrieben haben, insbesondere bezüglich der Dämpfungskontrolle und Spinwellenanregung in Yttrium-Eisen-Granat/Pt-Strukturen. Durch die Anwendung des *Spin Transfer Torque*-Effekts konnten wir eine effiziente Spinwellen-Dämpfungskontrolle in einem Heusler-System realisieren und konnten die Dämpfungskompensation in räumlich ausgedehnten Heusler-Platin-Wellenleitern aufzeigen. Dies ist ein weiterer Schritt in Richtung der Implementierung von Heusler-Materialien

in spintronische Anwendungen. Weiterhin untersuchten wir epitaktische Metallsysteme in Bezug auf das Spinpumpen. Als ein Modellsystem benutzten wir voll-epitaktische Fe/Pt-Doppelschichten mit hochgeordneten Grenzschichten. Ein Augenmerk lag dabei auf der epitaktischen Grenzschicht zwischen Fe und Pt, um besser den mikroskopischen Ursprung der *spin-mixing conductance* verstehen zu können. Im Forschungsfeld des spinkalorischen Transports haben wir neue Erkenntnisse auf die Auswirkungen der Temperatur und von Temperaturgradienten auf den parametrischen Pumpprozess in YIG/Pt Doppelschichten in einem großen Wellenvektorbereich gewonnen. Ebenso wurde ein starker Einfluss der Schichtdicke des magnetischen Isolators auf die zeitliche Dynamik des longitudinalen *Spin Seebeck*-Effekts gefunden.

Auf dem Feld der Außendarstellung veröffentlichten wir einen eingeladenen *Nature Physics* Review-Artikel über den letzten Stand der Technik und die wesentlichen Herausforderungen des Gebiets der Magnon-Spintronik und der Magnonik (*Magnon spintronics*, Nature Phys. **11**, 453 (2015)). Wir präsentierten unsere Arbeit über den Magnon-Transistor zu verschiedenen Gelegenheiten, insbesondere auf der CeBIT 2015, der größten Handelsmesse für Informationstechnologie. Ein weiteres Thema war die Entwicklung neuer Spintronik-Demonstratoren für die Automobilanwendung. Viel von dieser Arbeit wurde im Rahmen des *Magnetism Network of the Greater Region* (GRMN) und der *Spintronics Technology Platform Rhineland-Palatinate* (STeP) durchgeführt, welche beide in diesem Jahr zum Abschluss gebracht wurden.

Wir haben unsere sehr erfolgreiche Japanisch-Deutsche Forschungseinheit *Advanced Spintronic Materials and Transport Phenomena* - ASPIMATT (FG 1464) abgeschlossen. Diese wurde gemeinsam durchgeführt von Forschungsgruppen in Sendai, Mainz/Dresden und Kaiserslautern und gemeinsam gefördert durch die Japan Science and Technology Agency (JST) und die Deutsche Forschungsgemeinschaft (DFG). Ich möchte insbesondere den Professoren Yasuo Ando, Koki Takanashi und Claudia Felser für diese sehr fruchtbare und stimulierende und sehr erfreuliche Zusammenarbeit danken. In meiner Gruppe untersuchten wir im Wesentlichen lineare und nichtlineare Spinwelleneigenschaften in Heusler-Systemen.

Wieder einmal gab es einige Veränderungen in unserer Arbeitsgruppe. Philipp Pirro verließ uns für eine Postdoc-Stelle an dem Institut Jean Lamour der Universität Lorraine in Nancy, Frankreich, und arbeitet dort mit Stéphane Mangin zusammen. Er agiert auch als eine Verbindungsperson zwischen Nancy und Kaiserslautern, um die materialwissenschaftlichen Kompetenzen der Nancy-Gruppe mit unseren Kompetenzen in der Magnonenphysik zusammenzubringen. Ana Ruiz Calaforra, Thomas Brächer und Peter Clausen haben erfolgreich ihre Doktorarbeiten abgeschlossen. Ana und Thomas verließen uns für Postdoc-Positionen bei Spintec und CNRS in Grenoble. Milan Agrawal verließ uns für eine Stelle bei Infineon Technologies bei München.

Philipp Pirro erhielt den Preis des Freundeskreises der TU Kaiserslautern und Dmytro Bozhko erhielt zwei Posterauszeichnungen. Tobias Fischer, Frank Heussner, Stefan Klingler und Laura Mihalceanu beendeten erfolgreich ihre Diplomarbeiten und Martin Hutzel, Manuela Kratz, Matthias Monzel und Oliver Nick ihren Master im Lehramt Physik. Wir begrüßen Tobias Fischer, Frank Heussner und Laura Mihalceanu als neue Doktoranden und Timo Noack als neuen Diplomanden.

Unsere Arbeit wäre nicht ohne wertvolle Kooperationen mit Partnern aus der ganzen Welt möglich gewesen. Es sind zu viele um sie alle an dieser Stelle aufzulisten. Insbesondere möchten wir, in alphabetischer Reihenfolge, danken: Christoph Adelmann, Adekunle Adeyeye, Johan Åkerman, Yasuo Ando, Antonio Azevedo, Christian Back, Matthieu Bailleul, Gerrit Bauer, Arne Brataas, Giovanni Carlotti, Florin Ciubotaru, Frederick Casper, Russell Cowburn, Sergej Demokritov, Thibaut Devolder, Bernard Dieny, Marco Doms, Rembert Duine, Carsten Dubs, Ursula Ebels, Hajo Elmers,

Jürgen Fassbender, Gerhard Fecher, Claudia Felser, Albert Fert, Mark Freeman, Sebastian Goennenwein, John Gregg, Hubert Grimm, Dirk Grundler, Gianluca Gubbiotti, Konstantin Gusliyenko, Jaroslav Hamrle, Uwe Hartmann, Thomas Hauet, Michel Hehn, Jos Heremans, Atsufumi Hirohata, Axel Hoffmann, Koichiro Innomata, Gerhard Jakob, Xiaofeng Jin, Martin Jourdan, Gleb Kakazei, Boris Kalinikos, Alexy Karenowska, Sang-Koog Kim, Akihiro Kirihara, Olivier Klein, Mathias Kläui, Yuri Kobljanskyj, Peter Kopietz, Mikhail Kostylev, Tomohiro Koyama, Volodymyr Kruglyak, Takahide Kubota, Ronald Lehndorff, Joseph Losby, Jörg Lösch, Gregoire de Loubens, Sadamichi Maekawa, Stéphane Mangin, Gennadiy Melkov, Claudia and Tim Mewes, Shigemi Mizukami, Shuichi Murakami, Hiroshi Naganuma, Andrei Nikitin, Sergei Nikitov, Jean-Pierre Nozières, Kevin O'Grady, Hideo Ohno, Tereo Ono, Mikihiko Oogane, Yoshichika Otani, Stuart Parkin, Johannes Paul, Günter Reiss, Sergio Rezende, Caroline Ross, Manfred Rührig, Eiji Saitoh, John R. Sandercock, Rudi Schäfer, Gerd Schönhense, Helmut Schultheiss, Koji Sekiguchi, Jairo Sinova, Andrei Slavin, Rolf Slatter, Bob Stamps, Yoshishige Suzuki, Koki Takanashi, Vasyl Tiberkevich, Simon Trudel, Yaroslav Tserkovnyak, Ken-ichi Uchida, Alexey Ustinov, Bart van Wees und Mingzhong Wu.

Die Zusammenarbeit mit dem Fachbereich Physik der Technischen Universität Kaiserslautern (insbesondere mit Martin Aeschlimann, James Anglin, Sebastian Eggert, Michael Fleischhauer, Georg von Freymann, Jochen Kuhn, Herwig Ott, Hans-Christian Schneider, Volker Schünemann und Arthur Widera und ihren Arbeitsgruppen), Michael Kopnarski und seinem Team des Instituts für Oberflächen- und Schichtanalytik sowie Sandra Wolff und ihrem Team des Nano Structuring Centers waren sehr stimulierend. Wir sind sehr dankbar, Mitglied des Landesforschungszentrums für Optik und Materialwissenschaften (OPTIMAS) zu sein.

Ich möchte außerdem unseren Geldgebern danken: der Deutschen Forschungsgemeinschaft (DFG), dem Bundesministerium für Bildung und Forschung (BMBF), dem Deutschen Akademischen Austauschdienst (DAAD), der Europäischen Gemeinschaft(EFRE, INTAS, INTERREG), der Carl Zeiss-Stiftung, dem Land Rheinland-Pfalz und der Technischen Universität Kaiserslautern. In Bezug auf unsere Projekte in der angewandten Forschung möchte ich meine Dankbarkeit gegenüber der Sensitec GmbH und der Singulus Technologies AG, unseren starken Partnern in R&D von spintronischen Sensoren, zum Ausdruck bringen.

Mein besonderer Dank geht an Sascha Keller, Thomas Langner, Dieter Weller und Sibylle Müller für ihre Hilfe beim Erstellen dieses Berichtes und an das Team von Photo-Repro-Druck, TU Kaiserslautern.

Es ist mir eine besondere Freude, hiermit auch allen ehemaligen Gruppenmitgliedern einen Gruß zu senden. Möge dieser Bericht uns helfen, im Kontakt zu bleiben. Wenn Sie an unserer Arbeit interessiert sind, würde ich mich freuen, von Ihnen zu hören.

Mit den besten Wünschen für ein frohes Weihnachtsfest und ein gutes Neues Jahr

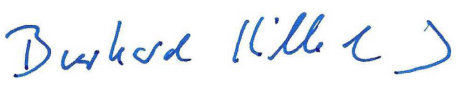

Kaiserslautern, im November 2015

Chapter 2: Personnel

2.1 Members of the group

Group leader:

Prof. Dr. Burkard Hillebrands

Senior scientists:

Dr. Andrii Chumak
Dr. Andrés Conca Parra
Dr. Britta Leven, Akad. Oberrätin
Jun. Prof. Dr. Evangelos Papaioannou
Dr. habil. Alexander Serga
Dr. Vitaliy Vasyuchka

Postdocs and long-term guest scientists:

Dr. Milan Agrawal	until 12/14
Dr. Thomas Brächer	03/15 - 05/15
Dr. Peter Clausen	since 07/15
Dr. Philipp Pirro	until 02/15
Dr. Ana Ruiz Calaforra	03/15 - 05/15

Ph.D. students:

M.Sc.	Dmytro Bozhko	
Dipl.-Phys.	Thomas Brächer	until 03/15
Dipl.-Phys.	Peter Clausen	until 07/15
Dipl.-Phys.	Tobias Fischer	since 11/15
Dipl.-Phys.	Frank Heussner	since 09/15
Dipl.-Phys.	Sascha Keller	
Dipl.-Phys.	Thomas Langner	
Dipl.-Phys.	Viktor Lauer	
Dipl.-Phys.	Thomas Meyer	
M.Sc.	Donata Passarello (IBM Research lab)	
M.Sc.	Ana Ruiz Calaforra	until 03/15

Diploma Students:

Tobias Fischer	until 05/15
Frank Heussner	until 01/15
Stefan Klingler	until 11/14
Laura Mihalceanu	until 07/15
Timo Noack	since 05/15

Master Students (Master of Education):

B.Ed. Martin Hutzel	12/14 - 05/15
B.Ed. Manuela Kratz	04/15 - 09/15
B.Ed. Matthias Monzel	04/15 - 09/15
B.Ed. Oliver Nick	12/14 - 05/15

Student Assistants:

Dipl.-Phys. Alexej Gaidoukov	02/15 - 06/15
Moritz Geilen	
Jochen Greser	until 06/15
Björn Heinz	
Philipp Jaeger	
Martin Kewenig	
Dipl.-Phys. Laura Mihalceanu	since 08/15
Hauke Georg Schäfer	since 04/15
Michael Schneider	
Matthias Schweizer	

Engineers and Technicians

Dipl.-Ing. (FH) Dieter Weller

Administration:

Sibylle Müller
Dr. Isabel Sattler

2.2 Visiting scientists, postdoctoral fellows and exchange students

(sorted by date of first arrival in our group)

Satoshi Iihama, Tohoku University, Sendai — 05.11. - 21.12.2014
Japan

Satoshi Iihama visited our group for the period of 2 months in the Framework of the Strategic Japanese-German Joint Research Program for Advanced Spintronic Materials and Transport Phenomena "ASPIMATT". He is a PhD student in the group of Prof. Dr. Yasuo Ando at the Tohoku university in Sendai. During his stay he used the facilities of the Nano Structuring Center NSC to microstructure FePd thin films. Subsequently, he performed BLS measurements using our setups to characterize the thin films as well as the microstructures.

Federico Montoncello, Dipartimento di Fisica e Scienze della Terra, Universita di Ferrara, Ferrara — 01.12. - 04.12.2014
Italy

Federico Montoncello visited us to discuss theoretical aspects of spin-wave properties. In particular we discussed the modification of bandwidth in complex structures and at magnetic transitions.

Vitalii Vitko, Department of Physical Electronics and Technology, St. Petersburg Electrotechnical University, St. Petersburg — 15.12. - 24.12.2014
Russia

Vitalii Vitko from the group of Prof. B. Kalinikos visited us in order to take part in our current investigations on microwave properties of thin ferromagnetic films, as well as to receive training in using the micromagnetic simulation program Mumax3.

Mikhail Kostylev, University of Western Australia, Perth — 07.03. - 16.03.2015
Australia

Prof. Mikhail Kostylev has visited our group in order to participate in the PhD defence of Thomas Brächer and to discuss our experimental results on the efficient spin-wave excitation and low-damping propagation in YIG-Pt bilayers.

Dr. Cecilia Holmqvist, Hans Skarsvåg, Norwegian University of Science and Technology Trondheim
Norway — 13.04. - 17.04.2015

Cecilia Holmqvist and Hans Skarsvåg have visited our group in the frame of the joint research within EU-FP7 project "Insulator Spintronics (InSpin)". We have spent a very useful time discussing the perspectives, trends, and problems in the field of insulator magnon spintronics. We also have defined a set of joint research directions in which the Kaiserslautern team will perform experimental studies while the Trondheim team will provide required theoretical support.

Dr. Alexy Karenowska, University of Oxford
United Kingdom — 26.04. - 28.04.2015

Dr. Alexy Karenowska is Early Career Fellow in Clarendon Laboratory of University of Oxford and our long-term collaborator. During her visit in Kaiserslautern we have discussed the field of macroscopic quantum phenomena and single magnon magnonics.

Prof. Andrei Slavin, Oakland University, Rochester, Michigan
USA — 18.06. - 24.06.2015, 16.07. - 24.07.2015

This year Prof. Andrei Slavin visited our group as a Visiting MAINZ Professor in order to jointly work on parametric and kinetic instabilities of parametrically driven dense magnon gases and on temporal dynamics of Bose-Einstein magnon and magnon-phonon condensates.

Prof. Gennadii Melkov, National Taras Shevchenko University of Kyiv
Ukraine — 06.07. - 23.08.2015

The regular visit of Prof. Melkov to our group was supported by the Deutsche Forschungsgemeinschaft in the frame of the SFB/Transregio 49 "Condensed Matter Systems with Variable Many-Body Interactions". During his stay he was mainly focusing on the investigation of phonon-magnon interactions in parametrically driven magnetic insulators and on phase induced magnon transport in thermal gradients.

Takafumi Nakano, Tohoku University, Sendai — 14.09. - 02.10.2015
Japan

For the period of three weeks in September, Takafumi Nakano, a PhD student in the group of Prof. Dr. Yasuo Ando at the Tohoku university in Sendai visited our group. During his stay, he characterized CoFeB thin films by means of BLS and presented his research to our group.

Assist. Prof. George Vourlias, Dr. Kostas Symeonidis, — 26.10. - 02.11.2015
Department of Physics, Aristotle University of Thessaloniki,
Department of Mechanical Engineering, University of Thessaly
Greece

Dr. George Vourlias is Assistant Professor in the Physics Department of Aristotle University of Thessaloniki. His research interests focus on materials growth, surface science and structural characterization of materials by X-ray methods. Dr. Kostas Simeonidis received his B.S. in Chemical Engineering and his PhD degree in Materials Science from Aristotle University of Thessaloniki. He is currently a postdoctoral fellow in the Department of Mechanical Engineering in University of Thessaly. His research interests are synthesis and engineering of magnetic nanoparticles for environmental applications. Their visit took place in the framework of bilateral German-Greek collaboration scheme DAAD PPP-IKYDA 2015.

Nikolaos I. Pliatsikas, Dimitrios Karfaridis, Aristotle University, — 30.10. - 06.11.2015
Thessaloniki
Greece

Nikolaos I. Pliatsikas and Dimitrios Karfaridis visited our group in the Framework of the bilateral German-Greek collaboration scheme DAAD PPP-IKYDA 2015. Nikolaos I. Pliatsikas is a PhD student in the group of Prof. Dr. P. Patsalas and Dimitrios Karfaridis is a Master student in the group of Prof. Dr. G. Vourlias at the Aristotle university in Thessaloniki.

2.3 Guest seminars

Ulrich Nowak 12.11.2014	Universität Konstanz, Germany *Magnon currents: propagation, localization and entropic torques* Special OPTIMAS seminar
Carsten Dubs 24.11.2014	Innovent e.V. Technologieentwicklung, Jena, Germany *Yttrium iron garnet (YIG) film growth and characterisation* Special group seminar
Sebastian T.B. Goennenwein 24.11.2014	Walther-Meißner-Institut, Bayerische Akademie der Wissenschaften, Garching, Germany *Spin currents in ferromagnet / normal metal heterostructures* Physics colloquium
Satoshi Iihama 01.12.2014	Department of Applied Physics, Tohoku University, Sendai, Japan *Magnetization dynamics and damping detected by all-optical pump-probe method* Special group seminar
Federico Montoncello 03.12.2014	Dipartimento di Fisica e Scienze della Terra, Università di Ferrara, Ferrara, Italy *Bandwidth variation of collective spin waves at the edge of magnetic transitions* Special seminar
Ron Jansen 04.12.2014	National Institute of Advanced Industrial Science and Technology (AIST), Spintronics Research Center, Tsukuba, Japan *Silicon Spintronics* Joint TR49 and Theoretical Physics colloquium
Peng Yan 16.01.2015	Johannes Gutenberg-Universität, Mainz, Germany *Dynamics of textured ferromagnetic cylinders and ferromagnetic bilayers* Special seminar
Hartmut Zabel 19.01.2015	Ruhr-Universität Bochum, Germany Johannes Gutenberg Universität, Mainz, Germany *Nanomagnetism explored by X-rays and neutrons* Physics colloquium
Tilmann Kuhn 22.01.2015	Westfälische Wilhelms-Universität Münster, Germany *Temporal and spatio-temporal dynamics of non-equilibrium magnon systems* Joint TR49 and Theoretical Physics Colloquium

Hans Huebl 28.01.2015	Walther-Meißner-Institut, Bayerische Akademie der Wissenschaften, Garching, Germany *Spins, strings and superconducting resonators: coupling harmonic oscillators in the solid state* Special seminar
Denys Makarov 06.02.2015	Institute for Integrative Nanosciences, IFW, Dresden, Germany *Curved magnetic nanomembranes* OPTIMAS Laser- und Quantenoptikseminar
Qi Wang 31.03.2015	University of Electronic Science and Technology of China State Key Laboratory of Electronic Thin Films and Integrated Devices, Chengdu, China *Spin wave in magnonic crystal* Special seminar
Yonatan Sivan 02.04.2015	Unit of Electro-Optics Engineering, Ben-Gurion University of the Negev, Israel *The non-local nature of free-carrier ultrafast nonlinearity theory and novel wave phenomena* Special seminar
Martin Weides 14.04.2015	Johannes Gutenberg Universität Mainz, Germany and Karlsruhe Institute of Technology (KIT), Germany *Coupling of magnons to superconducting qubits* Special seminar
Alexander Samardak 17.04.2015	Far Eastern Federal University, Vladivostok, Russia *Magnetic nanostructures: magnetization reversal, spin configurations and magnetotransport* Special seminar
Corinna Chudalla 18.05.2015	Referat für Technologie und Innovation, Patent- und Informationszentrum Rheinland Pfalz, Kaiserslautern, Germany *Patente und Arbeitnehmererfindungen* Special group seminar
Sebnem Tuncay 17.07.2015	Technische Universität München, Germany *Charge transfer between GaN and Pt interfaces studied by (conductive) atomic force microscopy* Special seminar
Thomas Hauet 20.07.2015	Institut Jean Lamour, Lorraine University - CNRS, Nancy, France *Towards spin transfer torque induced bubble dynamics* Special group seminar

Dmitry Turchinovich 23.07.2015	Max Planck Institute for Polymer Research, Mainz, Germany *Direct access to charge, lattice and spin dynamics in solids with ultrafast terahertz spectroscopy* Special seminar
Zakarya Lasmar 11.08.2015	Adam Mickiewicz University in Poznań, Poland *Spin Hall effect in graphene* Special seminar
Benjamin Jungfleisch 18.08.2015	Materials Science Division, Argonne National Laboratory, Argonne, IL, USA *Spin-torque driven magnetization dynamics by interface- and bulk spin-orbital phenomena* Special seminar
Takafumi Nakano 16.09.2015	Department of Applied Physics, Tohoku University, Sendai, Japan *Magnetic sensor based on magnetic tunnel junction with perpendicularly magnetized CoFeB sensing layers* Special seminar
Dazhi Hou 17.09.2015	Institute of Materials Research, Tohoku University, Sendai, Japan *Hall detection of magnetization due to spin pumping and spin Seebeck process* Special seminar
Dieter Weller 21.09.2015	HGST a Western Digital Company, San Jose, CA, USA *Future FePt heat assisted magnetic recording technology* Special OPTIMAS seminar
Eiji Saitoh 09.10.2015	Institute of Materials Research, Tohoku University, Sendai, Japan *Mechanical spintronics* OPTIMAS Laser- und Quantenoptikseminar
Sadamichi Maekawa 22.10.2015	Advanced Science Research Center (ASRC), Japan Atomic Energy Agency (JAEA), Tokai, Japan *Power spintronics* Special OPTIMAS seminar

2.4 Visits of group members at other laboratories

Evangelos Papaioannou	Uppsala Universitet, Uppsala, Sweden 04.02.2015 - 06.02.2015 Host: Prof. Björgvin Hjörvarsson
Matthias Schweizer	Center for Materials for Information Technology (MINT), Alabama, USA 04.06.2015 - 31.07.2015 Host: Prof. Paulo Araujo, Prof. Takao Suzuki
Alexander Serga	Oakland University, Rochester, Michigan, USA 10.09.2015 - 14.09.2015 Host: Prof. Andrei Slavin
Dmytro Bozhko	Faculty of Radiophysics, Taras Shevchenko National University of Kyiv, Ukraine 24.10.2015 - 30.10.2015 Host: Prof. Gennadiy A. Melkov

2.5 Group member photo gallery

Dr. Milan Agrawal
Postdoc

Dmytro Bozhko
Ph.D. student

Dr. Thomas Brächer
Postdoc

Dr. Andrii Chumak
Senior scientist

Dr. Peter Clausen
Postdoc

Dr. Andrés Conca Parra
Senior scientist

Tobias Fischer
Ph.D. student

Alexej Gaidoukov
Student assistant

Moritz Geilen
Student assistant

Jochen Greser
Student assistant

Björn Heinz
Student assistant

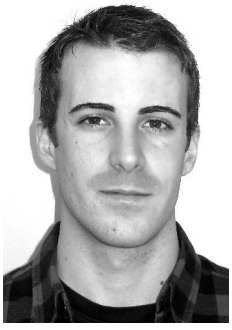

Frank Heussner
Ph.D. student

Prof. Dr. Burkard Hillebrands
Group leader

Martin Hutzel
Master student

Philipp Jaeger
Student assistant

Sascha Keller
Ph.D. student

Martin Kewenig
Student assistant

Stefan Klingler
Diploma student

Manuela Kratz
Master student

Thomas Langner
Ph.D. student

Viktor Lauer
Ph.D. student

Dr. Britta Leven
Senior scientist

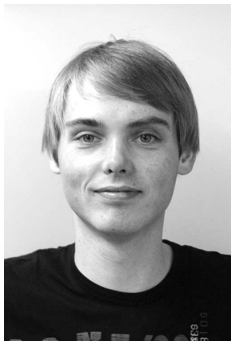

Thomas Meyer
Ph.D. student

Laura Mihalceanu
Diploma student

Matthias Monzel
Master student

Sibylle Müller
Secretary

Oliver Nick
Master student

Timo Noack
Diploma student

JProf. Dr. Evangelos Papaioannou
Senior scientist

Donata Passarello
Ph.D. student

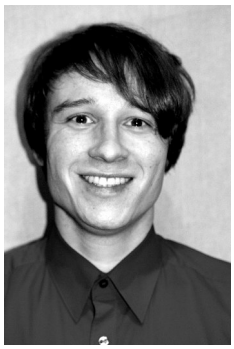

Dr. Philipp Pirro
Postdoc

Dr. Ana Ruiz Calaforra
Postdoc

Dr. Isabel Sattler
Administration

Hauke Georg Schäfer
Student assistant

Michael Schneider
Student assistant

Matthias Schweizer
Student assistant

Dr. Alexander Serga
Senior scientist

Dr. Vitaliy Vasyuchka
Senior scientist

Dieter Weller
Mechanical engineer

Chapter 3: Methods

3.1 Brillouin light scattering spectroscopy (BLS)

Brillouin light scattering spectroscopy (BLS) is the primary key technique in our laboratory to investigate the dynamic properties of magnetic materials and devices. It is based on the interaction of photons with the fundamental excitations of a solid such as magnons, the quanta of magnetic excitations. The interaction can be understood as an inelastic scattering process of the incident photons with magnons, taking into account energy and momentum conservation as indicated in Fig. 1.

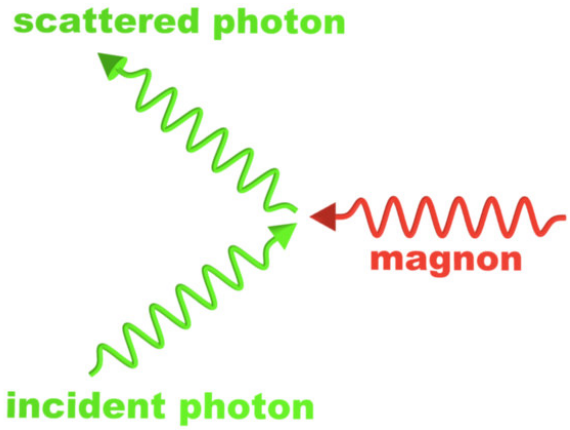

Fig. 1: Scheme of inelastic scattering of an incident photon by a magnon.

The detection of the inelastically scattered photons, i.e. the separation from the elastically scattered photons and the determination of the transferred energy, requires an interferometric technique with extremely high contrast and sensitivity. In our laboratory we implemented the (3+3) Tandem-Fabry-Pérot-Interferometer, designed by John R. Sandercock and schematically shown in Fig. 2. It consists of two Fabry-Pérot interferometers (FPI), each one passed three times by the inelastically scattered light. This approach results in a contrast better than 10^{10} for the separation of the elastically and inelastically scattered photons in a frequency range from 500 MHz up to 1 THz.

In the last decade we made significant progress in the improvement of BLS spectroscopy. The spatial resolution was pushed to the fundamental limit of classical optics by constructing a BLS-microscope (Fig. 3) with sophisticated active stabilization methods. Spin-wave transport phe-

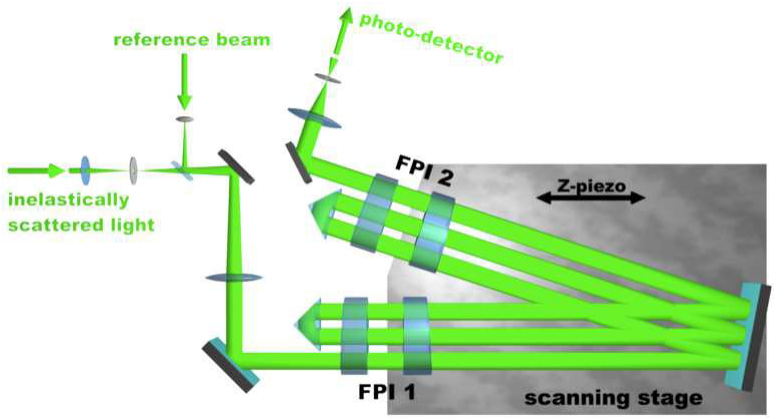

Fig. 2: Scheme of a (3+3) tandem Fabry-Pérot interferometer, designed and build by John R. Sandercock (JRS Scientific Instruments, Mettmenstetten, Switzerland)

nomena can be investigated by time, phase- and wave-vector resolution. Additionally, the typical in-plane measurement geometry has been extended by an out-of-plane electromagnet known from Kerr microscopy providing in-situ magnetic fields up to 1T perpendicular to the sample surface. This out-of-plane magnet can be implemented in one of the micro-focus BLS setups. In a further development during the past year, our BLS equipment needed to be upgraded towards new research fields. Integrating a blue laser with a wavelength of 491 nm into one of our micro-focus BLS setups we opened up the sensitive access to thin YIG films (with thicknesses of 100 nm and below) by largely increasing the sensitivity since the absorption is much higher at this wavelength.

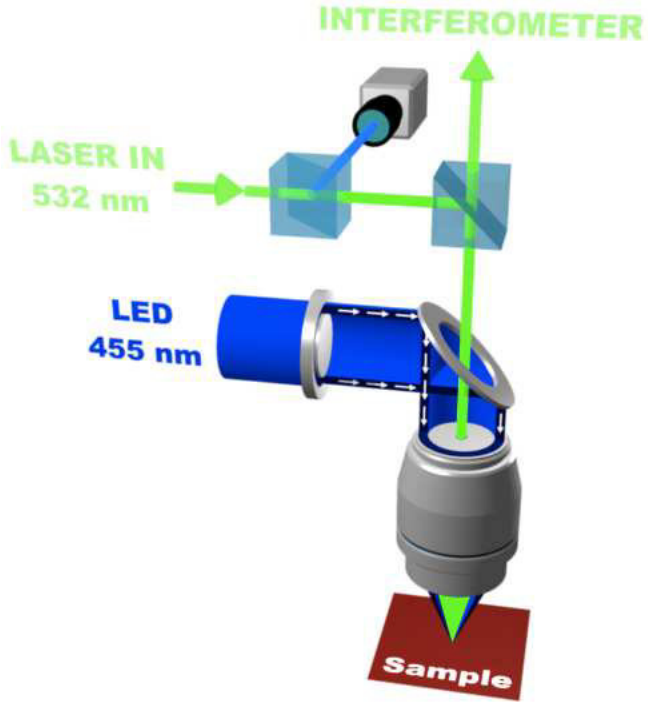

Fig. 3: Schematic setup of a BLS-microscope. The LED light is used to monitor the position of the laser focus on the sample by a CCD camera and to apply active position control to the sample stage.

A second recent advancement regarding our standard BLS techniques is the pulsed probe laser beam technique allowing for the detection of various evolution processes such as, e.g., the temperature evolution inside a sample. The special feature of this technique is that the focused laser beam combines the role of the magnon probe with the role of a local sample heater. Furthermore, the heating time is adjusted using amplitude modulation of the probing laser beam by an acousto-optic modulator (AOM). The scheme of the corresponding experimental setup, which consists of a YIG film sample, a microwave circuit, and a BLS laser system, is shown in Fig. 4.

The following list gives an overview of the different BLS setups available in our group:

BLS1: High-field electromagnet (1.2 T), standard BLS spectroscopy equipment. Time resolution, phase resolution, space resolution (50 µm), wave-vector resolution.

BLS2: High-field electromagnet (1.2 T), standard BLS spectroscopy equipment. Microscope stage with 250 nm spatial resolution and build-in time and phase resolution.

BLS3: High-field electromagnet (1.2 T), standard BLS spectroscopy equipment. Microscope stage with 250 nm spatial resolution and build-in time and phase resolution. Option to use blue laser ($\lambda = 491$ nm) or out-of-plane magnet unit.

BLS4: Electromagnet (0.1 T), standard BLS spectroscopy equipment. Microscope stage with 250 nm spatial resolution and build-in time and phase resolution.

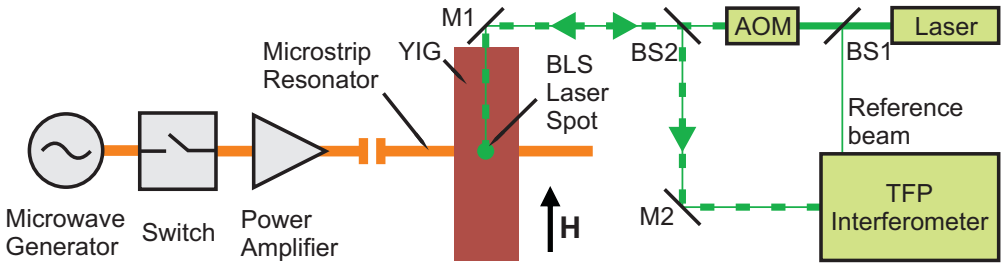

Fig. 4: Schematic illustration of the BLS setup with pulsed probe laser beam technique. On the left hand side, the microwave circuit consisting of a microwave source, switch and amplifier is shown. This circuit drives a microstrip resonator, which is placed below a YIG film. The arrow indicates the directions of the applied external bias magnetic field H. The green dot illustrates the focus position of the BLS laser. On the right hand side, the BLS laser beam path is indicated. The light of a solid-state laser ($\lambda = 532\,\mathrm{nm}$) is split by a beam splitter (BS1). The sample beam is sent to an acousto-optic modulator and the reference beam to the interferometer. The modulated sample beam is guided through the second beam splitter (BS2) and the mirror (M1) to the YIG film where it scatters. The scattered light is reflected again at M1 and deflect by BS2 to the Tandem Fabry-Pérot interferometer.

3.2 Microwave techniques

Brillouin light scattering (BLS) spectroscopy, as described in the previous section, is a powerful tool for the detection of spin waves and measurement of their characteristics. Nevertheless, it does not allow for spin-wave excitation. Thus, in many of our experiments BLS spectroscopy is combined with microwave techniques which ensure high-efficient generation of spin waves in magnetic structures. Spin waves are emitted by nano- and micro-sized microstrip antennas placed on the surfaces of magnetic thin films and is driven by a microwave signal in the GHz frequency range [1, 2]. Microwave sources in our laboratories generate signals of up to 70 GHz providing access to spin-waves in a very wide range of frequencies and wavenumbers. Furthermore, large powers (up to 200 W) provided by microwave amplifiers allow for the study of strongly nonlinear spin-wave dynamics as well as for quantum effects in parametrically-driven magnon gases. The microwave technique allows for the excitation of both, continuous spin waves as well as short spin-wave packets. Among other advantages, the pulsed technique enables the realization of time resolved (resolution down to 250 ps) BLS spectroscopy [3] shown in Fig. 1. The continuous microwave excitation, by-turn, allows realization of phase-resolved BLS spectroscopy [4, 5].

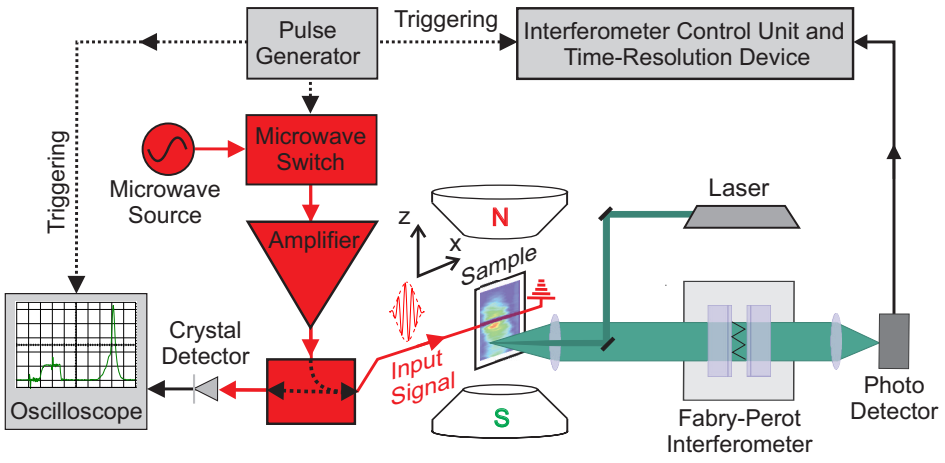

Fig. 1: Scheme of the microwave-assisted time- and space-resolved BLS setup

Besides the excitation of spin waves, the microwave technique is intensively used for high-sensitive (10^{-13} W) detection. Using the same antennas the magnetization precession is converted into microwave currents. These currents are amplified by low-noise amplifiers and analyzed using wide-band oscilloscopes, vector network analyzers or a spectrum analyzer [2]. A vector network analyzer is also used for the ferromagnetic resonance (FMR) measurements allowing determination of such characteristics of the magnetic thin films as magnetization saturation, exchange constant, and damping.

During the last year a modern microwave setup for broadband microwave analysis has been installed in our lab. This setup, schematically shown in Fig. 2, consists of the following complementary devices: vector network analyzer, spectrum analyzer, microwave signal generator, two high-power microwave amplifiers, and a magnet. It has a wide frequency bandwidth of up to 70 GHz which allows for the excitation of spin waves with wavelengths down to 30 nm. This helps us to perform measurements in the frame of modern nanometer-scale magnonics. The broadband microwave analysis can be conducted in both the CW and pulsed regime. The possibility to switch between CW and time-resolved measurements of the vector network analyzer gives us a unique opportunity to separate spin-wave signals from much larger electromagnetic leakages.

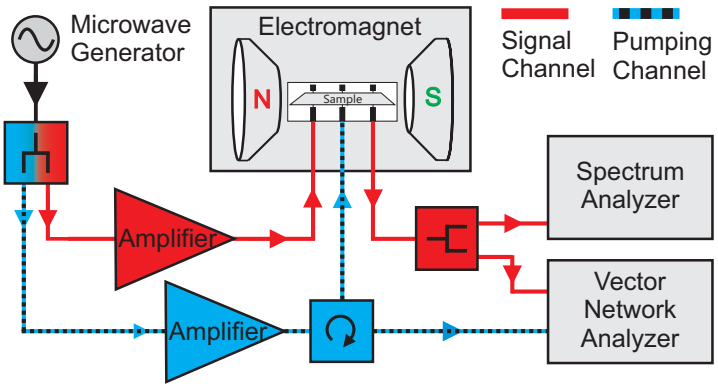

Fig. 2: Diagram of the experimental setup for microwave analysis with a wide frequency bandwidth up to 70 GHz

Our microwave techniques are amended by detection of spin waves using the inverse spin Hall effect [6] and were used recently for investigations of microwave-induced spin currents in a ferromagnetic-insulator | normal-metal bilayer system [7]. Furthermore, we have realized a magnon transistor [8], where the magnon-by-magnon control principle is demonstrated using the microwave technique.

References

[1] A.V. Chumak, V.I. Vasyuchka, A.A. Serga, B. Hillebrands, *Magnon spintronics*, Nat. Phys. **11**, 453 (2015).
[2] A.A. Serga, A.V. Chumak, B. Hillebrands, *YIG magnonics*, J. Phys. D **43**, 264002 (2010).
[3] O. Büttner, M. Bauer, S.O. Demokritov, B. Hillebrands, Yu.S. Kivshar, V. Grimalsky, Yu. Rapoport, A.N. Slavin, *Linear and nonlinear diffraction of dipolar spin waves in yttrium iron garnet films observed by space- and time-resolved Brillouin light scattering*, Phys. Rev. B **61**, 11576 (2000).
[4] A.A. Serga, T. Schneider, B. Hillebrands, S.O. Demokritov, M.P. Kostylev, *Phase-sensitive Brillouin light scattering spectroscopy from spin-wave packets*, Appl. Phys. Lett. **89**, 063506 (2006).
[5] K. Vogt, H. Schultheiss, S.J. Hermsdoerfer, P. Pirro, A.A. Serga, B. Hillebrands, *All-optical detection of phase fronts of propagating spin waves in a $Ni_{81}Fe_{19}$ microstripe*, Appl. Phys. Lett. **95**, 182508 (2009).
[6] A.V. Chumak, A.A. Serga, M.B. Jungfleisch, R. Neb, D.A. Bozhko, V.S. Tiberkevich, B. Hillebrands, *Direct detection of magnon spin transport by the inverse spin Hall effect*, Appl. Phys. Lett. **100**, 082405 (2012).

[7] M. Agrawal, A.A. Serga, V. Lauer, E.Th. Papaioannou, B. Hillebrands, V.I. Vasyuchka, *Microwave-induced spin currents in ferromagnetic-insulator|normal-metal bilayer system*, Appl. Phys. Lett. **105**, 092404 (2014).
[8] A.V. Chumak, A.A. Serga, B. Hillebrands, *Magnon transistor for all-magnon data processing*, Nat. Commun. **5**, 4700 (2014).

3.3 Magneto-optic Kerr effect magnetometry and microscopy (MOKE)

The magneto-optical Kerr effect (MOKE) is a well established technique to study magnetization properties. The effect is based on the fact, that the plane of polarization of light is rotated when the light is reflected from a magnetic material [1]. The physical origin of MOKE is the magnetic circular dichroism effect: exchange and spin-orbit coupling in a magnetic material lead to different absorption spectra for left- and right-circularly polarized light. Measuring the change of the polarization of the reflected beam (often referred to as Kerr angle Θ_{Kerr}) provides access to the magnetization state of the sample.

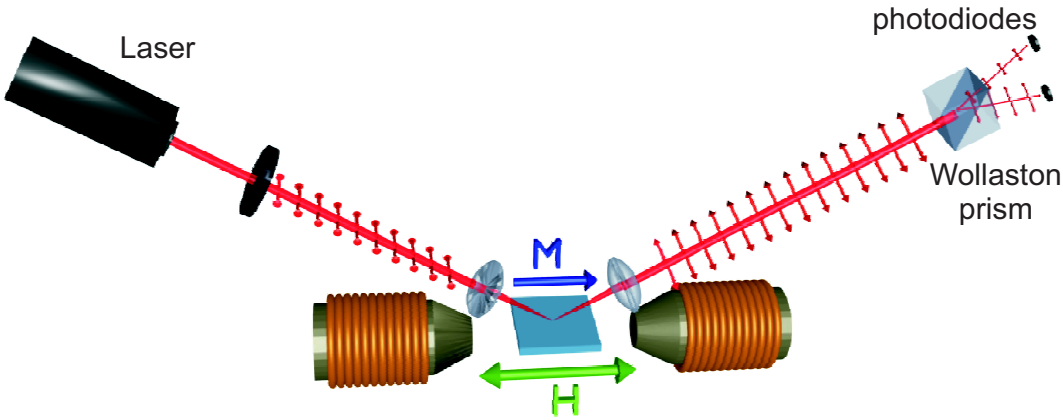

Fig. 1: Schematic setup of a longitudinal Kerr magnetometer.

With MOKE it is possible to study quasi-static magnetization reversal properties and magnetic anisotropies. When using a pulsed laser system it is also possible to study the time dependence of the magnetization under the influence of, e.g., a pulsed magnetic field or a microwave field. Since it is an optical technique it is non invasive, and the spatial resolution is only limited by the optical resolution. Thus, we are able to study the static and dynamic properties of magnetic thin films and magnetic structures with lateral dimension down to 1 µm.

Our group uses four different MOKE setups, all of them using the same principle. The light of a laser source is s-polarized through a thin-film polarizer. The beam is focused onto the sample. The polarization of the reflected light is analyzed by a detector unit that was developed and is built in our laboratory. A Wollaston prism divides the beam into two orthogonally polarized beams, which are monitored by a pair of photodiodes. The detector works as an opto-electrical bridge circuit to increase the signal-to-noise ratio. The obtained normalized differential signal $(I_1 - I_2)/(I_1 + I_2)$ is directly proportional to the Kerr angle Θ_{Kerr}.

Four experimental setups are available to investigate different scientific aspects:

Longitudinal Kerr magnetometer: Longitudinal MOKE geometry to probe quasi-static properties of magnetic thin films. Optical resolution $\sim 100\,\mu$m, magnetic field up to 2 T, automated sample positioning and rotation.

Microfocus Kerr microscope with rotation unit: Longitudinal MOKE geometry to probe quasi-static properties of micro-structured magnetic elements. Optical resolution $< 1\,\mu m$, magnetic field up to 0.6 T, automated sample positioning, rotation and stabilization.

Dual MOKE magnetometer: Two combined MOKE magnetometers working in parallel, one in longitudinal and one in polar geometry to study the quadratic MOKE effects on magnetic thin films. Optical resolution $\sim 100\,\mu m$, two orthogonal pairs of magnet coils to provide any in-plane field direction up to 0.25 T, automated sample positioning and rotation.

Time resolved scanning Kerr microscope: Longitudinal or polar MOKE geometry to study dynamic magnetization reversal properties of micro-structured elements. Optical resolution $<$ 500 nm, time resolution ~ 60 ps, magnetic field up to 150 mT, automated sample positioning and stabilization.

References

[1] J. Kerr, *On rotation of the plane of polarization by reflection from the pole of a magnet*, Phil. Mag. **4** (5), 321 (1877).

3.4 Molecular beam epitaxy (MBE)

The Molecular Beam Epitaxy (MBE) technique involves highly controlled evaporation of materials in an ultra-high vacuum chamber (pressure in the low 10^{-11} mbar region). This deposition from the vapor phase can lead to single crystal film growth. For this reason MBE possesses a dominant role in the world of nanotechnology regarding fabrication of materials for high performance applications.

Our group operates two Molecular Beam Epitaxy (MBE) growth clusters. Both systems are equipped with tools for cleaning the substrates, for controlling the evaporation from the sources and the film deposition, for *in-situ* structural and chemical characterization, as well as sample storage.

The first cluster is named MDA (Multidepositionsanlage). The MDA has been heavily loaded this year with the growth of magnetic structures. The growth chamber contains two Knudsen cells and one electron gun with 5 crucibles that are used to heat and evaporate the materials. The growth procedure is controlled *in-situ* by a quartz crystal. Additionally, *in-situ* Low-Energy Electron Diffraction (LEED) and Auger analytics can be performed. Furthermore, the linear construction of the sample holder reduces the total time for sample preparation largely.

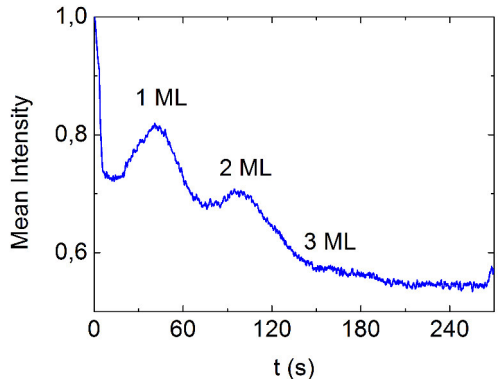

Fig. 1: RHEED oscillation observed for the growth of 3 ML Cr on top of Fe. RHEED offers unique advantages in controlling the growth procedure at the atomic level.

Our second cluster, named MBE, contains two Knudsen cells, and one electron gun with 5 crucibles. The growth procedure is controlled *in-situ* by a quartz crystal. One of the great advantages of our MBE system is the capability to control the *in-situ* growth by means of Reflection of High-Energy Electron Diffraction (RHEED). The characteristics of the RHEED technique is not to interfere with the deposition. An example of layer by layer deposition controlled by RHEED is shown in Fig. 1. This renders it as a unique tool for real-time structural characterization of the sample during the growth process. There is also the option for Low-Energy Electron Diffraction (LEED) and Auger analytics.

In addition to the aforementioned techniques and linked to the MBE, an scanning tunneling microscope (STM) set-up is used for *in-situ* atomic probing. This increases further the capabilities of our MBE chamber. STM is a unique tool for surface investigation of the evaporated samples,see Fig. 2. The cluster includes furthermore a load chamber for inserting samples in vacuum and preparation chamber. The latter is used for cleaning the samples since there is the possibility to heat up the samples to 800 °C . Furthermore, there is an option for optical coatings. The ionization chamber is equipped with a fine-focus noble gas keV ion source. A transfer chamber connects all the parts of the growth cluster while a repository chamber is also available. The MBE chamber has another unique feature: that of *in-situ* magnetic characterization with Brillouin light scattering (BLS) spectroscopy and Kerr effect magnetometry. The applied magnetic field can reach 1.2 T. There is an option for implementation of a cryostat.

The MBE evaporation technique offers unique advantages for the fabrication of patterned samples. The good control of the film growth and the directionality of the beam renders MBE suitable to grow materials on patterned masks. Patterned samples of extreme quality can be produced either with pre- or post treatment techniques.

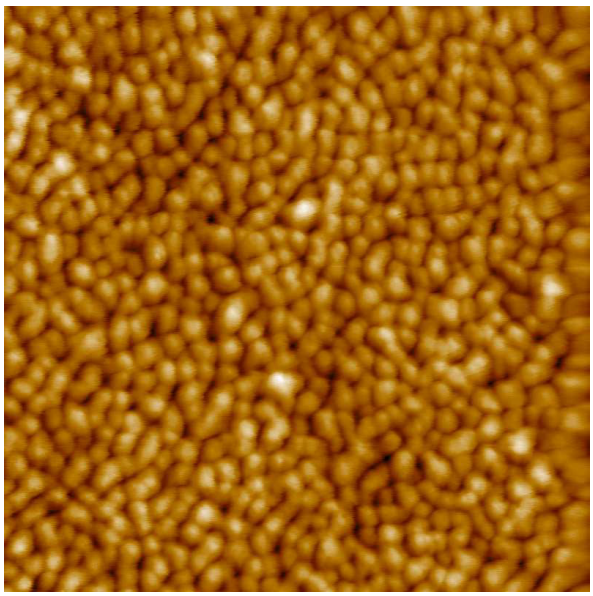

Fig. 2: *in-situ* scanning tunneling microscopy image (scale: 200 × 200 nm) of an Fe surface grown on a MgO substrate at 150 °C. The microstructural evolution of magnetic films define their magnetic properties.

2015 was a very successful year regarding both of our growth chambers. We have produced a series of different systems like epitaxial Fe/Pt bilayers, Fe/MgO/Pt trilayers, Fe/Au, Fe/Pd, FeRh, Co/Au alloys and bilayers for studies in magnetisation dynamics. We have also used YIG substrates to evaporate Au and Pt on top.

Chapter 4: Reports on Experimental Results

A. Magnon Gases and Condensates

In ferromagnetic materials atoms having unpaired electrons act as individual magnets. Their magnetism is mostly caused by the magnetic moments of the uncompensated electron spins. Since these atomic magnets tend to be oriented in the same direction due to quantum-mechanical exchange interaction, a macroscopic magnetic moment appears. As the atoms strongly interact, a reversal of a single atomic magnetic moment is not spatially localized but spreads through the solid as a wave of discrete magnetic momentum transfer. This wave is known as a spin wave, and in frame of second quantization it is associated with a quasi-particle named magnon. Weakly interacting magnons can be considered as a gas of magnetic bosonic quasi-particles and, therefore, this is referred to as a magnon gas.

Nowadays magnon gases are recognized as an excellent model environment for the experimental investigation of collective classical and quantum macroscopic properties of bosonic systems. Its potential is due to the wide controllability of the magnon density as well as of the spectral properties influencing the magnon-magnon interaction. For example, the dispersion branch of a magnon gas can be frequency shifted or otherwise modified by change in the strength or orientation of a bias magnetic field. The magnon population density can be effectively controlled by means of electromagnetic parametric pumping (see Gurevich and Melkov, Magnetization Oscillation and Waves, CRC, Cleveland, 1996). In the simplest case one photon of the pumping electromagnetic field excites two magnons with half the energy/frequency that propagate in opposite directions. Such a mechanism creates a huge quantity of phase correlated magnons, which are called a condensate of photon-coupled magnon pairs. The behavior of parametrically created magnon condensates, of gaseous magnon phases, and of Bose-Einstein condensates (BEC), which can be formed at the lowest energy state of a magnon gas, constitutes a hot research topic. The main goal of our work is to study the phase transition processes resulting in the formation of quantum macroscopic states of a magnon gas and to understand the role of magnon-magnon and magnon-phonon interactions in the properties of these correlated states of matter in comparison with the dynamics of ultra-cold quantum gases and quantum spin systems. We investigate the dynamics of the magnon system in a low-damping magnetic insulator (yttrium-iron-garnet, YIG) using wavevector- and time-resolved Brillouin light scattering (BLS) spectroscopy with special attention on the pump-free evolution of the magnetic medium after pumping. A focus lies on transport phenomena in magnon condensates including phase induced supercurrents.

Several very interesting findings are presented this year.

In Report 4.1 “Formation of Bose-Einstein magnon condensate via dipolar and exchange thermalization channels” we demonstrate the strong influence of the density of the parametrically pumped magnon pairs on the thermalization of the parametrically driven magnon gas and on the BEC formation. The BLS observations suggest two distinct channels of the thermalization process related to dipolar and exchange parts of the magnon gas spectrum. In the course of the pump action, the increasing magnon density causes a downward shift of the magnon spectrum due to the decrease in the saturation magnetization. This, consequently, leads to a transition from dipolar to exchange thermalization scenarios. As a result, the latter one becomes dominating at high pumping powers.

In Report 4.2 “Magnon supercurrent in a magnon Bose-Einstein condensate subject to a thermal gradient” we present further experimental and theoretical results on a magnon supercurrent excited in the magnon BEC by a laser-light induced thermal gradient. Such a current, which is driven by the

phase difference between the different BEC areas, leads to a magnon leakage from the focal point of the BLS probing laser beam and results, thus, in the enhanced decay in population of the freely evolving magnon condensate at the position of the laser spot. The developed theoretical model, which takes into account both the thermally induced phase shift and time-dependent stochastization of the BEC magnon phase, perfectly describes the experimental data.

In Report 4.3 “Stimulated thermalization of a parametrically driven magnon gas as a prerequisite for Bose-Einstein magnon condensation” we demonstrate both experimentally and theoretically that magnon condensation is preceded by the conversion of initially pumped magnons into a second group of frequency-degenerate magnons, which appear due to parametrically stimulated scattering of the initial magnons to a short-wavelength spectral region. In contrast to the first magnon group, in which wave vectors are orthogonal to the wave vectors of the magnons at the lowest energy states, the secondary magnons can effectively scatter to the bottom of the spectrum and condense there.

A. Magnonengase und -kondensate

In ferromagnetischen Materialien treten Atome, die ungepaarte Elektronen haben, als einzelne elementare Magnete auf. Ihr Magnetismus wird in der Regel durch die magnetischen Momente des nicht kompensierten Elektronenspins verursacht. Diese atomaren Magnete richten sich häufig aufgrund der quantenmechanischen Austauschwechselwirkung in einem Ferromagneten parallel zueinander aus. Daher beobachtet man ein makroskopisches magnetisches Moment. Da die Atome stark miteinander wechselwirken, wird das Umklappen eines einzelnen atomaren magnetischen Moments nicht räumlich lokalisiert sein, sondern breitet sich als Welle mit einem diskreten magnetischen Moment über den gesamten Festkörper aus. Diese Welle wird als Spinwelle bezeichnet und ist im Rahmen der zweiten Quantisierung mit einem Quasiteilchen, dem so ge-nannten Magnon, verbunden. Schwach miteinander wechselwirkende Magnonen können als Gas von magnetischen bosonischen Quasiteilchen angesehen werden und werden daher auch als Magnonengas bezeichnet.

Magnonengase sind unlängst als hervorragendes Modellsystem erkannt worden und dienen zur Untersuchung von korrelierten bosonischen Systemen mit sowohl klassischen Eigenschaften als auch makroskopischen Quanteneigenschaften. Ihr Potenzial liegt dabei in der guten Kontrollierbarkeit der Magnonendichte und den Eigenschaften des Spektrums, welches die Magnon-Magnon-Wechselwirkung beeinflusst. Zum Beispiel kann durch die Änderung der Richtung oder der Stärke eines externen Magnetfelds das Spektrum des Magnonengases in der Frequenz verschoben oder auch stark verändert werden. Der wirkungsvollste Mechanismus, die Dichte eines Magnonengases zu erhöhen, ist parametrisches Pumpen mittels Mikrowellen (s. Gurevich and Melkov, Magnetization Oscillation and Waves, CRC, Cleveland, 1996). Im einfachsten Fall erzeugt ein Photon des elektromagnetischen Pumpfeldes zwei Magnonen mit je der Hälfte der Energie/Frequenz des Photons, die sich in entgegengesetzte Richtungen ausbreiten. Dieser Mechanismus erzeugt eine große Anzahl von phasenkorrelierten Magnonen, ein sogenanntes Kondensat von photonengekoppelten Magnonenpaaren. Die Verhaltensweisen parametrisch erzeugter Magnonenkondensate, gasförmiger Magnonenzustände, und von magnonischen Bose-Einstein-Kondensaten (BEC), welche im Zustand niedrigster Energie des Magnonengases erzeugt werden können, bilden ein aktuelles Forschungsthema. Das Hauptziel unserer Forschung ist die Untersuchung der Phasenübergänge, die zu der Bildung von Zuständen mit makroskopischen Quanteneigenschaften in Magnonengasen führen, und das Verständnis der Funktion der Viel-Magnonen-Wechselwirkungen in diesen

korrelierten Zuständen der Materie im Vergleich mit der Dynamik von ultrakalten Quantengasen und Quanten-Spinsystemen. Wir untersuchen die Dynamik des Magnonensystems in einem magnetischen Isolator mit niedriger Dämpfung (Yttrium-Eisen-Granat, YIG) mit Hilfe von wellenvektor- und zeitaufgelöster Brillouin-Lichtstreuspektroskopie mit besonderem Augenmerk auf die pumpfreie Entwicklung des magnetischen Mediums nach dem Pumpprozess. Die besondere Aufmerksamkeit konzentriert sich auf Transportphänomene in Magnonenkondensaten, die phaseninduzierte Suprastrőme einbeziehen.

Dieses Jahr werden einige sehr interessante Ergebnisse vorgestellt.

In Bericht 4.1 “Formation of Bose-Einstein magnon condensate via dipolar and exchange thermalization channels” zeigen wir den starken Einfluss der parametrisch generierten Magnonenpaare auf die Thermalisierung des parametrisch getriebenen Magnonengases und auf die Bildung des BECs. Die BLS-Untersuchung legt zwei unterschiedliche Kanäle des Thermalisierungsprozesses nahe, die dem austausch- und dipoldominierten Teil des Magnonengasspektrums zuzuordnen sind. Im Laufe des Pumpprozesses verursacht die anwachsende Magnonendichte eine Absenkung der Sättigungsmagnetisierung und somit eine Verschiebung des Magnonenspektrums zu kleineren Frequenzen. Infolgedessen findet ein Wechsel von dipoldominierter zu austauschdominierter Thermalisierung statt und folglich dominiert bei hohen Pumpleistungen letztere.

In Bericht 4.2 “Magnon supercurrent in a magnon Bose-Einstein condensate subject to a thermal gradient” präsentieren wir weitere experimentelle und theoretische Ergebnisse über Suprastrőme, die im Magnonen-BEC durch Laserlicht induzierte thermische Gradienten entstehen. Dieser Strom, der durch die Phasendifferenz zwischen verschiedenen Bereichen des BECs angetrieben wird, führt zu einem Magnonenabfluss aus dem Fokus des BLS-Lasers und somit zu einer schnelleren Abnahme der pumpfreien BEC-Magnonendichte. Das entwickelte theoretische Modell, welches sowohl die thermisch induzierte Phasendifferenz als auch die zeitabhängige Dephasierung der BEC-Magnonenphase berücksichtigt, beschreibt die experimentellen Daten mit einer sehr guten Übereinstimmung.

In Bericht 4.3 “Stimulated thermalization of a parametrically driven magnon gas as a prerequisite for Bose-Einstein magnon condensation” zeigen wir sowohl experimentell als auch theoretisch, dass der Magnonenkondensation eine Umwandlung der anfangs gepumpten Magnonen in eine zweite Gruppe frequenzentarteter Magnonen vorhergeht, welche aufgrund einer parametrisch stimulieren Streuung der anfänglichen Magnonen in den austauschdominierten Spektralbereich in Erscheinung tritt. Im Gegensatz zu der anfänglichen Magnonengruppe, deren Wellenvektoren senkrecht zu den Wellenvektoren der Magnonen im Energieminimum stehen, können die Magnonen der zweiten Magnonengruppe effektiv in Richtung des Energieminimum streuen und dort kondensieren.

4.1 Formation of Bose-Einstein magnon condensate via dipolar and exchange thermalization channels

D.A. Bozhko, P. Clausen, A.V. Chumak, B. Hillebrands, and A.A. Serga

In collaboration with Yu.V. Kobljanskyj, Faculty of Radiophysics, Electronics and Computer Systems, Taras Shevchenko National University of Kyiv, 01601 Kyiv, Ukraine

In terms of the second quantization, a spin-wave ensemble of a magnetic sample can be treated as a gas of weakly interacting quasi-particles called magnons. Magnons have an integer spin and, therefore, obey the Bose-Einstein statistics. In 1991 it was predicted that external injection of magnons can increase the chemical potential up to the bottom of the spin-wave spectrum [1]. This results in the Bose-Einstein magnon condensation: the spontaneous appearance of a coherent state at the global energy minima of the spin-wave spectrum (see Fig. 1). In 2006, the parametric pumping technique [2, 3] was successfully used for the experimental observation of the Bose-Einstein condensate (BEC) of magnons at room temperature [4]. This discovery has attracted much interest to the physics of the parametrically driven magnon gases [5–12]. In this Report we provide experimental insight into the evolution of a magnon gas affected by the four-magnon scattering process in the presence of an external pumping field of different magnitudes. We show that the magnons initially pumped to the low wavenumber region of the perpendicular spin-wave branch (magnon wavevector $\mathbf{q} \perp \mathbf{H}_0$) scatter into the lowest energy states located at the longitudinal branch ($\mathbf{q} \parallel \mathbf{H}_0$) passing through both dipolar and exchange parts of the spectrum.

The measurements were performed using a low-damping single-crystal Yttrium Iron Garnet (YIG) film by means of a combined microwave and Brillouin light scattering (BLS) setup schematically shown in Fig. 2. The in-plane magnetized YIG sample with lateral dimensions $2 \times 10\,\mathrm{mm}^2$ and $6.7\,\mu\mathrm{m}$ thickness was placed on top of a $50\,\mu\mathrm{m}$ wide microstrip resonator, which was used to induce the pumping Oersted field.

The resonator was driven by 100 ns long microwave pulses at a carrier frequency of $f_\mathrm{p} = 13.74\,\mathrm{GHz}$

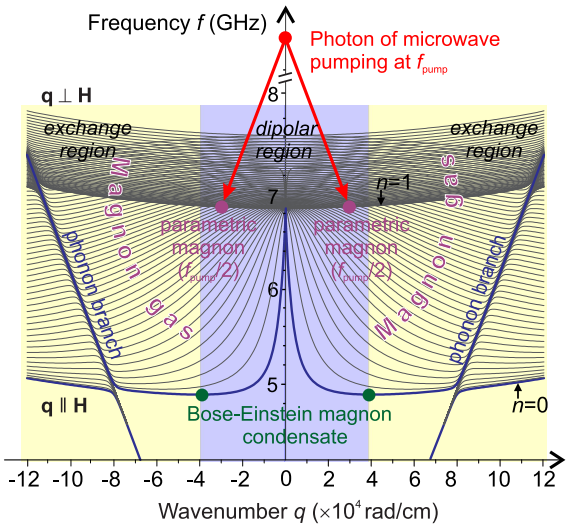

Fig. 1: The magnon spectrum calculated in dipole-exchange approximation for the first 47 thickness modes of an in-plane magnetized single crystal Yttrium Iron Garnet film of $6.7\,\mu\mathrm{m}$ thickness [13]. Parameters: external bias field $H_0 = 1735\,\mathrm{Oe}$, stiffness constant $\eta = 9.15 \cdot 10^{-2}\,\mathrm{cm}^2\,\mathrm{s}^{-1}$, saturation magnetization $4\pi M_\mathrm{s} = 1750\,\mathrm{G}$, total field of cubic crystallographic and uniaxial out of plane anisotropies $H_\mathrm{a} = -70\,\mathrm{Oe}$. Arrows indicate the magnon injection by parametric pumping. The initially pumped magnon group is marked by two dots. Dipolar and exchange spectral regions are greyed.

This work has been recently published in Low Temperature Physics/Fizika Nizkikh Temperatur **41**, 1024 (2015)

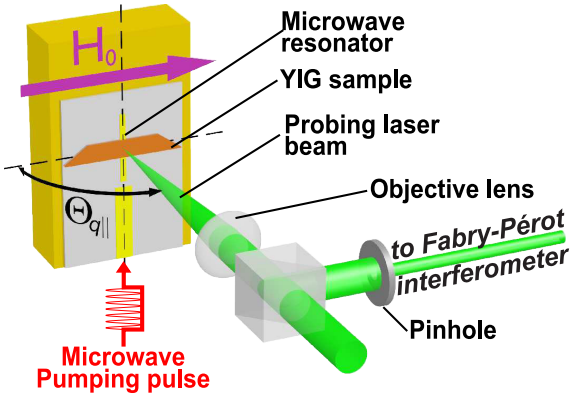

Fig. 2: Geometry of the experiment. The setup allows to vary the probing laser beam incidence angle $\Theta_{q\|}$ allowing for wavevector resolution. The YIG sample is placed on top of a microstrip resonator which is fabricated on top of an alumina substrate. Microwave pumping pulses are applied to the microstrip in order to drive the spin-wave system. The probing laser beam is directed through a beam splitter and focused by an objective lens onto the YIG sample. Inelastically scattered light is redirected to the Fabry-Pérot interferometer. An additional pinhole is used to increase the wavenumber resolution.

with peak powers P_p ranging from 1.25 W to 40 W. A pulse repetition time of 12.5 µs was chosen to give the system enough time to relax to the ground state and to prevent microwave-heating effects. The strength of the bias field $H_0 = 1735$ Oe has been chosen to allow for a pumping of the magnon pairs slightly above the FMR frequency.

The magnon dynamics was analyzed by means of time- and wavevector-resolved BLS spectroscopy [14]. The probing light beam of 532 nm wavelength and 32 mW power is generated by a single-mode solid-state laser. The wavevector resolution was $2 \cdot 10^3$ rad/cm (see Fig. 2). The frequency resolution of the BLS setup is 100 MHz.

Figure 3 shows a wavenumber-resolved BLS intensity maps of the time evolution of gaseous magnons with $\mathbf{q} \parallel \mathbf{H}_0$ within the frequency range from 4.7 GHz to 5.7 GHz, which includes the bottom of the magnon spectrum. The spectra are normalized to their maximum.

In the case of the highest pumping power $P_\mathrm{p} = 40$ W (see Fig. 3a), the first magnons appear at the bottom of the spin-wave spectrum already 30 ns after the pump pulse in the entire wavevector range of $(1/15) \cdot 10^4$ rad/cm. The center of the density distribution of the initially thermalized magnons lies in the *exchange* region of the spectrum at $7 \cdot 10^4$ rad/cm, which corresponds to the exchange thermalization channel (see Fig. 1). At the same time, the magnon density in a range of $(1/4) \cdot 10^4$ rad/cm, which corresponds to the dipolar spectral region (dipolar thermalization channel), is relatively weak (note the used logarithmic intensity scale). In the case of the lower microwave pumping power $P_\mathrm{p} = 10$ W shown in Fig. 3b, the first magnons appear after 50 ns delay time in the *dipolar* thermalization channel in the wavenumber range of $(1/5) \cdot 10^4$ rad/cm and only starting from 75 ns the exchange channel is populated (the corresponding thermalization channels are indicated with dashed guidelines for the eye in Fig. 3a–d). In Fig. 3c (pumping power $P_\mathrm{p} = 2.5$ W), the first magnons appear in the dipolar spectral region ($\sim 2 \cdot 10^4$ rad/cm). In Fig. 3d the pumping power is decreased to $P_\mathrm{p} = 1.25$ W. In this case two distinct areas of thermalization, which are separated by the energy minimum at a wavevector of $4 \cdot 10^4$ rad/cm, can be well recognized. The observed dynamics can be summarized as follows: the time of magnons appearance at the dipolar thermalization channel practically does not depend on the applied microwave power. Thermalized magnons appear in the exchange spectral area with a delay that strongly depends on the pumping power. This delay shortens with increasing pumped magnons density.

The explanation of the observed thermalization behavior is as follows. As it was already mentioned, the strength of the external magnetic field H_0 was chosen in such a way that in the case of the highest pump power the parametric magnons were injected into the exchange spectral area just above the FMR frequency (see Fig. 1). It is necessary to note that in this case the spin-wave spectrum is already shifted to lower frequencies by a huge amount of the injected magnons re-

ducing the magnetization of the sample. For a small quantity of the pumped magnons this shift is less pronounced and the spectral position of the magnon injection is located at or even below the FMR frequency. As a result, at the beginning of the pumping process, the parametric magnons are injected into the long-wavelength dipolar area [16] in all experimental cases presented in Fig. 3. This explains why in Fig. 3a–d the dipolar thermalization area always gets populated in the same way – as the magnon density increases during the action of the pumping pulse, the spectrum shifts down and the pumping point moves to the exchange area of the spectrum. As a result no more magnons are injected into the dipolar area. Thus, the resulting population of this thermalization channel does not change significantly with the increase in the pumping power from $P_\mathrm{p} = 2.5\,\mathrm{W}$ to $40\,\mathrm{W}$.

Another situation occurs in the exchange thermalization region. With increase of the pumping power, the magnon density increases faster, so this region starts to be populated earlier. Moreover, since the magnon number increases during the pumping process, the injection point continuously shifts towards the higher wavevectors. This leads to a spreading of thermalized magnons in the phase space (see exchange areas in Fig. 3a–c), and thus enhances the efficiency of the magnon gas thermalization. In addition, as it is shown in Ref. [17] (see also Report 4.3), at high pumping powers a second group of short-wavelength magnons excited at half of the pumping frequency significantly increases the population of the exchange thermalization channel.

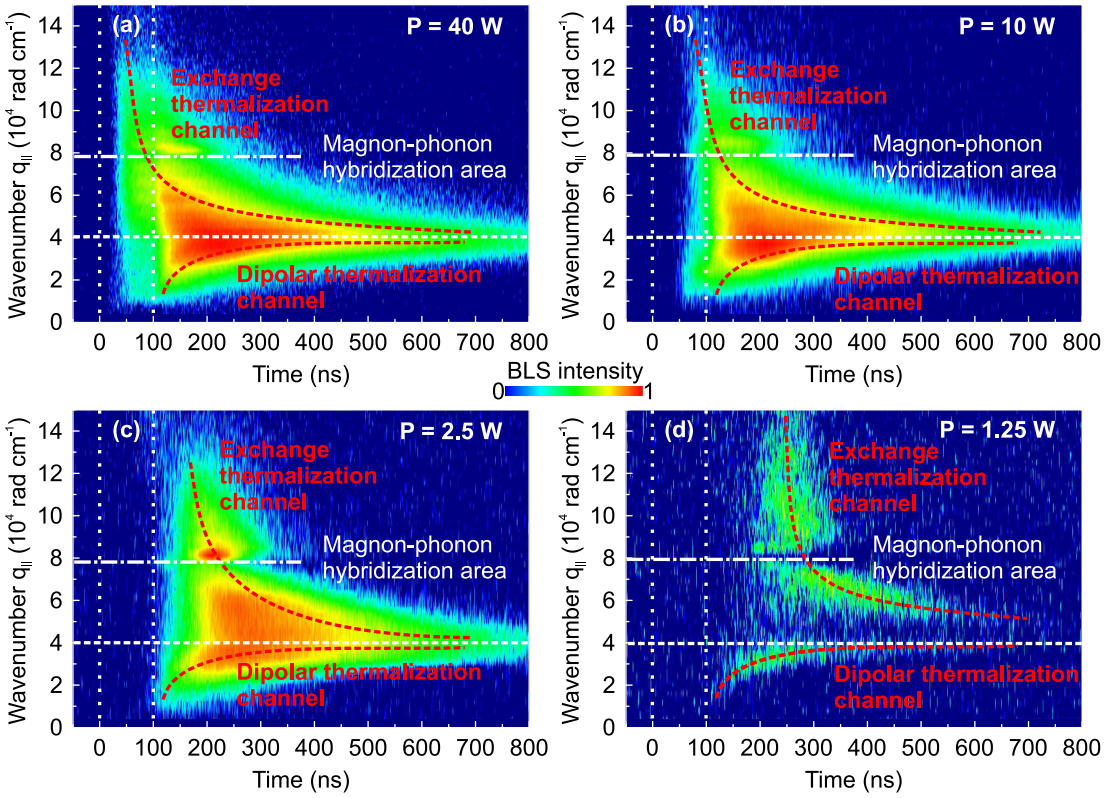

Fig. 3: Dependence of the density of thermalized magnons near the bottom of the spin-wave spectrum on the pumping power P_p for (a) $P_\mathrm{p} = 40\,\mathrm{W}$, (b) $P_\mathrm{p} = 10\,\mathrm{W}$, (c) $P_\mathrm{p} = 2.5\,\mathrm{W}$, (d) $P_\mathrm{p} = 1.25\,\mathrm{W}$. Vertical dotted lines mark the moments when the microwave pumping pulse was switched on and off. Dashed horizontal lines indicate the position of the global energy minima at $|\mathbf{q}| = 4 \cdot 10^4\,\mathrm{rad/cm}$ in the spin-wave spectrum. Dashed curves in panels (a)–(d) schematically show the time dependent transition paths of dipolar and exchange thermalized magnons to the bottom of the spin-wave spectrum. Dashed-dotted lines indicate the magnon-phonon hybridization area (see also Fig. 1).

In conclusion, we investigated the thermalization of the parametrically driven magnon gas and subsequent magnon Bose-Einstein formation in phase space. Our experimental findings suggest two channels of the thermalization process, which pass through dipolar and exchange areas of the spin-wave spectrum. During the pumping process, the increasing magnon density causes a shift of the spectrum due to the change in the saturation magnetization. This effect leads to corresponding shift towards higher wavevectors in the position of parametrically injected magnon pairs. It has been found that the dipolar thermalization channel doesn't change its qualitative behavior with increase of the pumping power. At the same time, the exchange channel becomes dominating at high pumping powers.

Financial support by the DFG within the SFB/TR49 and by the Graduate School Materials Science in Mainz is gratefully acknowledged.

References

[1] Yu.D. Kalafati, V.L. Safonov, *Theory of quasiequilibrium effects in a system of magnons excited by incoherent pumping*, Sov. Phys. JETP 73, 836 (1991).

[2] E. Schlömann, J.J. Green, U. Milano, *Recent developments in ferromagnetic resonance at high powerlevels*, J. Appl. Phys. **31**, 386S (1960).

[3] S.M. Rezende, F.M. de Aguiar, *Spin-wave instabilities, auto-oscillations, and chaos in yttrium-iron-garnet*, IEEE Proc. **78**, 6 (1990).

[4] S.O. Demokritov, V.E. Demidov, O. Dzyapko, G.A. Melkov, A.A. Serga, B. Hillebrands, A.N. Slavin, *Bose-Einstein condensation of quasi-equilibrium magnons at room temperature under pumping*, Nature **443**, 430 (2006).

[5] A.I. Bugrij, V.M. Loktev, *On the theory of Bose-Einstein condensation of quasiparticles: On the possibility of condensation of ferromagnons at high temperatures*, Low Temp. Phys. **33**, 37 (2007).

[6] S.M. Rezende, *Theory of coherence in Bose-Einstein condensation phenomena in a microwave-driven interacting magnon gas*, Phys. Rev. B **79**, 174411 (2009).

[7] V.E. Demidov, O. Dzyapko, S.O. Demokritov, G.A. Melkov, A.N. Slavin, *Thermalization of a parametrically driven magnon gas leading to Bose-Einstein condensation*, Phys. Rev. Lett. **99**, 037205 (2007).

[8] V.E. Demidov, O. Dzyapko, M. Buchmeier, T. Stockhoff, G. Schmitz, G.A. Melkov, S.O. Demokritov, *Magnon kinetics and Bose-Einstein condensation studied in phase space*, Phys. Rev. Lett. **101**, 257201 (2008).

[9] V. Demidov, O. Dzyapko, S. Demokritov, G. Melkov, A. Slavin, *Observation of spontaneous coherence in Bose-Einstein condensate of magnons*, Phys. Rev. Lett. **100**, 047205 (2008).

[10] A. Chumak, G. Melkov, V. Demidov, O. Dzyapko, V. Safonov, S. Demokritov, *Bose-Einstein condensation of magnons under incoherent pumping*, Phys. Rev. Lett. **102**, 187205 (2009).

[11] A.A. Serga, V.S. Tiberkevich, C.W. Sandweg, V.I. Vasyuchka, D.A. Bozhko, A.V. Chumak, T. Neumann, B. Obry, G.A. Melkov, A.N. Slavin, B. Hillebrands, *Bose-Einstein condensation in an ultra-hot gas of pumped magnons*, Nat. Commun. **5**, 4452 (2014).

[12] J. Hick, T. Kloss, P. Kopietz, *Thermalization of magnons in yttrium-iron garnet: Nonequilibrium functional renormalization group approach*, Phys. Rev. B **86**, 184417 (2012).

[13] B.A. Kalinikos, A.N. Slavin, *Theory of dipole-exchange spin wave spectrum for ferromagnetic films with mixed exchange boundary conditions*, J. Phys. C: Solid State Phys. **19**, 7013 (1986).

[14] C.W. Sandweg, M.B. Jungfleisch, V.I. Vasyucka, A.A. Serga, P. Clausen, H. Schultheiss, B. Hillebrands, A. Kreisel, P. Kopietz, *Wide-range wavevector selectivity of magnon gases in Brillouin light scattering spectroscopy*, Rev. Sci. Instrum. **81**, 073902 (2010).

[15] G.A. Melkov, V.L. Safonov, A.Y. Taranenko, S.V. Sholom, *Kinetic instability and bose condensation of nonequilibrium magnons*, J. Magn. Magn. Mater. **132**, 180 (1994).

[16] T. Neumann, A.A. Serga, V.I. Vasyuchka, B. Hillebrands, *Field-induced transition from parallel to perpendicular parametric pumping for a microstrip transducer*, Appl. Phys. Lett. **94**, 192502 (2009).

[17] P. Clausen, D.A. Bozhko, V.I. Vasyuchka, G.A. Melkov, B. Hillebrands, A.A. Serga, *Stimulated thermalization of a parametrically driven magnon gas as a prerequisite for Bose-Einstein magnon condensation*, Phys. Rev. B **91**, 220402(R) (2015).

4.2 Magnon supercurrent in a magnon Bose-Einstein condensate subject to a thermal gradient

P. Clausen, D.A. Bozhko, V.I. Vasyuchka, B. Hillebrands, and A.A. Serga

In collaboration with G.A. Melkov, Faculty of Radiophysics, Electronics and Computer System, Taras Shevchenko National University of Kyiv, 01601 Kyiv, Ukraine

Bose-Einstein condensation can be achieved either by decreasing the temperature of a boson gas or by increasing its density. The latter method is especially applicable to gases of weakly interacting quasi-particles like magnons, whose number can be effectively controlled by external electromagnetic pumping [1]. When a spin system is pumped, and when the injected magnons thermalize through scattering processes conserving both their number and the total energy, a Bose-Einstein condensate (BEC) may be formed at the lowest energy state of the energy-momentum spectrum. As the magnon BEC is localized in the global energy minimum, its group velocity is exactly zero and no energy transfer is associated with the magnon condensate. However, such a transfer is still possible due to the excitation of a magnon supercurrent [2–4], which can be driven by a gradient in the phase of the wavefunction of the magnon BEC. Here we provide experimental insight into the evolution of a magnon BEC in a thermal gradient generated by local laser heating, and we show that its transitional behavior can be understood using the concept of a magnon supercurrent.

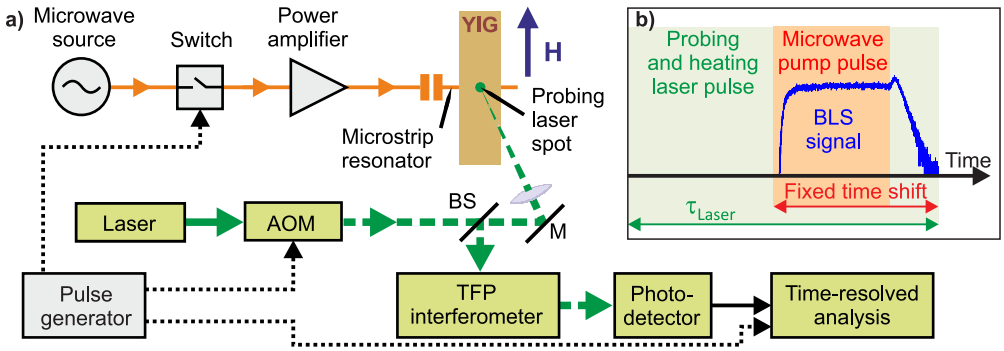

Fig. 1: a) Schematic illustration of the experimental setup. In the upper part of the figure the microwave circuit consisting of a microwave source, a switch and an amplifier is shown. This circuit drives a microstrip resonator, which is placed below the in-plane magnetized YIG film. The light from a solid-state laser is chopped by an acousto-optic modulator and guided through a beam splitter (BS) and a mirror (M) to the YIG film. There it scatters inelastically on magnons, and the frequency shifted component of the scattered light is selected by the tandem Fabry-Pérot (TFP) interferometer, detected, and analyzed in time. The time diagram b) presents relative time positions of the applied microwave pump pulse, the laser pulse, and the detected BLS signal.

We study the temporal evolution of a magnon BEC in a single-crystal yttrium iron garnet (YIG, $Y_3Fe_5O_{12}$) film by time-resolved Brillouin Light Scattering (BLS) spectroscopy [5]. The experimental setup, which consists of a YIG film, a microwave circuit, and a BLS system is schematically shown in Fig. 1a. The in-plane magnetized YIG sample is 5.6 µm thick, 5 mm long and 1 mm wide. The microwave pumping circuit consists of a microwave source, a switch and an amplifier. This circuit drives a 50 µm wide microstrip resonator, which is placed below the YIG film and tuned to

the pumping frequency of $f_p = 13.06\,\text{GHz}$. Magnons are injected into the YIG sample via parallel parametric pumping at a frequency of $f_p/2$. The strength of the bias field $\mu_0 H = 169.0\,\text{mT}$ is chosen to allow for magnon injection at the ferromagnetic resonance frequency (FMR), where the parallel pumping achieves its highest efficiency [6].

In our experiment, a focused laser beam combines the role of the magnon probe in the BLS experiment with the role of the local sample heater. The heating time is adjusted by chopping the probing laser beam using an acousto-optic modulator (AOM). The laser pulse duration τ_{Laser} is varied between 6 µs to 80 µs with a repetition time of 1 ms, allowing both for magnetic and temperature equilibration of the YIG film. The modulated probing beam is focused onto the surface of the YIG film sample in the middle of the microstrip resonator, where it has a maximal peak power of 9.5 mW. The radius r of the focal point is about 10 µm.

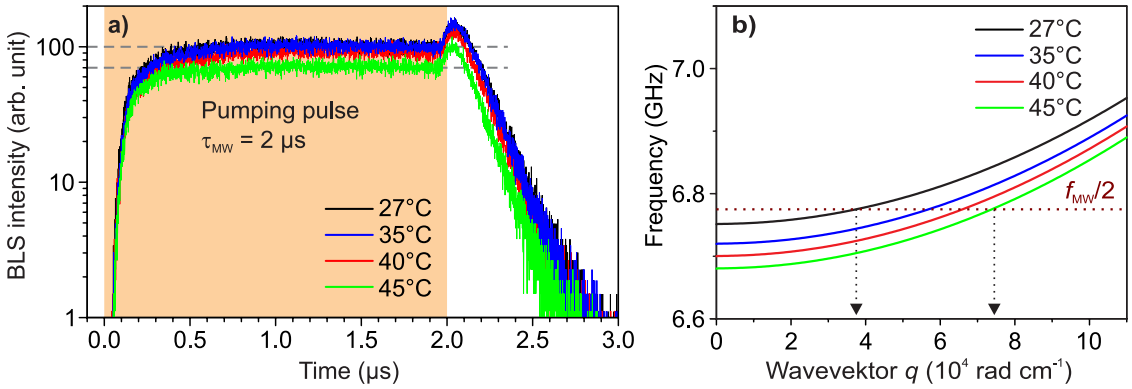

Fig. 2: Temperature dependent temporal dynamics of the magnon BEC. Panel a) shows the time-resolved Brillouin light scattering intensity for different uniform temperatures of the YIG film. The influence of the temperature on the spin-wave dispersion is shown in b).

In order to understand the temperature influenced magnon BEC dynamics one first needs to separate the effects caused by the spatially uniform change of a sample temperature from those caused by the formation of a temperature gradient. Therefore, in the first experiment we combined a low-power BLS probing light beam with an uniform air heating of the YIG film. Figure 2a shows the typical dynamics of the magnon BEC in this case. In course of the pump action, the magnon density, which is proportional to the intensity of the BLS signal, increases and saturates. After the parametric pumping is switched off, the magnon density jumps up due to the efficient BEC formation intensified by the evaporative cooling of the freely evolving magnon gas [7]. Afterwards the magnon density exponentially decreases due to conventional spin-wave relaxation. This behavior is the same for all temperatures in our experiment. Some decrease in the steady-state magnon density at higher temperatures is related to the lower efficiency of the parametric pumping. Due to a lowered saturation magnetization at higher temperatures the spectral branch of parametrically excited magnons shifts towards lower frequencies, see Fig. 2b. This shift increases the wavenumber of the injected magnons and, consequently, the threshold power of the parametric generation [6].

Now we focus on the temperature gradient dependent behaviour of the magnon condensate. Figure 3a shows the evolution of the magnon density at the bottom of the spin-wave spectrum for four different heating times, i.e. for four values of the temperature gradient, at a laser power of $P_{\text{Laser}} = 9.5\,\text{mW}$. For comparison, the black curve presents the time-dependent magnon dynamics measured using a much lower laser power of 0.4 mW. Similar to Fig. 2a, due to the pronounced

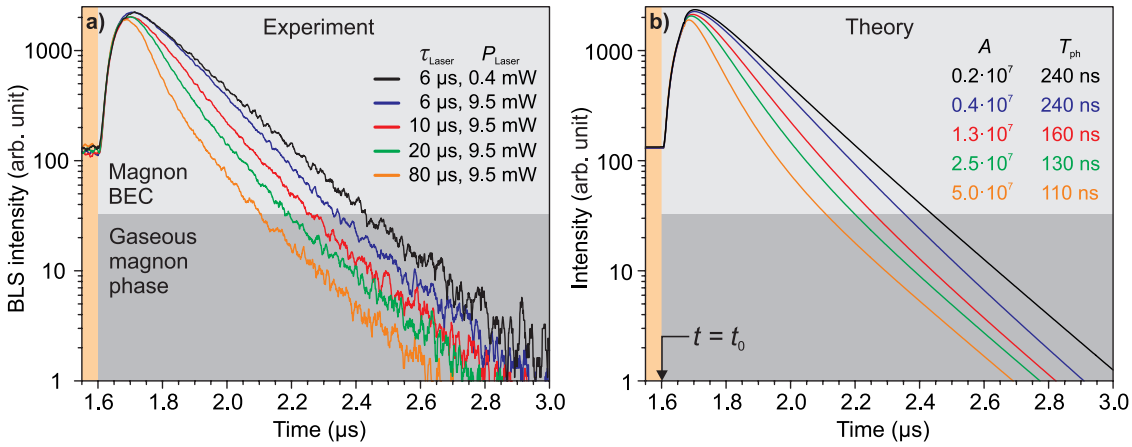

Fig. 3: a) Temporal dynamics of the magnon BEC under local laser heating. The increase of the laser pulse duration, and thus the heating time, leads to a faster relaxation of the BEC phase. The relaxation time of the residual gaseous magnons is independent of the heating. b) Calculations are done in accordance with Eq. 1.

BEC formation the magnon density rises sharply after the microwave pumping pulse is switched off [7]. Afterwards, the magnon density decreases. In the case of the low-power laser probing this decrease has an exponential form with a characteristic decay time τ of 240 ns, which corresponds well to the conventional values of a linear magnetic damping in YIG films [8].

At higher laser power the observed decrease in the magnon density cannot be described by one single exponential function anymore. Two different regimes of the magnon decay are clearly visible from the slopes of the BLS waveforms presented in Fig. 3a. These regimes are marked by the light gray and dark gray backgrounds. In the first regime, at high BLS intensities, the decay of the magnon density depends on the heating duration, i.e. on the temperature gradient in the laser focal point. In the second regime, at low BLS intensities, this decay is temperature independent and its rate coincides with the one observed in the low-laser-power experiment. It is remarkable that for all heating durations the transition between these two decay regimes occurs at approximately the same magnon density level, which can be associated with the transition from the condensed to the gaseous magnon phase.

We interpret these findings as follows. The magnon BEC is a spontaneously established coherent ground state, which possesses well defined frequency, wavevector, and phase [9]. The laser heating locally changes the saturation magnetization and, thus, induces a weak frequency shift $\Delta\omega$ between different parts of the magnon condensate. In the course of time this frequency shift results in an increasing phase gradient in the magnon BEC. As a result, a phase-gradient-induced magnon current or, in other words, a magnon supercurrent, flowing out of the hot region of the focal point, is excited. This efflux reduces the density of the magnon BEC in the probing point. After some time, the decrease in the magnon density results in the disappearance of the condensate, and thus in the disappearance of the supercurrent. Consequently, this leads to the restoration of the conventional relaxation dynamics associated with a residual incoherent magnon phase.

The magnon efflux can be written as $\Phi = 2n_c v_{sc}/r$, where n_c is the magnon BEC density, $v_{sc}(\Delta\phi) = \hbar\Delta\phi/m$ is the velocity of the phase-induced magnon flow, $r = S/V$ is the radius of the heated cylindrical volume V inside of the YIG film and S is the lateral area of this volume. $\hbar$ and $m = \hbar/2\eta$ are the Planck constant and the effective magnon mass, respectively. η is the exchange stiffness constant. The phase difference $\Delta\phi = \Delta\omega \cdot (t - t_0)/r$ increases along the time interval $t - t_0$ after the pump action is stopped at the moment of time t_0, see Fig. 3b.

The supercurrent influenced BEC dynamics can be described by a rate equation, which has already been used in Ref. [7] to explain the upward jump in the BEC density n_c after the end of the pump pulse, if we include an additional decay term associated with the efflux $\Phi = A(t-t_0)$:

$$\frac{1}{\Gamma}\frac{dn_c}{dt} = -\lambda n_{in} - n_c \cdot \left[1 - A\Theta(t_0)(t-t_0)e^{-\frac{t-t_0}{T_{ph}}}\right] + n_g^3 \quad . \tag{1}$$

The temperature gradient dependent parameter A is given by the equation $A = (2\hbar\Delta\omega)/(m\Gamma r^2)$. The relaxation frequency Γ corresponds to the conventional magnon decay, parameter λ defines the influence of the inflow of parametric magnons n_{in} on the BEC formation, $\Theta(t_0)$ is the Heaviside function, and n_g is the gaseous magnon density. The time-dependent exponential function in the new decay term contains a phase relaxation time T_{ph} and, thus, takes into account the loss in the coherency of the magnon BEC related to its finite lifetime. The value of T_{ph} is comparable with Γ and must decrease with increase of the sample temperature.

One can see from Fig. 3b that the theoretical curves, which are calculated in accordance with the proposed model, coincide with the experimental data (see Fig. 3a) very well. As it is expected, the parameter A increases and the time T_{ph} decreases with increase in the laser power and the heating duration. Thus, the reported results provide further experimental and theoretical evidence of a magnon supercurrent at room temperature.

Financial support from the Deutsche Forschungsgemeinschaft within the SFB/TR 49 and from the State Fund for Fundamental Research of Ukraine (SFFR) is gratefully acknowledged. D.B. is supported by a fellowship of the Graduate School Material Sciences in Mainz (MAINZ) through DFG funding of the Excellence Initiative (GSC-266).

References

[1] S.O. Demokritov, V.E. Demidov, O. Dzyapko, G.A. Melkov, A.A. Serga, B. Hillebrands, A.N. Slavin, *Bose-Einstein condensation of quasi-equilibrium magnons at room temperature under pumping*, Nature **443**, 430 (2006).

[2] A.S. Borovik-Romanov, Yu.M. Bun'kov, V.V. Dmitriev, Yu.M. Mukharskiy, *Long-lived induction signal in superfluid ^{3}He-B*, JETP Letters **40**, 1033 (1984).

[3] A.S. Borovik-Romanov, Yu.M. Bun'kov, A. de Vaard, V.V. Dmitriev, V. Makrotsieva, Yu.M. Mukharskiy, D.A. Sergatskov, *Observation of a spin-current analog of the Josephson effect*, JETP Letters **47**, 400 (1988).

[4] K. Nakata, K.A. van Hoogdalem, P. Simon, D. Loss, *Josephson and persistent spin currents in Bose-Einstein condensates of magnons*, Phys. Rev. B **90**, 144419 (2014).

[5] O. Büttner, M. Bauer, S. Demokritov, B. Hillebrands, Y. Kivshar, V. Grimalsky, Y. Rapoport, A.N. Slavin, *Linear and nonlinear diffraction of dipolar spin waves in yttrium iron garnet films observed by space- and time-resolved Brillouin light scattering*, Phys. Rev. B **61**, 576 (2000).

[6] A.A. Serga, C.W. Sandweg, V.I. Vasyuchka, M.B. Jungfleisch, B. Hillebrands, A. Kreisel, P. Kopietz, M.P. Kostylev, *Brillouin light scattering spectroscopy of parametrically excited dipole-exchange magnons*, Phys. Rev. B **86**, 134403 (2012).

[7] A.A. Serga, V.S. Tiberkevich, C.W. Sandweg, V.I. Vasyuchka, D.A. Bozhko, A.V. Chumak, T. Neumann, B. Obry, G.A. Melkov, A.N. Slavin, B. Hillebrands, *Bose-Einstein condensation in an ultra-hot gas of pumped magnons*, Nat. Commun. **5**, 3452 (2014).

[8] V. Cherepanov, I. Kolokolov, V. L'vov, *The saga of YIG: spectra, thermodynamics, interaction and relaxation of magnons in a complex magnet*, Phys. Rep. – Rev. Sec. Phys. Lett. **229**, 81 (1993).

[9] P. Nowik-Boltyk, O. Dzyapko, V.E. Demidov, N.G. Berloff, S.O. Demokritov, *Spatially non-uniform ground state and quantized vortices in a two-component Bose-Einstein condensate of magnons*, Sci. Rep. **2**, 482 (2012).

4.3 Stimulated thermalization of a parametrically driven magnon gas as a prerequisite for Bose-Einstein magnon condensation

P. Clausen, D.A. Bozhko, V.I. Vasyuchka, B. Hillebrands, and A.A. Serga

In collaboration with G.A. Melkov, Faculty of Radiophysics, Electronics and Computer Systems, Taras Shevchenko National University of Kyiv, 01601 Kyiv, Ukraine

Here, we provide experimental insight into the evolution of a magnon gas affected by four-magnon scattering in the presence of an external pumping field. We claim that the magnons initially pumped to the transversal branch of the spin-wave spectrum (magnon wavevector $\mathbf{q} \perp \mathbf{H}$) do not scatter into the lowest energy states located at the longitudinal branch ($\mathbf{q} \parallel \mathbf{H}$). Instead, the formation of a Bose-Einstein condensate (BEC) [1] at the bottom of the spin-wave spectrum is associated with the parametric excitation of a second group of short-wavelength magnons propagating at an angle $\angle(\mathbf{q},\mathbf{H}) < 90°$. Simultaneously, the initially excited transversal magnon group is suppressed to the near thermal level by a mutual action of the second magnon group and the external pumping field.

The measurements were performed using a low-damping ferrimagnetic film of yttrium iron garnet (YIG, $Y_3Fe_5O_{12}$) by means of a combined microwave and Brillouin light scattering (BLS) setup schematically shown in Fig. 1a. The in-plane magnetized YIG-film sample of 6.7 µm thickness with dimensions $2 \times 10\,\mathrm{mm}^2$ was placed on top of a 50 µm wide microstrip resonator, which was used to induce the pumping Oersted field $\mathbf{h}(t)$. The resonator was driven by microwave pulses at a carrier frequency of $f_\mathrm{p} = \omega_\mathrm{p}/2\pi = 13.74\,\mathrm{GHz}$ with peak power P_p ranging from 1 mW to 4 W. The duration of the pump pulses was chosen to 100 ns. A pulse repetition time of 5 µs was sufficiently long to ensure the relaxation of the magnon system to the ground state after each pumping event and to exclude microwave-heating effects.

In course of the parallel pumping process the photons of the microwave pumping field split into magnon pairs with opposite wavevectors at half of the pumping frequency as illustrated in Fig. 1b. The strength of the bias field $\mu_0 H = 173.5\,\mathrm{mT}$ has been chosen to allow for a pumping of the magnon pairs slightly above the ferromagnetic resonance frequency (FMR). In this case, the parallel pumping process achieves its highest efficiency because the magnons are pumped to the transversal spectral branch, which has the lowest threshold of the parametric instability [2].

It looks obvious that with increase in the pumping power P_p the number of parametric magnons must grow. However, as it was reported by us in the previous Annual Report [3], the increase of P_p above 10 mW leads to a decrease in the observed magnon density. Moreover, at pumping levels that are sufficient for the formation of the magnon BEC the parametric magnons are practically non-detectable. The conventional four-magnon scattering processes cannot be assumed as a reason for the observed disappearance of the parametrically pumped magnon group. During the action of the external pumping this nonlinear mechanism can only limit but not reduce the number of the parametric magnons: the decrease in their density would lead to the consequent decrease of the scattering efficiency and, thus, to a density saturation.

The phenomenon can be understood if one takes into account the role of the external pumping field in the four-magnon scattering process and the possible excitation of a few groups of parametric

This work has been recently published in Phys. Rev. B [7]

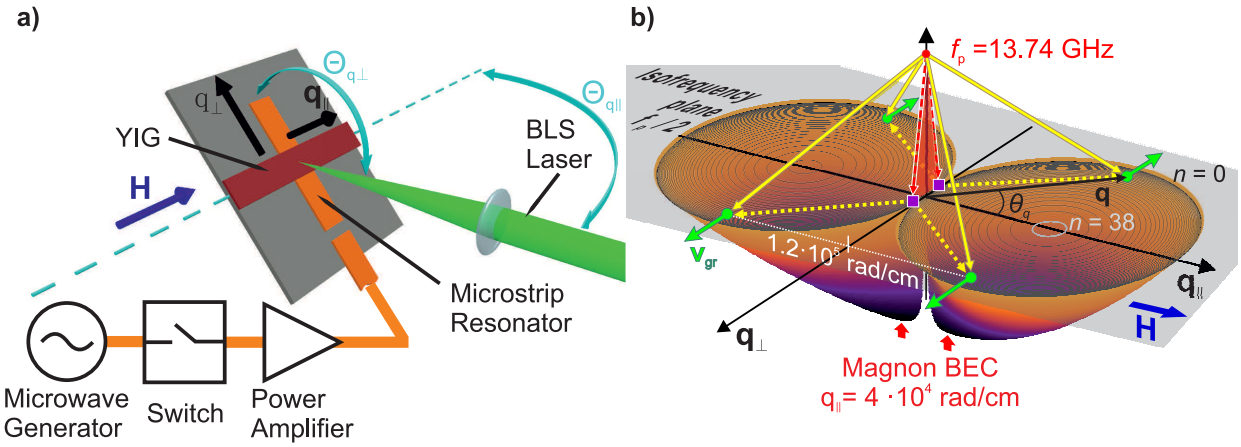

Fig. 1: a) Sketch of the experimental setup. $\mathbf{H}$ is a bias magnetic field. $\mathbf{q}_\parallel$ and $\mathbf{q}_\perp$ are in-plane wavevectors of the transversal ($\mathbf{q} \perp \mathbf{H}$) and longitudinal ($\mathbf{q} \parallel \mathbf{H}$) magnons. The setup is tiltable by the angles $\Theta_{q\perp}$ and $\Theta_{q\parallel}$ allowing for wavevector resolution. b) The magnon spectrum calculated for the first 38 thickness modes n [4]. The shadowed area between the dashed arrows illustrates the magnon injection by parametric pumping. The initially pumped magnon group is marked by two squares. The second magnon group is shown by four dots and the arrows indicate the group velocities of the secondary magnons. The long arrows outline the parametrically stimulated magnon scattering.

magnons *well separated in phase space*. For example, after the excitation of two magnon groups the total pumping process will consist of three components: the action of the external pumping field and the reactions of the first and the second groups. This can lead to the *suppression* of the first group of parametric magnons.

In order to verify the proposed model, we performed an experiment on detection of the second magnon group using the time- and angle-resolving BLS setup [5, 6] shown in Fig. 1a with a time resolution of 1 ns. A probing laser beam with a power of 5 mW and a wavelength of 532 nm was focused to a focal spot with a diameter of 50 µm in the middle of the microstrip resonator. The wavevector selection was realized by changing the angles $\Theta_{q\perp}$ and $\Theta_{q\parallel}$ between the sample and the incident light beam. It allowed us to increase the detectable wavenumber range up to $15 \cdot 10^4$ rad/cm for both transversal and longitudinal magnons. The wavevector resolution was set to $2 \cdot 10^3$ rad/cm by a pinhole in the path to the interferometer.

Figure 2a shows the color-coded BLS intensity map measured in time and wavevector space in the frequency range from 6.5 GHz to 7.5 GHz for magnons with $\mathbf{q} \perp \mathbf{H}$. The two dashed lines indicate the 100 ns long microwave pumping pulse. The parametrically injected magnons with a frequency of $f_\mathrm{p}/2$ appear first at wavenumbers in the range from $1.5 \cdot 10^4$ rad/cm to $3 \cdot 10^4$ rad/cm. Such a broad excitation range is due to the flatness of the perpendicular magnon branch near the FMR frequency. In the course of the approximately next 5 ns, some of the injected magnons redistribute towards smaller and higher wavenumbers. The short scattering time is a consequence of the high rate of magnon-scattering processes due to the high population of the first magnon group. The BLS signal from the parametrically injected magnons rapidly decreases and, approximately 20 ns after the start of the pumping pulse, the first magnon group is completely vanished. At the same time, a weak BLS signal, which appears at wavenumbers between $11.0 \cdot 10^4$ rad/cm and $13.5 \cdot 10^4$ rad/cm and which is visible up to the end of the pump pulse, clearly provides evidence for the excitation of the second magnon group. It is noteworthy that the dynamics of the magnon groups c_1 and c_2 in Fig. 2d, which was numerically calculated in Ref. [7], qualitatively corresponds to the experimental time-dependent profiles of magnon densities shown in Fig. 2c.

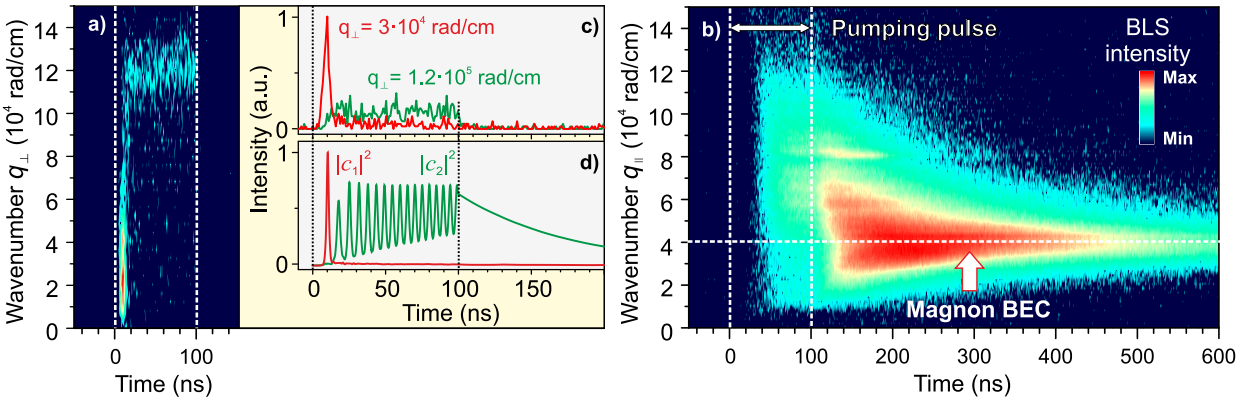

Fig. 2: Logarithmic BLS intensity maps of a) parametrically injected magnons ($\mathbf{q} \perp \mathbf{H}$) at $f_p/2$ and b) the magnon gas ($\mathbf{q} \parallel \mathbf{H}$) at the bottom of the spin-wave spectrum. c) Change in the density of the first and the second magnon groups extracted from the intensity map in panel a) for the given wavenumbers $q_\perp$. d) Calculated time-dependent variations in the densities $|c_1|^2$ and $|c_2|^2$ of the first and the secondary groups of parametric magnons [7]. The long decay tail of the second magnon group c_2 is due to neglecting the nonlinear decay caused by the conventional four-magnon scattering processes. The intensity oscillations are caused by a periodic dephasing between this magnon group and the total pumping field.

Figure 2b represents a wavenumber-resolved BLS intensity map of magnons with $\mathbf{q} \parallel \mathbf{H}$ within the frequency range from 4.7 GHz to 5.7 GHz, which includes the bottom of the magnon spectrum. One can see that the first thermalized magnons appear already 30 ns after the rising flank of the pumping pulse. However, during the pump pulse the formation of the magnon BEC is prevented by the extremely high effective temperature of the parametrically driven magnon gas [8]. After the end of the pumping, the magnon temperature rapidly decreases due to the evaporative supercooling process [8] and magnons form the Bose-Einstein condensate in the global energy minimum at $4 \cdot 10^4$ rad/cm (see Fig. 1b). By comparing Fig. 2a and Fig. 2b one can see that the appearance of thermalized magnons at the bottom of the spin-wave spectrum correlates with the excitation of the second group of parametric magnons with a wavevector component $q_\perp$ beyond $11 \cdot 10^4$ rad/cm.

This correlation can be understood from the momentum conservation law. It is obvious that no magnon-magnon scattering process within the initially excited transversal magnon group is able to turn the magnon wavevector from $\mathbf{q} \perp \mathbf{H}$ to $\mathbf{q} \parallel \mathbf{H}$ orientation. At the same time, such wavevector conversion can easily occur if the second magnon group possesses a sufficiently large wavevector component along $\mathbf{H}$.

It is hard to predict the exact value of the polar angle $\theta_2 = \angle(\mathbf{q}, \mathbf{H})$ of the second group as no general solution of this problem exists for a magnetic film of finite thickness. However, it is expected that this angle significantly differs from 90°. For example, in an unbounded medium the secondary wave group could be excited under the angle $\theta_2 \simeq 50°$ [9]. The situation is even more complicated for a spatially localized pumping realized as in our case by the narrow microstrip resonator: because excited waves can leak from the pumping area their losses strongly depend on their group velocities $\mathbf{v}_{gr}$. The first magnon group with $\theta_1 = 90°$ propagates along the microstrip resonator and, thus, does not suffer any radiation losses. Practically all other magnons with $\theta_q \neq 90°$ can easily leak out of the 50 µm wide pumping area and their excitation thresholds rise up significantly [10]. However, there are magnons with $\theta_q \neq 90°$ whose group velocities are still directed along the microstrip resonator. Four of such spectral positions ($n = 12$, $\theta_q = 35°$, $q = 21.6 \cdot 10^4$ rad/cm, $q_\perp = \pm 12 \cdot 10^4$ rad/cm) forming the second magnon group are marked by the green dots on the isofrequency plane $f_p/2$ in Fig. 1b. As a result, the stimulated scattering

brakes the orthogonality between the first magnon group ($\theta_q = 90°$) and magnons from the bottom of the spin-wave spectrum ($\theta_q = 0$), and thus creates the prerequisites for Bose-Einstein condensation. Our evaluation shows that the second magnon group can further scatter by the conventional four-magnon scattering mechanism between the neighboring modes while conserving energy and momentum. Such intermodal scattering processes are allowed down to the minimum of the first $n = 0$ mode where the BEC is formed at $q_{\parallel} = 4 \cdot 10^4\,\mathrm{rad/cm}$ (and $\theta_q = 0$) as shown in Fig. 1b.

In conclusion, our experimental findings suggest distinctly different phases of the thermalization process of a parametrically driven magnon gas: First, energy degenerated, parametrically magnons are generated, which, secondly, scatter in a multistage magnon transfer process to the bottom of the magnon spectrum. Thus, the parametrically stimulated magnon thermalization is assumed to be the essential precondition for the formation of the magnon Bose-Einstein condensate.

We thank T. Brächer for fruitful discussions. Financial support from the Deutsche Forschungsgemeinschaft within the SFB/TR 49 and from the State Fund for Fundamental Research of Ukraine (SFFR) is gratefully acknowledged. D.B. was supported by a fellowship of the Graduate School Material Sciences in Mainz (MAINZ) through DFG funding of the Excellence Initiative (GSC-266).

References

[1] S.O. Demokritov, V.E. Demidov, O. Dzyapko, G.A. Melkov, A.A. Serga, B. Hillebrands, A.N. Slavin, *Bose-Einstein condensation of quasi-equilibrium magnons at room temperature under pumping*, Nature **443**, 430 (2006).

[2] A.A. Serga, C.W. Sandweg, V.I. Vasyuchka, M.B. Jungfleisch, B. Hillebrands, A. Kreisel, P. Kopietz, M.P. Kostylev, *Brillouin light scattering spectroscopy of parametrically excited dipole-exchange magnons*, Phys. Rev. B **86**, 134403 (2012).

[3] P. Clausen, D.A. Bozhko, V.I. Vasyuchka, B. Hillebrands, A.A. Serga, *Stimulated thermalization of a parametrically driven magnon gas and Bose-Einstein condensation of dipole-exchange magnons*, Annual Report 2014: http://www.physik.uni-kl.de/hillebrands/publications/annual-reports/annual-report-2014.

[4] B.A. Kalinikos, A.N. Slavin, *Theory of dipole-exchange spin wave spectrum for ferromagnetic films with mixed exchange boundary conditions*, J. Phys. C: Solid State Phys. **19**, 7013 (1986).

[5] O. Büttner, M. Bauer, S.O. Demokritov, B. Hillebrands, Yu.S. Kivshar, V. Grimalsky, Yu. Rapoport, A.N. Slavin, *Linear and nonlinear diffraction of dipolar spin waves in yttrium iron garnet films observed by space- and time-resolved Brillouin light scattering*, Phys. Rev. B **61**, 11576 (2000).

[6] C.W. Sandweg, M.B. Jungfleisch, V.I. Vasyuchka, A.A. Serga, P. Clausen, H. Schultheiss, B. Hillebrands, A. Kreisel, P. Kopietz, *Wide-range wavevector selectivity of magnon gases in Brillouin light scattering spectroscopy*, Rev. Sci. Instrum. **81**, 073902 (2010).

[7] P. Clausen, D.A. Bozhko, V.I. Vasyuchka, B. Hillebrands, G.A. Melkov, A.A. Serga, *Stimulated thermalization of a parametrically driven magnon gas as a prerequisite for Bose-Einstein magnon condensation*, Phys. Rev. B **91**, 220402(R) (2015).

[8] A.A. Serga, V.S. Tiberkevich, C.W. Sandweg, V.I. Vasyuchka, D.A. Bozhko, A.V. Chumak, T. Neumann, B. Obry, G.A. Melkov, A.N. Slavin, B. Hillebrands, *Bose-Einstein condensation in an ultra-hot gas of pumped magnons*, Nat. Commun. **5**, 4452 (2014).

[9] V.V. Zautkin, V.E. Zakharov, V.S. L'vov, S.L. Musher, S.S. Starobinets, *Parallel spin-wave pumping in yttrium garnet single crystals*, Sov. Phys. JETP **35**, 926 (1972).

[10] T. Neumann, A.A. Serga, V.I. Vasyuchka, B. Hillebrands, *Field-induced transition from parallel to perpendicular parametric pumping for a microstrip transducer*, Appl. Phys. Lett. **94**, 192502 (2009).

B. Insulator Magnon Spintronics

The field of science that refers to information transport and processing by spin waves is known as magnonics. This name relates to the magnon – the spin-wave quantum associated with the flip of a single spin. The usage of magnonic approaches in the field of spintronics, hitherto dealing with electron-carried spin currents, gave birth to the field of magnon spintronics. This field is currently emerging, and considers magnon-based data buses, data processing elements operating with analogous and digital information, as well as converters between the magnon subsystem and the electron-carried spin and charge currents.

In this context, a magnetic insulator such as yttrium iron garnet (YIG) is of particular interest for magnon spintronics due to its extremely small damping parameter that ensures transport of spin information over macroscopic distances up to centimeters. Moreover, a magnetic insulator provides Joule-heat-free transfer and processing of spin information. Therefore, this year we have split our results in the frame of magnon spintronics into two parts: "Insulator Magnon Spintronics" and "Metallic Magnon Spintronics" that are presented in the corresponding Chapters of this Annual Report.

The first Report of the Chapter (Report 4.4) is devoted to the experimental studies of the excitation of the Damon-Eshbach surface spin waves in YIG/Pt bi-layers by inductive microstrip antennas. YIG/Pt systems represent a special material class for spintronics due to high values of the Spin Hall angle in Pt and small magnetic loss in YIG. The spin-wave dynamics in YIG/Pt structures rises up many question like the shielding effect by a thin metal layer, increase of spin-wave loss in YIG due to spin pumping to the Pt layer etc. In our studies we have found that the spin-wave amplitude decreases significantly due to the resistive losses attributed to the eddy currents induced in a Pt film by a propagating spin wave. At the same time, we have proposed a novel excitation geometry that enables a reduction of the excitation of the eddy currents and leads to a large increase in the spin-wave transmission (up to 1000 times).

In Report 4.5 we present a continuation of our studies on the spin-wave majority gate using numerical simulations. This three-input device is of especial interest for magnon spintronics since it can perform majority logic operations as well as AND, OR, NAND, and NOR logic operations. In the previous report we have presented a fully-functional in-plane magnetized majority gate which, hovewer, was challenged by two major issues: (*i*) very weak spin-wave transmission from the input to the output of order of 11 %, and (*ii*) parasitic excitation of short-wavelength exchange waves that disturbs reading out of data. In this Report 4.5 we present the design of an out-of-plane magnetized majority gate of new asymmetric layout (see also Cover Page). Isotropic forward volume waves used to overcome both these obstacles. Thus, there are no any exchange wave excitation in the new majority gate and the spin-wave transmission reached 64 % in our studies.

Finally, in Report 4.6 we present experimental studies on the spin-wave damping variation in YIG structures by a dc current passed through an adjacent Pt layer. The spin-wave relaxation was determined via the threshold of the parametric instability measured by Brillouin light scattering spectroscopy. The application of a dc current to the Pt layer led to the formation of a spin-polarized electron current normal to the film plane due to the spin Hall effect. This spin current exerted a spin transfer torque in the YIG film and, thus, changed the spin-wave damping. Depending on the polarity of the applied dc current with respect to the magnetization direction, the damping could be increased or decreased. The variation in the relaxation frequency of $\pm 7.5\,\%$ was achieved for an applied dc current density of $5 \cdot 10^{10}\,\mathrm{A/m^2}$. It is also worth to mention that this value of the current density agrees well with the theoretical predictions and with the latest experimental

results obtained by the group of O. Klein (CNRS, France). At the same time, it exceeds the values published before by other groups by up to four orders of magnitude.

B. Isolator-Magnon-Spintronik

Die Magnonik umfasst das Fachgebiet, das sich mit der Informationsübertragung und -verarbeitung mittels Spinwellen befasst. Die Bezeichnung bezieht sich auf das Magnon, das Quant einer Spinwelle, welches einem einzelnen Spin-Flip entspricht. Die Verwendung magnonischer Konzepte in der Spintronik, welche sich bis dahin nur ladungsgebundener Spinströme bediente, brachte das Fachgebiet der Magnon-Spintronik hervor. Dieses Forschungsfeld befindet sich momentan im großen Wachstum und befasst sich mit Magnon-basierter Datenübertragung und Komponenten zur Datenverarbeitung von analogen und digitalen Informationen, sowie mit Umwandlern zwischen dem magnonischen Untersystem und den elektronen-basierten Spin- und Ladungsströmen.

In diesem Zusammenhang ist ein magnetischer Isolator wie das Yttrium-Eisen-Granat (YIG) für die Magnon-Spintronik besonderes interessant, da dieses Material aufgrund seines äußerst geringen Dämpfungsparameters den Transport von Spin-Informationen über makroskopische Entfernungen bis in den Zentimeterbereich ermöglicht. Darüberhinaus erlaubt ein magnetischer Isolator Spin-Informationen ohne Beeinträchtigung durch Joulsche Erwärmung zu übertragen und zu verarbeiten. Daher haben wir dieses Jahr unsere Ergebnisse im Rahmen der Magnon-Spintronik in zwei Bereiche unterteilt, “Magnon-Spintronik in Isolatoren” und “Magnon-Spintronik in Metallen”, die in den entsprechenden Kapiteln dieses Jahresberichts vorgestellt werden.

Der erste Bericht (Bericht 4.4) befasst sich mit der experimentellen Untersuchung über die Erzeugung von Damon-Eshbach Oberflächenspinwellen in YIG/Pt Doppelschichten mit Hilfe induktiver Mikrostreifenantennen. YIG/Pt-Systeme sind von besonderem Interesse für die Spintronik aufgrund des großen Spin-Hall-Winkels im Pt und der geringen magnetischen Verluste im YIG. Die Spinwellendynamik in YIG/Pt-Strukturen wirft viele Fragestellungen auf, wie zum Beispiel nach dem Abschirmungseffekt durch eine dünne Metallschicht, die Erhöhung der Spinwellenverluste durch das Spinpumpen in die Pt-Schicht, usw. Bei unseren Untersuchungen fanden wir heraus, dass sich die Spinwellenamplitude aufgrund Ohmscher Verluste erheblich verringert, da propagierende Spinwellen in der Pt-Schicht Wirbelströme induzieren. Zugleich haben wir eine neuartige Anregungsgeometrie vorgeschlagen, die die Entstehung von Wirbelströmen reduziert und zu einem erheblichen Anstieg (bis zu 1000-fach) der Spinwellenübertragung führt.

Im nächsten Bericht 4.5 zeigen wir die Fortsetzung unserer Untersuchungen über das Spinwellenmajoritätsgatter anhand numerischer Simulationen. Dieses Bauteil mit drei Eingängen ist für die Magnon-Spintronik von besonderer Bedeutung, da es Rechenoperationen entsprechend einer Majoritätslogik durchführen kann, sowie als AND, OR, NAND und NOR-Gatter verwendet werden kann. Im vorigen Jahresbericht haben wir ein vollfunktionierendes in-plane magnetisiertes Majoritätsgatter vorgestellt und dabei zwei Herausforderungen ermittelt: (*i*) sehr geringe Spinwellenübertrag vom Eingang zum Ausgang in der Größenordnung von 11 % und (*ii*) parasitäre Anregung kurzwelliger Austauschspinwellen, die die Datenauslesung erschweren. In diesem Bericht 4.5 zeigen wir ein out-of-plane magnetisiertes Majoritätsgatter, welches mit einem neuen asymmetrischen Design (siehe auch Deckblatt) und mit isotropen Forwärtsvolumenwellen beide Hürden überwindet. Auf diese Weise werden im neuen Majoritätsgatter keine Austauschspinwellen angeregt und die Spinwellenübertragung erreicht 64 % in unseren Untersuchungen.

In Bericht 4.6 zeigen wir schließlich experimentelle Untersuchungen über die Änderung der Spin-

wellendämpfung in YIG Strukturen verursacht durch einen Gleichstromfluß durch eine angrenzende Pt-Schicht. Die Spinwellenrelaxation wurde anhand der Schwelle für die parametrische Instabilität ermittelt, die mit Hilfe der Brillouin-Lichtstreuung untersucht wurde. Ein Gleichstrom, der durch die Pt-Schicht floss, bewirkte durch den Spin Hall Effekt die Entstehung eines spinpolarisierten Elektronenstroms senkrecht zur Filmebene. Dieser Spinstrom übte ein Spintransfer-Drehmoment in der YIG-Schicht aus, der die Spinwellendämpfung änderte. Abhängig von der Polung des Gleichstroms in Bezug auf die Richtung der Magnetisierung konnte die Dämpfung erhöht oder verringert werden. Eine Variation der Relaxationsfrequenz von $\pm 7.5\,\%$ wurde bei einer Stromdichte von $5 \cdot 10^{10}\,\mathrm{A/m^2}$ erreicht. Es sollte auch erwähnt werden, dass dieser Stromdichtewert gut mit den theoretischen Erwartungen und mit den letzten experimentell erzielten Ergebnissen in der Gruppe von O. Klein (CNRS, Frankreich) übereinstimmt. Zugleich übersteigt es die Werte, die zuvor von anderen Gruppen veröffentlicht wurden, um bis zu vier Größenordnungen.

4.4 Spin-wave excitation, propagation and amplification in YIG/Pt bilayers

D.A. Bozhko, M. Agrawal, B. Hillebrands, and A.A. Serga

In collaboration with M.P. Kostylev, School of Physics, M013, University of Western Australia, Crawley, WA 6009, Australia

Magnonics addresses the transfer and processing of information using spin waves (SW) and their quanta, magnons. One of the main challenges for this field is the finite lifetime of magnons even in a low-damping material such as single crystal yttrium-iron-garnet (YIG) [1]. A possible way to overcome this issue is the compensation of SW damping via transfer of a spin torque to a magnetic medium by a spin-polarized electron current generated in an adjacent non-magnetic metal layer with high spin-orbit interaction. The decrease in the damping of spin waves propagating in a YIG film covered with a current conducting Pt film has already been reported [2,3]. However, the initial spin-wave attenuation in such a structure was unacceptably high for practical applications ($\simeq 35\,$dB in Ref. [2]). Therefore, it is an important task to determine the origin of the excessive spin-wave damping in YIG-Pt bi-layers and find a way to reduce this harmful effect. The latter will only be possible if this damping does not correspond to the spin-pumping effect – the process of a back transfer of a spin torque from magnons exited in a magnetic medium to a non-magnetic layer.

Here, we show that in a YIG-Pt bi-layer the SW amplitude significantly decreases, compared to a single YIG film, due to the resistive losses attributed to the microwave eddy currents induced in a Pt film by a propagating spin wave. By introducing a novel excitation geometry, where the Pt layer faces the ground plane of a microstrip line structure, we suppressed the excitation of the eddy currents in this Pt layer and, thus, achieved a large increase in the transmission of the Damon-Eshbach surface spin wave (up to 1000 times). At the same time, no visible influence of an external dc current applied to the Pt film on the SW amplitude in the YIG-Pt bi-layer was observed in our experiments with YIG films of micrometer thickness.

The experiments were performed using 2 mm wide and 15 mm long SW waveguides prepared from a 6.7 µm thick YIG film grown by liquid phase epitaxy on a 500 µm thick gallium-gadolinium garnet (GGG) substrate. A Pt layer of 10 nm thickness was deposited on top of the YIG surface. Spin waves were emitted and received by two short-circuited gold-wire antennas of 50 µm diameter placed 6 mm apart from each other (see Fig. 1). Spin-wave propagation was studied in a frequency band from 6.2 to 6.5 GHz using a vector network analyzer (Anritsu MS46322A). A relatively small level of the applied microwave power of 0.5 mW was chosen to prevent the development of non-linear effects for the propagating spin waves. An external bias magnetic field $H_0 = 1600\,$Oe was applied in the YIG film plane perpendicularly to the SW propagation direction. Thus, the excitation geometry for the Damon-Eshbach (DE) surface spin wave was implemented [1].

The reference experiment was performed in a conventional excitation geometry (as in Ref. [2]),

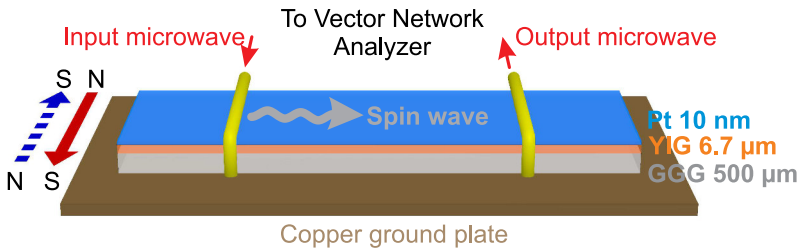

Fig. 1: Sketch of the conventional SW excitation geometry.

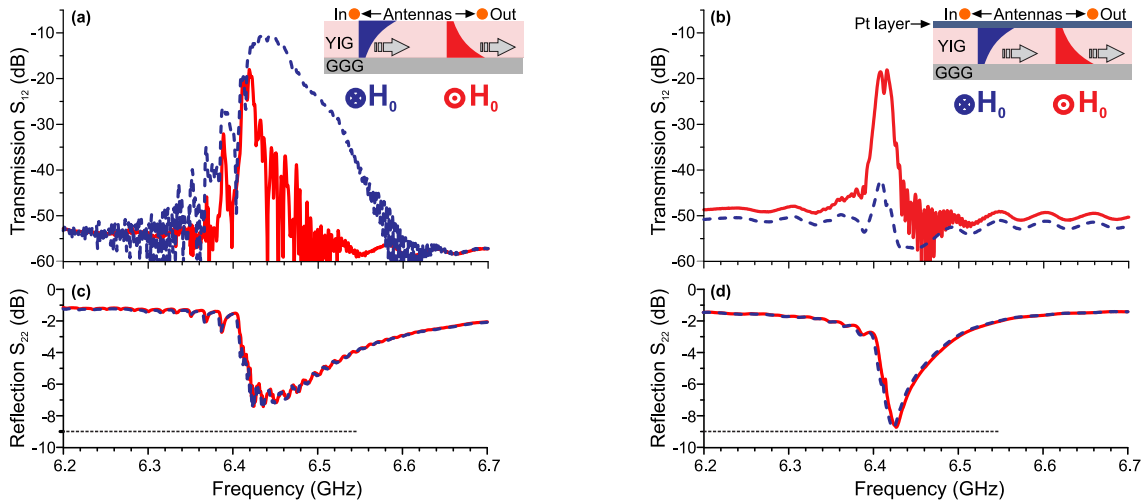

Fig. 2: Conventional excitation geometry. A YIG film is positioned directly under the antennas. The localization of a Damon-Eshbach wave depends on the direction of the bias magnetic field H_0 (see insets). Dashed/blue lines correspond to the bias magnetic field pointing into the drawing plane. Solid/red lines correspond to the bias magnetic field pointing out of the drawing plane. (a) Transmission (S_{12}) characteristic of the bare YIG waveguide. (b) Transmission (S_{12}) characteristic of the YIG waveguide covered with 10 nm Pt layer. (c) Excitation efficiency by the input antenna (S_{22}) for the bare YIG waveguide. (d) Excitation efficiency by the input antenna (S_{22}) for the YIG waveguide covered with 10 nm Pt layer.

when a YIG film lays directly under the antennas (see Fig. 1 and insets in Fig. 2). In the case of a bare YIG film – i.e. without any Pt coating (Fig. 2a), the DE spin wave, which propagates near the YIG surface touching the antennas (see the sketch of spin-wave distribution over the YIG film thickness in inset in Fig. 2a), possesses relatively low minimal transmission losses of around 10 dB at 6.42 GHz. The DE wave localized at the opposite film surface shows one order of magnitude weaker transmission. This well known effect relates to the nonreciprocal excitation of a DE wave, whose efficiency depends on the relative orientation of the bias magnetic field H_0 and the SW propagation direction [1, 4]. In spite of the pronounced difference in the transmission characteristics, the efficiencies of SW excitation, which are inversely proportional to the microwave reflection from the input antenna S_{22}, are identical for two opposite orientations of the bias magnetic field (see Fig. 2c). That is because in both cases the input antenna radiates spin waves in two opposite directions but only one of the emitted waves reaches the output antenna.

In the case of the Pt-covered YIG film, the excitation efficiency remains almost the same as for the bare YIG waveguide (compare Fig. 2d to Fig. 2c) but the transmission of the DE wave localized near the Pt layer is strongly suppressed (see the dashed curve in Fig. 2b). This suppression can be associated either with eddy currents excited in the high-resistive ($R_{\mathrm{Pt}} = 218\,\Omega$) Pt layer by stray fields of the propagating spin wave or with the spin-pumping effect at the YIG-Pt interface.

At the second stage of our studies, in order to distinguish between these two damping mechanisms, the YIG film was facing the ground plate (see Fig. 3b). It is expected that if the Pt film is placed in direct contact with the bulk copper plate, than the eddy currents will mostly flow in the low resistive ground plate. Hence, no additional Ohmic losses due to currents in Pt are expected. At the same time, the spin pumping effect should remain unchanged. The SW excitation efficiencies shown in Fig. 2c and Fig. 2d for the bare and Pt-covered YIG waveguides are close to those obtained in the conventional excitation geometry (see Fig. 2c). At the same time, one can see from Figs 3a, b that the wave, which propagates close to the Pt layer, experiences now no excessive damping and shows the same transmission losses as the wave in the bare YIG film. This fact explicitly confirms our

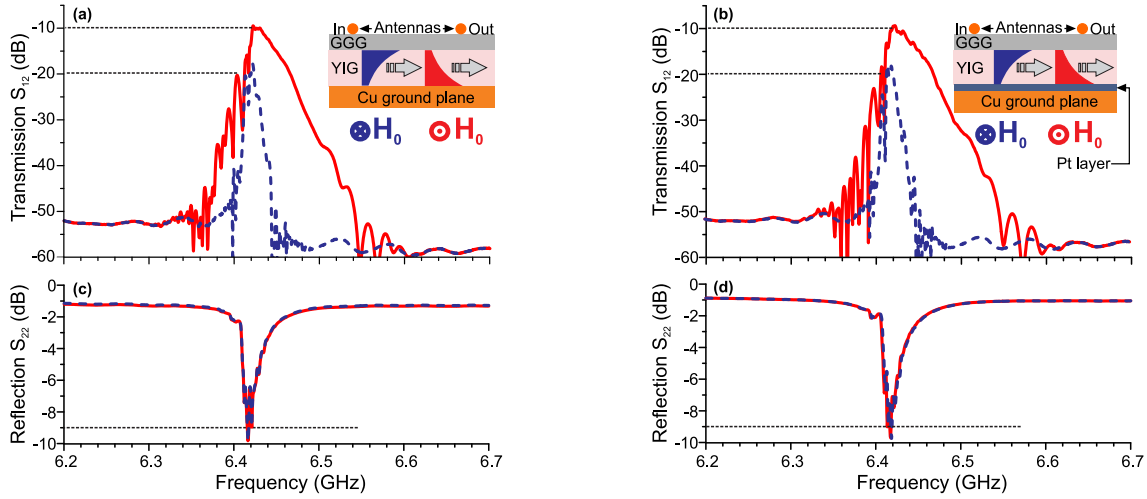

Fig. 3: Inverted excitation geometry. The YIG waveguide is positioned directly on the copper ground plate. Dashed/blue lines correspond to the bias magnetic field pointing into the drawing plane. Solid/red lines correspond to the bias magnetic field pointing out of the drawing plane. (a) Transmission (S_{12}) characteristics of the bare YIG waveguide. (b) Transmission (S_{12}) characteristics of the YIG waveguide covered with 10 nm Pt layer. (c) Excitation efficiency of the input antenna (S_{22}) for the bare YIG waveguide. (d) Excitation efficiency of the input antenna (S_{22}) for the YIG waveguide covered with a 10 nm Pt layer. Insets demonstrate schematic representations of the surface spin wave localizations for different directions of a bias magnetic field.

assumption about the significant contribution of the SW induced eddy currents to the SW damping in Pt-YIG bi-layers.

It should be noted that in the proposed excitation geometry spin waves are excited by microwave currents flowing in the ground plate rather than through the microstrip antenna separated from the

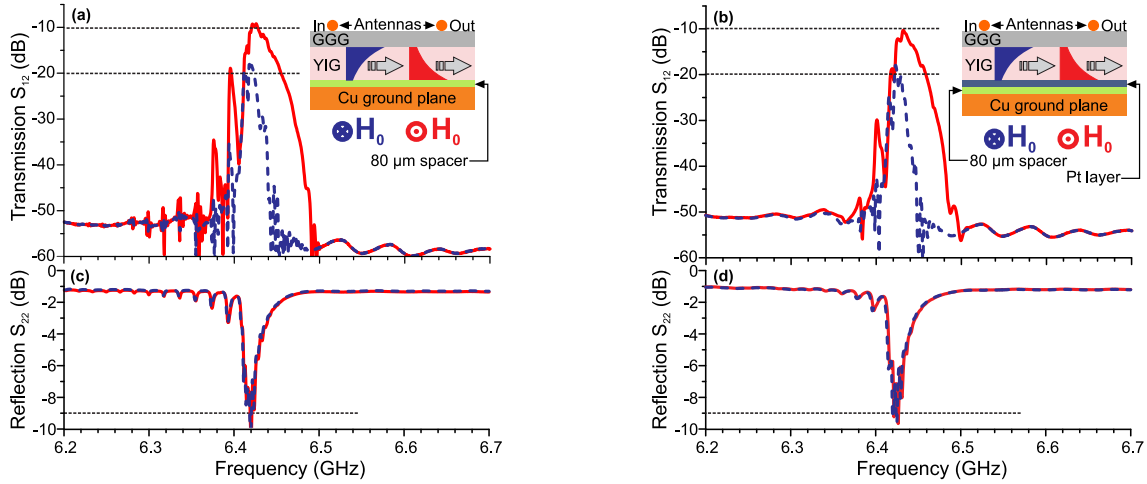

Fig. 4: Inverted excitation geometry. The YIG waveguide is positioned near the copper ground plate. An additional 80 µm thick dielectric spacer layer is introduced to electrically decouple the Pt layer from ground. Dashed/blue lines correspond to the bias magnetic field pointing into the drawing plane. Solid/red lines correspond to the bias magnetic field pointing out of the drawing plane. (a) Transmission (S_{12}) characteristics of the bare YIG waveguide. (b) Transmission (S_{12}) characteristics of the YIG waveguide covered with 10 nm Pt layer. (c) Excitation efficiency of the input antenna (S_{22}) for the bare YIG waveguide. (d) Excitation efficiency of the input antenna (S_{22}) for the YIG waveguide covered with a 10 nm Pt layer. Insets demonstrate schematic representations of the surface spin wave localizations for different directions of a bias magnetic field .

YIG film by the thick GGG layer. This decreases the excitation efficiency of short-wavelength spin waves because in the continuous ground plate the microwave currents are localized more weakly than in the narrow microstrip. However, the change in the electrodynamic boundary conditions due to placing a highly conducting layer near the surface of the YIG film [5] makes the DE dispersion relation steeper, i.e., increases the eigen-frequencies of the excited long-wavelength spin waves. The related increase in the SW group velocity decreases the SW propagation time and consequently the SW transmission losses. As a result, the SW transmission frequency band remains rather wide.

The described geometry enables the surface spin waves to propagate rather long distances through the Pt-covered YIG-film waveguides. However, no application of a dc electric current to such a structure is possible because of electric contact between the Pt layer and the Cu ground plate. In order to settle the issue, a 80 µm thick dielectric spacer was placed between the sample and the ground plate (see inset in Fig. 4a, b). In this case, the minimal transmission losses (Figs. 4a, b) remain the same as in the previous measurements (see Fig. 2, and Figs. 3a, b), but the transmission bandwidth turns to be significantly narrower. The reasons for this narrowing are obvious. A microwave magnetic field induced by microwave currents flowing in the ground plate is becoming more uniform with increase in the distance to the ground plate. This leads to a reduction of the excited SW wavenumbers and, alongside with the vanishing of the effect of metallization, to a decrease in the frequency bandwidth. However, the coupling between the Pt layer and the ground plate appears to be high enough to shunt the Pt film and reduce, thus, the eddy currents related SW losses.

At the final stage, we used the circuit shown in inset in Fig. 4b in order to check the ability to control the SW damping by a dc electric current applied to the Pt layer. To avoid spurious heating effects, overlapping 20 ns and 350 ns long microwave and dc current pulses were applied with 100 Hz repetition rate. It is remarkable that in the studied structure the highest SW transmission corresponds to the case when the DE wave is localized at the YIG-Pt interface. In the absence of the externally applied dc electric current, such localization results in rather high dc voltages induced in the Pt layer by the combined action of the spin pumping and inverse spin Hall effects. However, no influence of both positive and negative electric currents $I_{\mathrm{dc}} = \pm 370\,\mathrm{mA}$ on the SW amplitude was measured in the entire SW frequency band.

In conclusion, we have demonstrated that by using a novel spin-wave circuitry, where a Pt-covered YIG-film waveguide faces the ground plane of a microstrip line structure, it is possible to reduce the excitation of SW-related eddy currents in the Pt layer and achieve, thus, in a YIG-Pt bi-layer the same transmission losses for the Damon-Eshbach surface spin wave as in a bare YIG film. At the same time, no influence of a dc electric current applied to the Pt layer on the amplitude of SW pulses propagating in the relatively thick YIG waveguide of 6.7 µm thickness was observed in our experiments.

Financial support by EU-FET grant InSpin 612759 and by the Graduate School Materials Science in Mainz is gratefully acknowledged.

References

[1] A.A Serga, A.V Chumak, B. Hillebrands, *YIG magnonics*, J. Phys. D: Appl. Phys. **43**, 264002 (2010).
[2] Z. Wang, Y. Sun, M. Wu, V. Tiberkevich, A. Slavin, *Control of spin waves in a thin film ferromagnetic insulator through interfacial spin scattering*, Phys. Rev. Lett. **107**, 146602 (2011).
[3] E. Padrón-Hernández, A. Azevedo, S.M. Rezende, *Amplification of spin waves in yttrium iron garnet films through the spin Hall effect*, Appl. Phys. Lett. **99**, 192511 (2011).
[4] V.E. Demidov, M.P. Kostylev, K. Rott, P. Krzysteczko, G. Reiss, S.O. Demokritov, *Excitation of microwaveguide modes by a stripe antenna*, Appl. Phys. Lett. **95**, 112509 (2009).
[5] J.P. Parekh, K.W. Chang, H.S. Tuan, *Propagation characteristics of magnetostatic waves*, Circuits, Systems and Signal Processing **4**, 9 (1985).

4.5 Out-of-plane magnetized majority gate

A.V. Chumak, S. Klingler, P. Pirro†, T. Brächer‡, B. Leven, and B. Hillebrands*

**Current affiliation: Walther-Meißner-Institut, Bayerische Akademie der Wissenschaften, 85748 Garching, Germany*

†Current affiliation: Institut Jean Lamour, Université Lorraine, CNRS, 54506 Vandœuvre-lès-Nancy, France

‡Current affiliation: Univ. Grenoble Alpes, CNRS, CEA, INACSPINTEC, 17, rue des Martyrs 38054, Grenoble, France

Steadily advancing progress in modern information technology pushes the computation capabilities of common silicon-based digital logics towards fundamental limits. A potential alternative is wave-based computing. In particular, logic elements and devices based on collective excitations of the magnetization in the solid state - spin waves and their quanta magnons - attract attention [2–6]. In a spin-wave device the information can be encoded into the phase or amplitude of the wave, and the information can be processed by employing interference between different waves as well as nonlinear interactions [6].

A cornerstone of wave-based logic elements is the majority gate, since it allows for a simple implementation of complex logic circuits and the processing of several boolean operations with a single gate structure [7]. In a previous study [8], we introduced the design of an in-plane magnetized majority gate. It consists of three input waveguides where spin waves are excited, a symmetric spin-wave combiner that merges the different input waveguides, and an output waveguide where a spin wave propagates with the same phase as the majority of the input waves. We showed, that parasitic scattering processes into higher dipolar modes, which occur in such a device/devices, can be suppressed with a suitable waveguide geometry. But still, the output signal is influenced by short-wavelength exchange spin waves [8].

In this Report we demonstrate an out-of-plane magnetized spin-wave majority gate that operates with isotropic forward volume magneto-static spin waves (FVMSWs) and overcomes the aforementioned limitations of the in-plane magnetized gates.

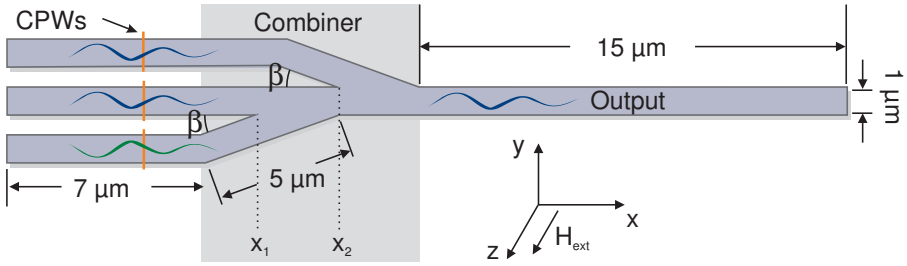

Fig. 1: Geometry of the majority gate. Spin waves are excited with coplanar waveguides in the input spin-wave waveguides. The input waveguides are bended under an angle β and merged to the center input arm at the positions x_1 and x_2 in the combiner region, where the spin waves interfere. The amplitude and phase of the spin wave in the output waveguide are consequently determined by the phase of the input spin waves.

This work has been recently published in Applied Physics Letters [1].

The simulations are performed for Yttrium-Iron-Garnet-(YIG)-structures with a thickness of 100 nm [9]. The following material parameters have been used: a saturation magnetization of $M_s = 140\,\mathrm{kA/m}$, an exchange constant of $A = 3.5\,\mathrm{pJ/m}$ and a Gilbert damping of $\alpha = 5 \cdot 10^{-4}$. The small damping of YIG allows for the spin-wave propagation over millimeter distances [10] and, thus, for the construction of complex magnonic networks [11]. The majority gate structure is investigated with numerical simulations using MuMax2 (see [1] for details).

In Fig. 1 the design of an out-of-plane magnetized majority gate is shown. It consists of three parallel input waveguides, where the spin waves are excited and the information is encoded into the spin-wave phase. In the combiner the input waveguides are bent under an angle $\beta = 20°$ towards the center waveguide, to overlay the spin waves and allow for their interference with each other. The bent parts have a length of 5 µm and merge with the center waveguide at the positions x_1 and x_2, respectively. With this asymmetric design the spin waves mainly propagate into the direction of the connected output waveguide, rather than into the direction of other inputs. Thus, a high spin-wave energy transmission from one of the majority gate inputs to the output of about 64% was achieved [1].

In general, the majority logic operation requires the simultaneous excitation of spin waves in all three inputs. For this, all spin-wave signals are equalized. As equalizing parameters for input 2 we reveal an attenuation factor of 0.7 and a phase shift of $\Delta\phi = -0.35\pi$ with respect to input 3. The spin-wave excitation in input 1 has to be attenuated by a factor of 0.5 and the excitation phase has to be shifted by $\Delta\phi = -0.64\pi$ relative to input 3. The different equalizing factors can be ascribed to the asymmetric gate geometry. In a real device these shifts can be realized e.g. by a small displacement of the antenna positions or by the use of nanomagnets as phase shifters [12]. With this equalizing parameters the output signals of every single input coincide, and all possible input combinations can be simulated.

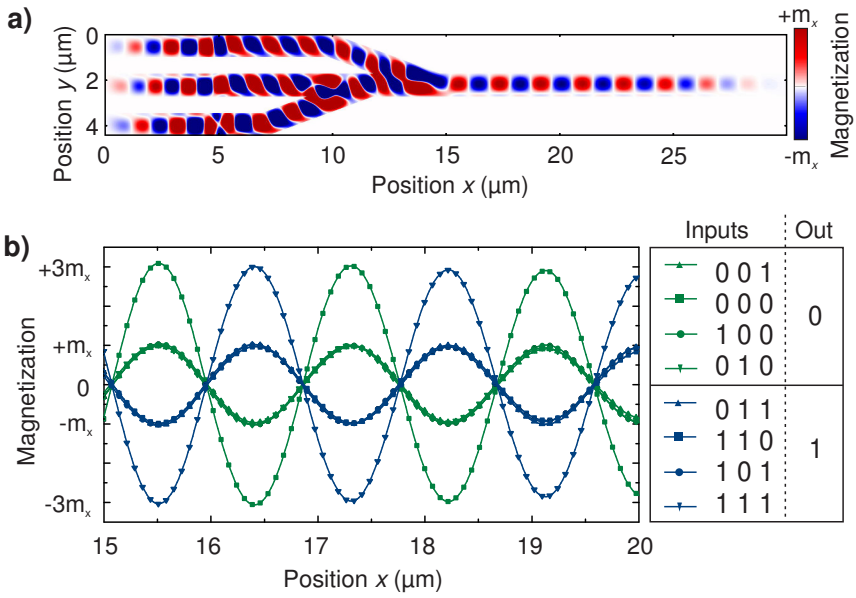

Fig. 2: (Color online) a) Spatial magnetization distribution of a fixed time step for the 1-0-0 operation. b) All input combinations are displayed in one graph. Input combinations with the same majority phase are in phase. Input combinations with different majority phases are out of phase.

In Fig. 2a the x-component of the magnetization distribution m_x is shown for a logic 1-0-0 ex-

citation (logic values from top to bottom) at a fixed time step. This means, that the spin waves in the upper input are excited with an additional phase shift of π, whereas the spin waves in the center and bottom waveguide are excited without an additional phase shift. At the edge of the waveguides one can see a small area where the magnetization is inverted. This is the result of an overlapping edge-mode [13] that propagates on the edge of the waveguide and decays exponentially into the waveguide width. Due to its small amplitude, no negative influences of this effect have to be expected. In Fig. 2b the magnetization m_x of every possible input combination is shown for the same time step. The sinusoidal shape of the magnetization distributions is clearly visible. All spin-waves with a majority phase of "0"are in phase and are exactly out of phase to the spin waves with a majority phase of "1". This is the clear signature of the majority function, which can be seen by comparing the results with the truth table (in the legend) in Fig. 2b [1]. From the magnetization distributions one can easily extract a wavelength of about 1.8 µm. Additionally, the amplitudes of the spin waves in the output waveguide fit very well to the theoretical predictions: if all three input waves are in phase, the amplitude in the output waveguide is three times larger than for every other case. Since the information is encoded in the spin-wave phase, the different output amplitudes are not essential for the information content of the spin wave. However, if the output signal is forwarded to another logic gate, the amplitude has to be normalized before, e.g. by employing parametric amplification [10, 14] or by embedding a magnon transistor [11].

To demonstrate that the spin-wave majority gate allows for a full set of logic operations, input 3 can be chosen as a control input. At a fixed readout position, e.g. at $x = 15.5\,\mu\text{m}$, one can perform AND-operations between inputs 1 and 2 when the spin waves in input 3 are excited without any additional phase shift. At the same readout position OR-operations can be performed when the spin waves in input 3 are excited with an additional phase shift of π. By shifting the readout position by one half of the wavelength, e.g. to 16.4 µm, the output phase of the spin wave is shifted by π and thus, NAND- and NOR-operations are performed dependending on the control input signal. In total, four different logic operations can be processed with a single majority gate.

One of the main advantages of the out-of-plane magnetized majority gate presented here, as compared to the in-plane-magnetized gate [8], is that the interference pattern shown in Fig. 2a is not disturbed by the scattering processes into higher dipolar spin waves or exchange spin waves. This can be understood by examining the dispersion relations [15] for the first three width modes n of the waveguide that are shown in Fig. 3. Here, n is the number of anti-nodes across the waveguide width. In the simulations dynamic demagnetization effects are automatically included, but not in the dispersion relations. To include such effects in the dispersion relations an effective stripe width [16] of 1.42 µm was used. Furthermore, one can extract a wavevector of $k = 3.8\,\text{rad}/\mu\text{m}$, a wavelength of $\lambda = 1.7\,\mu\text{m}$ and a group velocity of $v_g = 0.13\,\mu\text{m}/\text{ns}$ from the dispersion relation at the excitation frequency f. Together with the decay time of the spin wave of $\tau = 566\,\text{ns}$, which can be calculated from the material parameters [17], one obtains a decay length $\lambda_{\text{dec}} = v_g\tau = 73\,\mu\text{m}$

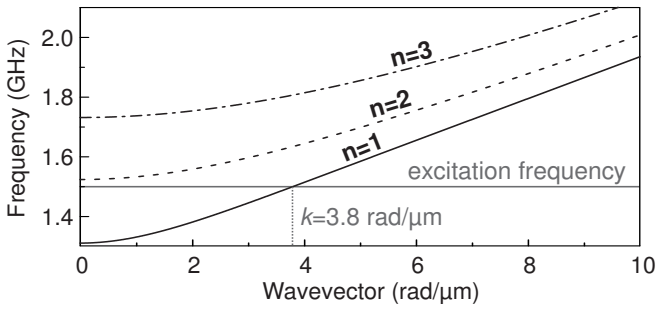

Fig. 3: Dispersion relations for different width modes for a perpendicular magnetized stripe with an effective width of 1.42 µm. For an excitation frequency of 1.5 GHz no higher width modes can exist in the waveguide.

that is much larger than the size of the microstructures.

The proposed spin-wave majority gate has a large down-scaling potential. The smallest YIG structures reported nowadays have sizes of the order of a few hundreds of nanometers [18]. However, the same technology [9, 18] allows for the reduction of the sizes below hundred nanometers. The fundamental limitation of the feature size is given by the YIG lattice constant, which is about 1.24 nm [19]. In such structures the energy of the spin waves is dominated by the exchange energy, which guarantees for isotropic spin-wave dispersions and high group velocities of spin waves.

In summary, a fully functional, asymmetric magnonic majority gate design for the use with isotropic forward volume magnetostatic waves has been presented. It was shown, that the output signal is not disturbed by parasitic scattering processes into higher spin-wave modes. This results in a very clear interference pattern in the output waveguide. The data processing and transmission occured in the pure spin-wave system, which makes the gate suitable for an integration into complex magnonic networks with various daisy-chained spin-wave devices [6].

This research has been supported by the EU-FET grant InSpin 612759.

References

[1] S. Klingler, P. Pirro, T. Brächer, B. Leven, B. Hillebrands, A. V. Chumak, *Spin-wave logic devices based on isotropic forward volume magnetostatic waves*, Appl. Phys. Lett. **106**, 212406 (2015).
[2] V. V. Kruglyak, S. O. Demokritov, D. Grundler, *Magnonics*, J. Phys. D **43**, 264001 (2010).
[3] B. Lenk, H. Ulrichs, F. Garbs, M. Münzenberg, *The building blocks of magnonics*. Phys. Rep. **507**, 107 (2011).
[4] A. Khitun, M. Bao, K. L. Wang, *Magnonic logic circuits*, J. Phys. D **43**, 264005 (2010).
[5] M. Krawczyk, D. Grundler, *Review and prospects of magnonic crystals and devices with reprogrammable band structure*, J. Phys. Condens. Matter **26**, 123202 (2014).
[6] A. V. Chumak, V. I. Vasyuchka, A. A. Serga, B. Hillebrands, *Magnon spintronics*, Nature Phys. **11**, 453 (2015).
[7] A. Khitun, K. L. Wang, *Spin wave magnetic nanofabric: A new approach to spin-based logic circuitry*, IEEE Trans. Magn. **44**, 2141 (2008).
[8] S. Klingler, P. Pirro, T. Brächer, B. Leven, B. Hillebrands, A. V. Chumak, *Design of a spin-wave majority gate employing mode selection*, Appl. Phys. Lett. **105**, 152410 (2014).
[9] P. Pirro, T. Brächer, A. V. Chumak, B. Lägel, C. Dubs, O. Surzhenko, P. Görnert, B. Leven, B. Hillebrands, *Spin-wave excitation and propagation in microstructured waveguides of yttrium iron garnet/Pt bilayers*, Appl. Phys. Lett. **104**, 012402 (2014)
[10] A. A. Serga, A. V. Chumak, B. Hillebrands, *YIG magnonics*, J. Phys. D **43**, 264002 (2010).
[11] A. V. Chumak, A. A. Serga, B. Hillebrands, *Magnon transistor for all-magnon data processing*, Nat. Commun. **5**, 4700 (2014).
[12] Y. Au, M. Dvornik, O. Dmytriiev, V. V. Kruglyak, *Nanoscale spin wave valve and phase shifter*, Appl. Phys. Lett. **100**, 172408 (2012).
[13] I. Lisenkov, V. Tyberkevych, A. Slavin, P. Bondarenko, B. A. Ivanov, E. Bankowski, T. Meitzler, S. Nikitov, *Spin-wave edge modes in finite arrays of dipolarly coupled magnetic nanopillars*, Phys. Rev. B **90**, 104417 (2014).
[14] T. Brächer, P. Pirro, T. Meyer, F. Heussner, B. Lägel, A. A. Serga, B. Hillebrands, *Parallel parametric amplification of coherently excited propagating spin waves in a microscopic $Ni_{81}Fe_{19}$ waveguide*, Appl. Phys. Lett. **104**, 202408 (2014).
[15] B. A. Kalinikos, A. N. Slavin, *Theory of dipole-exchange spin wave spectrum for ferromagnetic films with mixed exchange boundary conditions*, J. Phys. C: Solid State Phys. **19**, 7013 (1986).
[16] K. Guslienko, S. Demokritov, B. Hillebrands, A. N. Slavin, *Effective dipolar boundary conditions for dynamic magnetization in thin magnetic stripes*, Phys. Rev. B **66**, 132402 (2002).
[17] C. E. Patton, in *Magnetic oxides*, edited by D. J. Craik (John Wiley, London, 1975), pp. 575 - 645.
[18] C. Hahn, V. V. Naletov, G. de Loubens, O. Klein, O. d'Allivy Kelly, A. Anane, R. Bernard, E. Jacquet, P. Bortolotti, V. Cros, J. L. Prieto, M. Mũnoz, *Measurement of the intrinsic damping constant in individual nanodisks of $Y_3Fe_5O_{12}$ and $Y_3Fe_5O_{12}|Pt$*, Appl. Phys. Lett. **104**, 152410 (2014).
[19] V. Cherepanov, I. Kolokolov, V. L'vov, *The saga of YIG: Spectra, thermodynamics, interaction and relaxation of magnons in a complex magnet*, Phys. Rep. **229**, 81 (1993).

4.6 Spin-transfer torque based damping control of parametrically excited spin waves in a magnetic insulator

V. Lauer, D.A. Bozhko, T. Brächer, P. Pirro†, V.I. Vasyuchka, A.A. Serga, M.B. Jungfleisch‡, M. Agrawal, B. Hillebrands, and A.V. Chumak*

In collaboration with Yu.V. Kobljanskyj and G.A. Melkov, Faculty of Radiophysics, Electronics and Computer Systems, Taras Shevchenko National University of Kyiv, 01601 Kyiv, Ukraine;
C. Dubs, Innovent e.V., Prüssingstraße 27B, 07745 Jena, Germany.

**Current affiliation: Univ. Grenoble Alpes, CNRS, CEA, INAC-SPINTEC, 17, rue des Martyrs 38054, Grenoble, France.*
†Current affiliation: Institut Jean Lamour, Université Lorraine, CNRS, 54506 Vandœuvre-lès-Nancy, France.
‡Current affiliation: Materials Science Division, Argonne National Laboratory, Argonne, Illinois 60439, USA.

The injection of a spin current into a magnetic film can generate a spin-transfer torque (STT) that acts on the magnetization [2], and allows for tuning of the damping [3–6] as well as for the excitation of magnetization precession in the film [7, 8]. A preferred method to generate a spin current in a non-magnetic metal with large spin-orbit interaction is based on the spin Hall effect (SHE) [9]. One of the advantages of the SHE is that it does not require a dc charge current in the magnetic layer and, thus, allows for the application of a STT to a magnetic dielectric such as yttrium iron garnet (YIG) [10]. YIG is of particular interest for magnon spintronics [11, 12] due to its extremely small damping parameter [13]. Moreover, a great advantage of the SHE is that a STT can be applied not only locally but to a large area of a magnetic film [4] and, thus, can be potentially used to compensate the damping in a whole complex magnonic circuit [12].

In this work, we use a YIG/Pt bilayer of macroscopic size to investigate SHE-STT damping variation. In contrast, most experimental studies concerning the SHE-STT damping reduction up to the creation of auto-oscillations in metallic samples [3, 5] as well as in YIG structures [6, 8] were performed with laterally-confined nano- or micro-structures [14]. Our sample consists of a YIG/Pt bilayer with lateral dimensions of 4 mm × 2 mm, and film thicknesses of $t_{\mathrm{YIG}} = 100\,\mathrm{nm}$ and $t_{\mathrm{Pt}} = 10\,\mathrm{nm}$. The YIG film is grown by liquid phase epitaxy on a gadolinium gallium garnet (GGG) substrate and the Pt film is deposited afterwards using plasma cleaning and RF sputtering. Various characterization parameters of the used sample can be found in Ref. [1].

Our investigation of the SHE-STT damping variation is based on the analysis of the threshold of the parametric instability. Figure 1 shows a sketch of the experimental arrangement, in which the parametric instability threshold is measured in the parallel pumping geometry [11]. An external biasing field H_{appl} magnetizes the YIG film in-plane along the x-axis. The parametric excitation of spin waves is achieved by an alternating pumping magnetic field h_{p} oriented parallel to H_{appl}. For this purpose, a microwave signal at a fixed frequency of $f_{\mathrm{p}} = 14\,\mathrm{GHz}$ is applied to a Cu microstrip antenna placed close to the sample. Spin waves are excited at half of the pumping frequency ($f_{\mathrm{sw}} = 7\,\mathrm{GHz}$) as soon as the pumping field amplitude h_{p} overcomes a critical threshold value h_{th}

This work has been recently uploaded to arXiv [1].

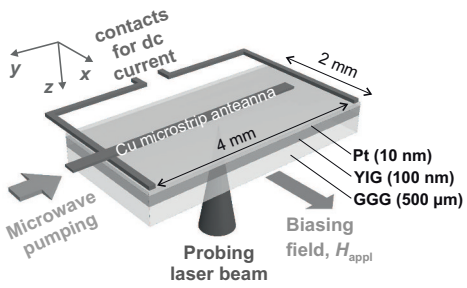

Fig. 1: Sketch of the sample and the setup in the parallel pumping geometry used for the parametric excitation of spin waves and their detection by BLS spectroscopy. The externally applied biasing field and the pumping field in the examined area of the sample are both aligned along to the x-direction, the charge current is applied in-plane along the y-direction.

which depends on H_{appl}. BLS spectroscopy enables the detection of spin waves with wavenumbers in a range of $k \lesssim 10^4\,\mathrm{rad/cm}$ when the probing laser beam is perpendicular to the film plane in our experiment. Au wires are mounted to the edges of the sample to apply an in-plane dc current to the Pt film along the y-axis allowing the SHE to generate an out-of-plane spin current (along the z-direction) in the Pt film that, in turn, exerts a STT on the YIG magnetization at the YIG/Pt interface. A maximal current of 1 A is used, corresponding to a current density of $j_{\mathrm{c}} = 5 \cdot 10^{10}\,\mathrm{A/m^2}$. In order to reduce the influence of Joule heating in the Pt film, the experiment is performed in the pulsed regime with a pulse duration of 10 µs and a repetition time of 1 ms. All measurements presented here are performed at room temperature.

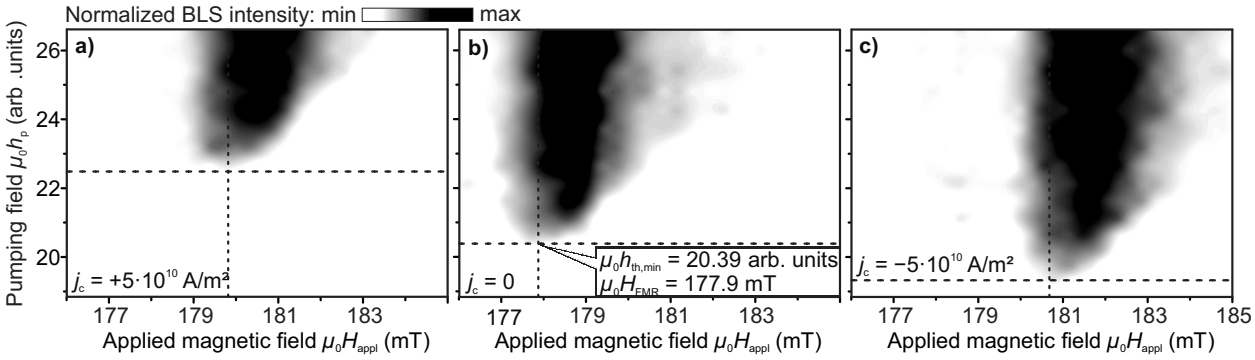

Fig. 2: BLS intensity of parametrically pumped spin waves while scanning the pumping field h_{p} and the biasing field H_{appl} (in $+x$-direction) for different applied current densities j_{c} (in $+y$-direction).

For each dc current density j_{c}, the BLS measurements are performed by scanning over the pumping field h_{p} and the applied biasing field H_{appl}. Figures 2a-c exemplary show BLS intensities of parametrically excited spin waves when H_{appl} is in $+x$-direction and the dc current is in $+y$-direction. The applied current densities are (a) $j_{\mathrm{c}} = +5 \cdot 10^{10}\,\mathrm{A/m^2}$, (b) reference measurement $j_{\mathrm{c}} = 0$, (c) $j_{\mathrm{c}} = -5 \cdot 10^{10}\,\mathrm{A/m^2}$. Bright areas in the intensity graphs correspond to the case $h_{\mathrm{p}} < h_{\mathrm{th}}$ when no detectable spin waves are parametrically excited. The horizontal dashed lines indicate the minimal threshold values $h_{\mathrm{th,min}}$ at the resonant field values H_{FMR} (vertical dashed lines), which correspond to spin waves with $k \to 0$. For the further study, only the variations of H_{FMR} (shown in Fig. 3a) and $h_{\mathrm{th,min}}$ (shown in Fig. 3c) are analyzed as functions of the applied dc current.

The variation of H_{FMR} as function of j_{c} can be described by the Kittel equation

$$f_{\mathrm{sw}} = \gamma\mu_0 \sqrt{(H_{\mathrm{FMR}} + H_{\mathrm{ind}}(j_{\mathrm{c}})) \cdot (H_{\mathrm{FMR}} + H_{\mathrm{ind}}(j_{\mathrm{c}}) + M_{\mathrm{s}}(j_{\mathrm{c}}))}. \tag{1}$$

Here, $\gamma = 28\,\mathrm{GHz/T}$ denotes the gyromagnetic ratio, μ_0 is the vacuum permeability, $\mu_0 H_{\mathrm{ind}}(j_{\mathrm{c}}) = a \cdot j_{\mathrm{c}}$ accounts for the Oersted field induced by the dc current, and $M_{\mathrm{s}}(j_{\mathrm{c}}) = M_{\mathrm{s}}(0) \cdot (1 - b \cdot {j_{\mathrm{c}}}^2)$

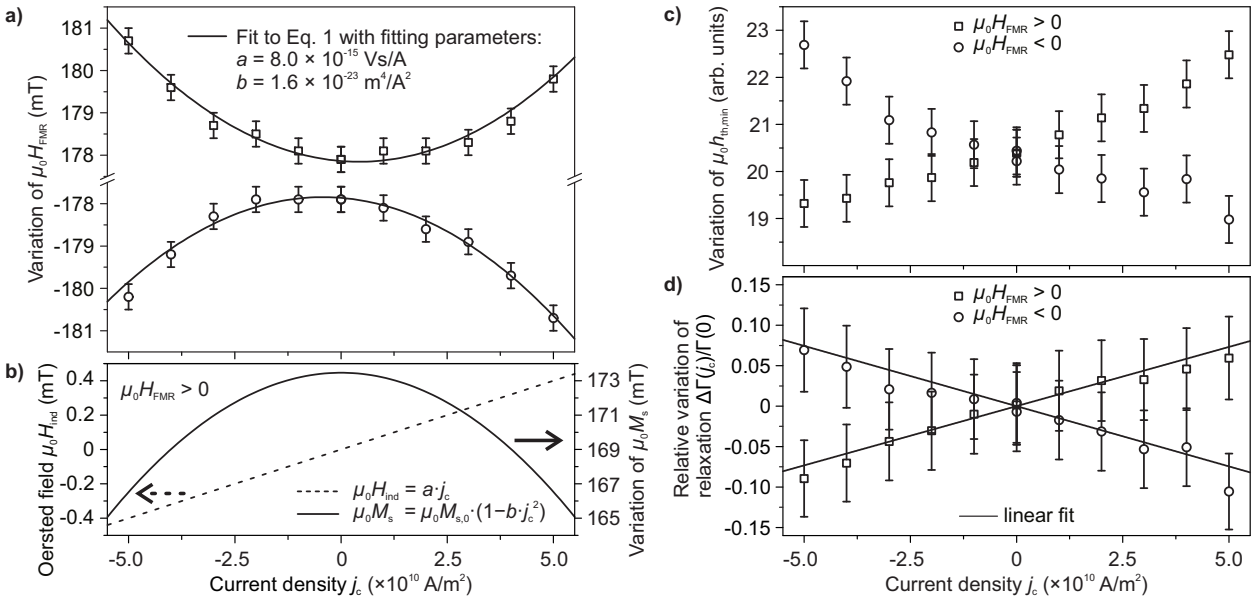

Fig. 3: a) H_{FMR} values as functions of j_{c} obtained from BLS measurements. The solid lines are fits to Eq. 1. b) The induced Oersted field and the variation of the saturation magnetization as functions of j_{c}, when the applied biasing field is in $+x$-direction ($H_{\mathrm{FMR}} > 0$). c) $h_{\mathrm{th,min}}$ values as functions of j_{c} obtained from BLS measurements. d) Relative change of the relaxation frequency Γ. The solid lines are linear fits.

accounts for the decrease of the saturation magnetization of the YIG film caused by Joule heating in the Pt. The fit of Eq. 1 to the data points (solid lines in Fig. 3a) yield the fitting parameters $a = 8.0 \cdot 10^{-15}\,\mathrm{Vs/A}$ and $b = 1.6 \cdot 10^{-23}\,\mathrm{m^4/A^2}$. Figure 3b presents the variations of the Oersted field H_{ind} and the saturation magnetization M_{s} as function of j_{c} according to the obtained values for a and b.

The variation of $h_{\mathrm{th,min}}$ as function of j_{c} (see Fig. 3c) depends on the orientation of the dc current with respect to the applied field and can be understood in terms of the SHE-STT combination. The damping in the YIG film and consequently $h_{\mathrm{th,min}}$ decreases if the spin current is oriented from Pt to YIG (in $+z$-direction according to our experimental geometry), whereas the damping increases if the spin current is reversed. The relaxation frequency Γ of spin waves with $k \to 0$ reads [15]

$$\Gamma(j_{\mathrm{c}}) = \frac{\pi}{2}\frac{\gamma^2}{f_{\mathrm{sw}}} \cdot \mu_0 M_{\mathrm{s}}(j_{\mathrm{c}}) \cdot \mu_0 h_{\mathrm{th,min}}(j_{\mathrm{c}}). \tag{2}$$

Figure 3d shows $\Delta\Gamma(j_{\mathrm{c}})/\Gamma(0) = (\Gamma(j_{\mathrm{c}}) - \Gamma(0))/\Gamma(0)$, the relative variation of the relaxation frequency as function of j_{c} calculated from the $h_{\mathrm{th,min}}$ values of Fig. 3b and the M_{s} values of Fig. 3c. Γ is changed by approximately 7.5 % for the highest applied current densities of $j_{\mathrm{c}} = \pm 5 \cdot 10^{10}\,\mathrm{A/m^2}$ in our experiment. In order to estimate the required critical current density for the complete compensation of damping, and for the triggering of auto-oscillations in our experiments, an extrapolation of the linear fit to $\Gamma(j_{\mathrm{c}}) = 0$ is performed, yielding a value of $j_{\mathrm{c,crit}}^{\mathrm{exp}} \approx 6.7 \cdot 10^{11}\,\mathrm{A/m^2}$. This value agrees well with the results obtained with patterned structures [6], and with the theoretically estimated value of $j_{\mathrm{c,crit}}^{\mathrm{theo}} \approx 8.3 \cdot 10^{11}\,\mathrm{A/m^2}$ calculated on the basis of the analytical expressions provided in Ref. [6]. For this calculation, the parameters of our system (see Ref. [1]), a spin diffusion length of $\lambda = 3.4\,\mathrm{nm}$, and a spin Hall angle of $\theta_{\mathrm{SH}} = 0.056$ are used [16], neglecting the influence of heating effects. Additional reference measurements performed in a geometry which eliminates the SHE-STT combination demonstrate no variation of Γ due to the spin Seebeck effect within the error bars (not shown).

In summary, the threshold of the parametric excitation of spin waves in a macroscopic YIG/Pt bilayer is detected by BLS spectroscopy. A change of the damping in the YIG due to SHE-STT is observed when a dc current is passed through the adjacent Pt film. Based on our calculations, including current induced Joule heating and Oersted fields, the damping is found to change linearly with the current. The linearity suggests that the role of nonlinear multi-magnon scattering processes is negligible for the damping variation in the analyzed range (below 10% change of Γ). The maximum used current density of $j_c = \pm 5 \cdot 10^{10}\,\mathrm{A/m^2}$ results in a damping variation of $\pm 7.5\%$. Thus, the complete damping compensation in the system is estimated at $j_{c,crit}^{exp} \approx 6.7 \cdot 10^{11}\,\mathrm{A/m^2}$ which is in agreement with the theoretical estimation. The SHE-STT-based damping compensation below the auto-oscillatory regime can potentially be used to realize complex magnonic circuits with ultra-low effective losses [12].

This research has been supported by the EU-FET grant InSpin 612759.

References

[1] V. Lauer, D.A. Bozhko, T. Brächer, P. Pirro, V.I. Vasyuchka, A.A. Serga, M.B. Jungfleisch, M. Agrawal, Yu.V. Kobljanskyj, G.A. Melkov, C. Dubs B. Hillebrands, A.V. Chumak, *Spin-transfer torque based damping control of parametrically excited spin waves in a magnetic insulator*, arXiv:1508.07517 (2015).

[2] A.N. Slavin, V.S. Tiberkevich, *Nonlinear auto-oscillator theory of microwave generation by spin-polarized current*, IEEE Trans. Magn. **45**, 1875-1918 (2009)

[3] I.N. Krivorotov, N.C. Emley, J.C. Sankey, S.I. Kiselev, D.C. Ralph, R.A. Buhrman, *Time-domain measurements of nanomagnet dynamics driven by spin-transfer torques*, Science **307**, 228-231 (2005).

[4] K. Ando, S. Takahashi, K. Harii, K. Sasage, J. Ieda, S. Maekawa, E. Saitoh, *Electric manipulation of spin relaxation using the spin Hall effect*, Phys. Rev. Lett. **101**, 036601 (2008).

[5] V.E. Demidov, S. Urazhdin, E.R. J. Edwards, S.O. Demokritov, *Wide-range control of ferromagnetic resonance by spin Hall effect*, Appl. Phys. Lett. **99**, 172501 (2011).

[6] A. Hamadeh, O. d'Allivy Kelly, C. Hahn, H. Meley, R. Bernard, A.H. Molpeceres, V.V. Naletov, M. Viret, A. Anane, V. Cros, S.O. Demokritov, J.L. Prieto, M. Muñoz, G. de Loubens, O. Klein, *Full control of the spin-wave damping in a magnetic insulator using spin-orbit torque*, Phys. Rev. Lett. **113**, 197203 (2014).

[7] V.E. Demidov, S. Urazhdin, S.O. Demokritov, *Direct observation and mapping of spin waves emitted by spin-torque nano-oscillators*, Nature Mater. **9**, 984-988 (2010).

[8] M. Collet, X. De Milly, O. D'Allivy-Kelly, V.V. Naletov, R. Bernard, P. Bortolotti, V.E. Demidov, S.O. Demokritov, J.L. Prieto, M. Muñoz, A. Anane, V. Cros, G. De Loubens, O. Klein, *Generation of coherent spin-wave modes in Yttrium Iron Garnet microdiscs by spin-orbit torque*, arXiv:1504.01512 (2015).

[9] J.E. Hirsch, *Spin Hall effect*, Phys. Rev. Lett. **83**, 1834-1837 (1999).

[10] J. Xiao, G.E.W. Bauer, *Spin-wave excitation in magnetic insulators by spin-transfer torque*, Phys. Rev. Lett. **108**, 217204 (2012).

[11] A.A. Serga, A.V. Chumak, B. Hillebrands, *YIG magnonics*, J. Phys. D **43**, 264002 (2010).

[12] A.V. Chumak, V.I. Vasyuchka, A.A. Serga, B. Hillebrands, *Magnon spintronics*, Nature Physics **11**, 453 (2015).

[13] P. Pirro, T. Brächer, A.V. Chumak, B. Lägel, C. Dubs, O. Surzhenko, P. Görnert, B. Leven, B. Hillebrands, *Spin-wave excitation and propagation in microstructured waveguides of yttrium iron garnet/Pt bilayers*, Appl. Phys. Lett. **104**, 012402 (2014).

[14] Remark on the used references: Only experimental results which have been reproduced by other groups and approved by scientific community are cited here.

[15] A.G. Gurevich, G.A. Melkov, *Magnetization oscillations and waves*, (CRC Press, 1996).

[16] J.C. Rojas-Sánchez, N. Reyren, P. Laczkowski, W. Savero, J.P. Attané, C. Deranlot, M. Jamet, J.M. George, L. Vila, H. Jaffrès, *Spin pumping and inverse spin Hall effect in platinum: The essential role of spin-memory loss at metallic interfaces*, Phys. Rev. Lett. **112**, 106602 (2014).

C. Metallic Magnon Spintronics

The combination of standard spintronics with spin-wave dynamics led to the emergence of the field of *magnon spintronics*. This field aims at the magnon-to-charge current conversion and for magnon-based data processing devices. A magnon, i.e. the quantum of a spin wave, carries an angular momentum or spin and can be used for storage, processing and transport of spin information, building on its outstanding properties such as long lifetime and potential for dissipationless transport. Furthermore, the utilization of spin Hall effects to create and detect spin currents and magnetization dynamics has pushed *magnon spintronics* even further. The use of metallic systems of ferromagnetic metal/non-magnetic metal bilayers has proven to be the highest efficient systems of the charge-to-spin conversion and vice versa. In this section we focus on spin Hall related effects like spin pumping and inverse spin Hall effect (ISHE) by addressing high-quality epitaxial metallic systems and phase-dependent parallel parametric amplification of spin waves in the non-adiabatic regime in a micro-structured Py waveguide.

In particular, the first of our four reports of the chapter, Report 4.7, describes a detailed study of ferromagnetic resonance (FMR) measurements in fully epitaxial Fe/Pt samples. Such an FMR analysis provides the basis for understanding the spin pumping effect where a microwave field typically excites the magnetization of a ferromagnetic layer at the ferromagnetic resonance and that leads to a generation of a spin current in the attached non-magnetic layer. By changing the Pt thickness we observe an increase of the measured effective Gilbert damping (α_{eff}) for the Fe/Pt bilayers that already reaches saturation at Pt thickness of 1 nm. We compare our data with different reference samples and we point out the big importance of choosing the reference for α_{eff}. Furthermore, we reveal the different contributions that can affect the enhancement of α_{eff}. The spin mixing conductance is calculated with respect to the most appropriate reference sample.

Report 4.8 adresses to the conversion of a magnon current into a charge current via the spin pumping effect in Fe/Pt sample series. We show the influence of the crystal structure on the spin pumping experiments. The excitation either along the easy or along the hard magnetization axis provides distinct differences of the spin pumping excitation. By using the ISHE we have recorded the signal due to spin pumping at two different applied magnetic field values at the same frequency along the hard axis. This is a result from the strong anisotropic nature of our samples. The symmetric as well the antisymmetric components of the measured voltage due to ISHE are decreasing with the Pt thickness due to the shielding of the microwave excitation by the Pt layer and the spin diffusion length in Pt.

Report 4.9 presents the influence of an insulating MgO layer inserted between the Fe and Pt layers on the spin pumping. The good growth of MgO on Fe and the tunneling properties of MgO renders the Fe/MgO/Pt system a very interesting candidate to reveal the physical mechanisms of spin pumping in such structures. We show that the effective Gilbert damping α_{eff} is decreasing with the MgO thickness. However the measured voltage is increasing for thicker MgO barriers. Furthermore, the symmetric part of the signal increases with the MgO thickness.

Report 4.10 addresses a microstructured Py waveguide for converting the phase information of a spin wave into an amplitude information by employing localized parallel parametric pumping in the non-adiabatic regime. The wave-nature of magnons allows use to code the information not only in the amplitude but also in the phase of the spin waves, which provides an additional degree of freedom. Therefore the phase-to-amplitude conversion may help to combine *magnon spintronics* with today's complementary metal-oxide-semiconductor (CMOS) technology. The maximal and minimal amplification of the signal wave in our waveguide varies by a high factor of 10, which

ensures a high reliability of the readout process and increases the sensitivity of detection of small signals.

C. Magnon-Spintronik in Metallen

Die Kombination von Standard-Spintronik und Spinwellendynamik führte zur Entstehung des Feldes der *Magnon-Spintronik*. Dieses Forschungsgebiet hat die Konversion von Magnonen- zu Ladungsträgerströmen und die Entwicklung Magnonen-basierter Datenverarbeitungsgeräte zum Ziel. Ein Magnon, d.h. das Quant einer Spinwelle, trägt einen Drehimpuls und kann zur Speicherung, Prozessierung und zum Transport einer Spin-Information Verwendung finden, basierend auf seinen hervorstechenden Eigenschaften wie großer Lebensdauer und potenziell verlustfreiem Transport. Weiterhin wurde die *Magnon-Spintronik* durch die Ausnutzung des Spin-Hall-Effekts zur Erzeugung und Detektion von Spinströmen und Magnetisierungsdynamik vorangetrieben. Metallische Systeme aus ferromagnetischem Metall/nichtmagnetischem Metall-Doppelschichten erwiesen sich als höchsteffiziente Systeme zur Ladungsträger-zu-Spin Konversion und umgekehrt. In diesem Abschnitt konzentrieren wir uns auf die Spin-Hall zugehörigen Effekte wie Spin Pumping und inversem Spin Hall Effekt (ISHE) durch die Addressierung der hohen Qualität epitaktischer Metallsysteme und auf phasensensitive parallele parametrische Verstärkung von Spinwellen in dem nicht-adiabatischen Regime in mikrostrukturierten Py-Wellenleitern.

Insbesondere der erste unserer vier Berichte dieser Sektion, Bericht 4.7, beschäftigt sich mit einer detailierten Studie ferromagnetischer Resonanz (FMR) -Messungen in vollepitaktischen Fe/Pt-Proben. Solche FMR-Analysen liefern die Grundlage für das Verständnis des Spin-Pumping-Effekts, wo typischerweise ein Mikrowellenfeld die Magnetisierung einer ferromagnetischen Schicht zur ferromagnetischen Resonanz anregt und zur Erzeugung von Spinströmen in die anliegende nichtmagnetische Schicht führt. Durch Variierung der Pt-Schichtdicke beobachten wir einen Anstieg der gemessenen effektiven Gilbert-Dämpfung (α_{eff}) bei den Fe/Pt-Doppelschicht-Proben, die bereits bei Pt-Schichtdicken von 1 nm in Sättigung übergeht. Wir vergleichen unsere Daten mit verschiedenen Referenzproben und zeigen wie wichtig die Wahl der Referenz für α_{eff} ist. Weiterhin zeigen wir die unterschiedlichen Beiträge auf, die zu einem erhöhten Wert α_{eff} beitragen. Die “spin mixing conductance” wird dann in Bezug auf die am besten geeignete Referenzprobe berechnet.

Bericht 4.8 bezieht sich auf die Umwandlung von Magnonenströmen in Ladungsströme durch den Spin-Pumping-Effekt und addressiert die in Bericht 4.7 vorher genannte Fe/Pt-Probenserie. Hier beschreiben wir den Einfluss der Kristallstruktur auf die Spin-Pumping-Experimente. Die Anregung entlang der magnetisch leichten oder der harten Achse weist deutliche Unterschiede in der Spin-Pumping-Anregung auf. Durch die Verwendung des ISHE wurde das Signal aufgrund von Spin- Pumping bei zwei verschiedenen Werten des externen magnetischen Felds bei gleicher Frequenz entlang der harten Achse gemessen. Die Ursache dessen liegt in der stark anisotropen Natur der Proben. Die symmetrische als auch die antisymmetrische Komponente der gemessenen Spannung aufgrund des ISHE nehmen mit steigender Pt-Schichtdicke wegen der Abschirmung der Mikrowellenanregung aufgrund der Pt-Schicht und der Spin-Diffusionslänge in Pt ab.

In Bericht 4.9 wird der Einfluss einer isolierenden MgO-Schicht, eingefügt zwischen der Fe- und Pt-Schicht, auf das Spin-Pumping präsentiert. Das gute Wachstum von MgO auf Fe und dessen Tunnel-Eigenschaften macht das Fe/MgO/Pt-System zu einem sehr interessanten Kandidaten, um den physikalischen Mechanismus des Spin-Pumping in solchen Strukturen zu enthüllen. Wir

zeigen, dass die effektive Gilbert-Dämpfung α_{eff} mit der MgO-Schichtdicke abnimmt, hingegen aber die gemessene Spannung mit dickeren MgO-Barrieren zunimmt. Weiterhin nimmt der symmetrische Anteil des Signals mit der MgO-Schichtdicke zu.

Bericht 4.10 verwendet ein wohlbekanntes metallisches System in anderer Weise für die *Magnon-Spintronik*: In einem mikrostrukturierten Py-Wellenleiter konvertieren wir die Phaseninformation einer Spinwelle in eine Amplitudeninformation durch die Anwendung von lokalisertem parallelem parametrischen Pumpen im nicht-adiabatischem Regime. Die Wellennatur des Magnons erlaubt es uns die Information nicht nur in der Amplitude, sondern auch in der Phase einer Spinwelle zu kodieren, was einen zusätzlichen Freiheitsgrad erschließt. Demnach könnte die Phasen-zu-Amplituden-Umwandlung aus diesem Bericht helfen die *Magnon-Spintronik* mit der heutigen komplementären Metalloxid-Halbleiter-Technologie (CMOS) zu verbinden. Die maximale und minimale Verstärkung der Signalwelle in unserem Wellenleiter variiert um einen hohen Faktor von 10, was eine hohe Zuverlässigkeit für den Ausleseprozess und eine Erhöhung der Empfindlichkeit für die Detektion von kleinen Signalen sicherstellt.

4.7 Study of fully epitaxial Fe/Pt bilayers for spin pumping by ferromagnetic resonance spectroscopy

A. Conca, S. Keller, L. Mihalceanu, B. Hillebrands, and E.Th. Papaioannou

The generation of pure spin currents without accompanying charge current is of large importance for present spintronics and is called to play a critical role in the design of future spintronic devices. The creation and injection of a spin current into a non-magnetic (NM) material from a ferromagnetic (FM) one is commonly referred to as spin pumping. In spin pumping experiments [1, 2], the magnetization of a ferromagnetic layer is typically excited by a microwave field and the generation of the spin current is maximized when the ferromagnetic resonance (FMR) condition is fulfilled.

In the last years a large interest in the measurement of spin pumping properties in FM/NM layers with metallic [3–9] and non-metallic [10, 11] FM layers have been reported. In many cases the spin current is detected using the inverse spin Hall effect (ISHE). Here we report on a study of spin pumping on the FMR properties of fully epitaxial Fe(100)/Pt layer systems and discuss the possible origin of the different observed phenomena.

Figure 1a shows a typical sample FMR spectrum with the real and imaginary part of the transmission parameter $\tilde{S}_{12}$ for a Fe(12 nm)/Pt(10 nm) bilayer system for a frequency of 14.8 GHz. Following the approach used by Kalarickal *et al.* [12] the spectra were fitted (lines) using the expression

$$\tilde{S}_{12}(H_{\mathrm{ext}}) = S_0 + S(H_{\mathrm{ext}})e^{i\phi} \quad \text{with} \quad S(H_{\mathrm{ext}}) = A \cdot \frac{1}{H_{\mathrm{FMR}}^2 - H_{\mathrm{ext}}(H_{\mathrm{ext}} - i\Delta H)} \quad , \tag{1}$$

where H_{ext} is the external applied field, H_{FMR} the resonance field and ΔH is the linewidth. S_0 and A are an offset and a scaling parameter, respectively. ϕ is a phase-shift adjustment parameter. With the extracted data, the dependence of the resonance frequency on the external applied is used to obtain the effective saturation magnetization M_{eff} using Kittel's formula [13] for measurements where H_{ext} is parallel to the easy axis:

$$f_{\mathrm{FMR}} = \frac{|\gamma|\,\mu_0}{2\pi}\sqrt{(H_{\mathrm{ext}} + H_{\mathrm{ani}})(H_{\mathrm{ext}} + H_{\mathrm{ani}} + M_{\mathrm{eff}})} \quad , \tag{2}$$

where H_{ani} is the anisotropy field and γ is the gyromagnetic ratio. An example of this is shown in Fig. 1b for a Fe/MgO(10 nm) reference sample. The Gilbert damping parameter α is accessible

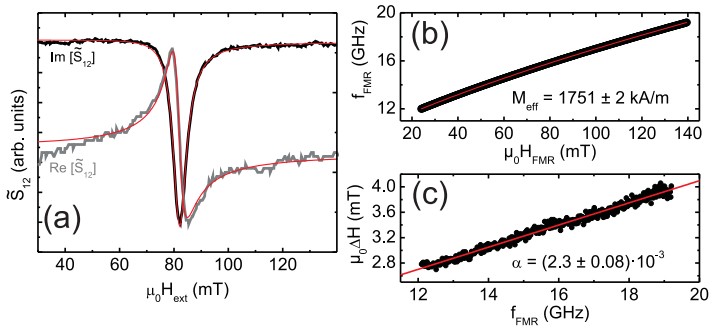

Fig. 1: (a) Exemplary FMR spectrum for a Fe(12nm)/Pt(10nm) bilayer measured at 14.8 GHz showing the real and imaginary part of $\tilde{S}_{12}$. (b) Dependence of the resonance frequency on the applied field for a Fe(12nm)/MgO(10nm) reference sample. The line is a fit to Kittel's formula [13] (Eq. 2). (c) Dependence of the resonance linewidth on the frequency for the same sample. The line is a linear fit to Eq. 3.

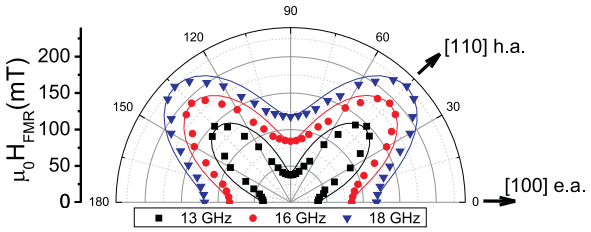

Fig. 2: Dependence of the resonance field H_{FMR} on the azimuthal in-plane angle ϕ for three fixed resonance frequencies for a Fe(12 nm)/MgO(10 nm) sample. The lines are fits to Eq. 4. The crystallographic Fe directions and the magnetic easy (e.a.) and hard axis (h.a.) are labeled.

via the dependence of the linewidth on the resonance frequency as shown in Fig. 1c for the same sample. The line is a linear fit to

$$\Delta H = \Delta H_0 + \frac{4\pi\alpha f_{\mathrm{FMR}}}{\gamma} \quad . \tag{3}$$

Here, ΔH_0 is the inhomogenous broadening and is related to film quality.

The study of the in-plane anisotropic properties of the samples was performed by measuring the resonance field H_{FMR} dependence on the azimuthal angle. Figure 2 shows the H_{FMR} angular dependence for three fixed frequencies for a Fe(12 nm)/MgO(10 nm) reference sample. A four-fold anisotropy, as expected for the cubic lattice of Fe can clearly be recognized. Assuming a perfect collinearity between magnetization vector and external field, and with no additional anisotropy contributions, H_{FMR} can be modeled as [14]:

$$H_{\mathrm{FMR}} = \tilde{H}_{\mathrm{FMR}} + \frac{2K_1}{M_s}\cos(4\phi) \quad , \tag{4}$$

where K_1 is the biaxial anisotropy constant and ϕ the in-plane azimuthal angle. The fraction $\frac{2K_1}{M_s}$ is directly the anisotropy field H_{ani}. The lines in Fig. 2 are fits to this formula from which a value of $H_{\mathrm{ani}} = 52.4 \pm 0.8\,\mathrm{mT}$ is extracted. Using the known saturation magnetization of Fe, $1750\,\mathrm{kA/m}$ (measured for instance by VSM in Ref [15]), we obtain a value for K_1 of $45850 \pm 70\,\mathrm{J/m^3}$. This value is very close to the value of $44500 \pm 600\,\mathrm{J/m^3}$ or $39000\,\mathrm{J/m^3}$ reported for thin films [16, 17] and still lower than the bulk value [18], $48000 \pm 1000\,\mathrm{J/m^3}$. The obtained value for K_1, together with the one extracted from the Kittel fit for this same sample, $M_{\mathrm{eff}} = 1751 \pm 2\,\mathrm{kA/m}$, proves the high quality properties of the films.

Figure 3b shows the dependence of the measured effective Gilbert damping parameter α_{eff} on the Pt thickness. The values for the reference samples Fe/MgO and Fe/MgO/Pt and for Fe/Al bilayers are shown. We observe an increase of the measured α_{eff} for the Fe/Pt bilayers compared with the MgO reference layers and a saturation point is found already for the smallest of our Pt thickness (1 nm). The measured α_{eff} can be separated into different contributions:

$$\alpha_{\mathrm{eff}} = \alpha_0 + \alpha_{\mathrm{mpe}} + \alpha_{\mathrm{sp}} + \alpha_{\mathrm{i}} \quad . \tag{5}$$

Here α_0 is the intrinsic damping parameter which can be defined as characteristic of the material under investigation (growth conditions however may influence it strongly), α_{mpe} is the contribution due to the dynamic coupling between the ordered spins in Pt due to the magnetic proximity effect (MPE) and the Fe magnetization, α_{sp} is the result of the losses by the spin current generated in the ferromagnetic layer by the precession of the magnetization and that flows into the Pt layer (spin pumping), and α_{i} is the increase of damping due to other interfacial effects.

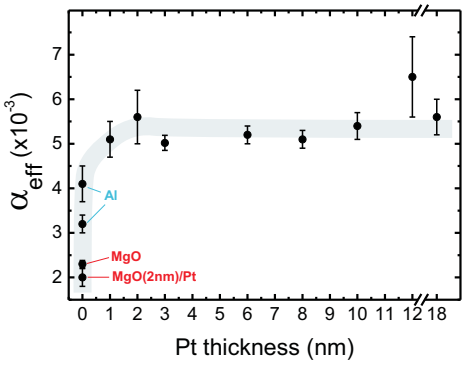

Fig. 3: Dependence of the effective damping parameter α_{eff} on the Pt thickness for Fe/Pt bilayers. For comparison also the values for the reference samples (Fe/Al, Fe/MgO and Fe/MgO/Pt) are shown. The line is a guide to the eye.

The relative weights of α_{mpe} and α_{sp} in their contribution to α_{eff} is still under discussion in the magnetism community. Some results in the literature limit the influence of the MPE in metallic FM/Pt bilayers. By inserting a thin metallic and non magnetic interlayer with a large spin diffusion length λ_{sd} it is possible to eliminate the MPE without a strong reduction of the injected spin current. Zhang *et al.* [6] showed that the introduction of a thin Cu interlayer in Co/Pt has a reduced impact in the measured spin Hall angle and therefore MPE has only a small influence in the FM/Pt layers. However, a different conclusion can be extracted from data reported elsewhere for the same layer system [8]. There the increase in α_{eff} compared to Co/Al reference samples for Co/Pt is a factor of two larger than for Co/Cu/Pt pointing to similar values for α_{mpe} and α_{sp}. Other studies with NiFe/Pt and CoFeB/Pt and several different metallic interlayers seems to point in the same direction [7].

The contribution due to spin pumping is related to the spin mixing conductance, which describes the interaction of the spins with the magnetization at the FM/NM interface [1]:

$$\Delta\alpha_{\mathrm{sp}} = \frac{\gamma\hbar}{4\pi M_s\, d_{\mathrm{FM}}} g^{\uparrow\downarrow} \quad . \tag{6}$$

It has to be pointed out that this formula is only valid in the case of a Gilbert-like damping, i.e. with $\Delta H \propto f_{\mathrm{FMR}}$ as in Eq. 3. This is always the observed situation in our samples. The theoretical description [2] of the spin mixing conductance $g^{\uparrow\downarrow}$ for FM/NM interfaces indicates that the value is only defined by the nature of the material used as NM and for this reason it must be the same for all FM/Pt combinations. However, the relative weights of α_{mpe} and α_{sp} may be different depending on interface quality being the roughness one of the critical parameters. Since the separation of contributions is not possible, it is more correct to speak of an effective spin mixing conductance $g_{\mathrm{eff}}^{\uparrow\downarrow}$ for the values obtained using Eq. 6.

In any case, the use of Eq. 6 requires the identification of an adequate reference layer system where the losses by spin pumping and MPE are close to zero allowing for the measurement of the value for α_0. This is a critical point since by the contribution of interfacial effects, α_{i} can lead to a wrong estimation of $g_{\mathrm{eff}}^{\uparrow\downarrow}$. For our estimation we deposited four reference samples corresponding to two kinds of interfaces, Fe/Al and Fe/MgO. For obvious reasons the MPE contribution is zero. Since MgO blocks spin pumping [19] also the contribution α_{sp} vanishes. Both systems (see Fig. 3), the Fe/MgO and the Fe/MgO/Pt show, considering the error bars, the same value for α_{eff}. This value ($(2.15 \pm 0.15) \times 10^{-3}$, average of both systems) is identified as α_0 and it is compatible with literature results [20]. The case for the Fe/Al samples is different and shows how important it is to choose a correct reference layer system. Spin pumping is indeed taking place also here but due to the large λ_{sd} of $350 - 600\,\mathrm{nm}$ in Al, the increase in damping should be negligible and a value close to α_0 is expected. However, as seen in Fig. 3, a larger value of $(3.7 \pm 0.5) \times 10^{-3}$ is measured.

This can be only a result of the additional interface contributions included in α_{i}.

For the calculation of $\Delta\alpha_{\mathrm{eff}}$ we average all the values obtained for the Fe/Pt bilayers. With this a value of $g_{\mathrm{eff}}^{\uparrow\downarrow} = (4.9 \pm 0.5) \times 10^{19}\,\mathrm{m}^{-2}$ is obtained. Our value lays in the upper range of the typical values reported for NiFe/Pt bilayers [3–7] and it is very similar to the values reported for Co/Pt or CoFeB/Pt [7, 8]. Still, the variation of values for $g_{\mathrm{eff}}^{\uparrow\downarrow}$ in the literature is large. We believe that this is due the different contribution of the interface effects included in α_{i}, also affecting the choice of the reference layer and the different strength of α_{mpe}.

Financial support by Carl Zeiss Stiftung is acknowledged.

References

[1] Y. Tserkovnyak, A. Brataas, G.E.W. Bauer, B.I. Halperin, *Nonlocal magnetization dynamics in ferromagnetic heterostructures*, Rev. Mod. Phys., **77**, No. 4, 1375 (2005).

[2] Y. Tserkovnyak, A. Brataas, G.E.W. Bauer, *Dynamic exchange coupling in magnetic bilayers*, Phys. Rev. Lett. **88**, 117601 (2002).

[3] A. Azevedo, L.H. Vilela-Leão, R.L. Rodríguez-Suárez, A.F. Lacerda Santos, S.M. Rezende, *Spin pumping and anisotropic magnetoresistance voltages in magnetic bilayers*, Phys. Rev. B **83**, 144402 (2011).

[4] M. Obstbaum, M. Härtinger, H.G. Bauer, T. Meier, F. Swientek, C.H. Back, G. Woltersdorf, *Inverse spin Hall effect in $Ni_{81}Fe_{19}$/normal-metal bilayers*, Phys. Rev. B **89**, 060407(R) (2014).

[5] Z. Feng, J. Hu, L. Sun, B. You, D .Wu, J. Du, W. Zhang, A. Hu, Y. Yang, D.M. Tang, B.S. Zhang, H.F. Ding, *Spin Hall angle quantification from spin pumping and microwave photoresistance*, Phys. Rev. B **85**, 214423 (2012).

[6] W. Zhang, W. Han, X. Jiang, S.-H. Yang, S.S.P. Parkin, *Role of transparency of platinum-ferromagnet interfaces in determining the intrinsic magnitude of the spin Hall effect*, Nat. Physics **11**, 496 (2015).

[7] A. Ruiz-Calaforra, T. Brächer, V. Lauer, P. Pirro, B. Heinz, M. Geilen, A.V. Chumak, A. Conca, B. Leven, B. Hillebrands, *The role of the non-magnetic material in spin pumping and magnetization dynamics in NiFe and CoFeB multilayer systems*, J. Appl. Phys. **117**, 163901 (2015).

[8] J.-C. Rojas-Sánchez, N. Reyren, P. Laczkowski, W. Savero, J.-P. Attané, C. Deranlot, M. Jamet, *Spin pumping and ISHE in Pt: The essential role of spin-memory loss at metallic interfaces*, Phys. Rev. Lett. **112**, 106602 (2014).

[9] E.Th. Papaioannou, P. Fuhrmann, M.B. Jungfleisch, T. Brächer, P. Pirro, V. Lauer, J. Lösch, B. Hillebrands, *Optimizing the spin-pumping induced inverse spin Hall voltage by crystal growth in Fe/Pt bilayers*, Appl. Phys. Lett. **103**, 162401 (2013).

[10] Y. Sun, H. Chang, M. Kabatek, Y.-Y. Song, Z. Wang, M. Jantz, W. Schneider, M. Wu, E. Montoya, B. Kardasz, B. Heinrich, S.G.E. te Velthuis, H. Schultheiss, A. Hoffmann, *Damping in yttrium iron garnet nanoscale films capped by platinum*, Phys. Rev. Lett. **111**, 106601 (2013).

[11] B. Heinrich, C. Burrowes, E. Montoya, B. Kardasz, E. Girt, Y.-Y. Song, Y. Sun, M. Wu, *Spin pumping at the magnetic insulator (YIG)/normal metal (Au) interfaces*, Phys. Rev. Lett. **107**, 066604 (2011).

[12] S.S. Kalarickal, P. Krivosik, M. Wu, C.E. Patton, M.L. Schneider, P. Kabos, T.J. Silva, J.P. Nibarger, *Ferromagnetic resonance linewidth in metallic thin films*, J. Appl. Phys. **99**, 093909 (2006).

[13] C. Kittel, *On the theory of ferromagnetic resonance absorption*, Phys. Rev. **73**, 155 (1948).

[14] B. Heinrich, J.F. Cochran, M. Kowalewski, J. Kirschner, Z. Celinski, A.S. Arrott, K. Myrtle, *Magnetic anisotropies and exchange coupling in ultrathin fcc Co(001) structures*, Phys. Rev. B, **44**, 9348 (1991).

[15] F. Bonell, S. Andrieu, F. Bertran, P. Lefèvre, A.T. Ibrahimi, E. Snoeck, C. Tiusan, F. Montaigne, *MgO-based magnetic tunnel junctions using Fe-V electrodes*, IEEE Trans. Magn. **45**, NO. 10, 3467 (2009).

[16] N.A. Morley, M.R.J Gibbs, E. Ahmad, I.G. Will, Y.B. Xu, *Magnetostriction and magnetocrystalline anisotropy constants of ultrathin epitaxial Fe films on GaAs*, J. Phys.: Condens. Matter **17**, 1201 (2005).

[17] H. Ikeya, Y. Takahashi, N. Inaba, F. Kirino, M. Ohtake, M. Futamoto, *Magnetic properties of Fe thin films on GaAs deposited by RF magnetron sputtering*, J. of Physics: Conference Series **266**, 012116 (2011).

[18] C.D. Graham, Jr., *Magnetocrystalline anisotropy constants of Fe at room temperature and below*, Phys. Rev. **112**, 1117 (1958).

[19] K. Eid, R. Fonck, M.A. Darwish, W.P. Pratt, *CPP magnetoresistance properties of Ru and Co/Ru interfaces*, J. Bass, J. Appl. Phys. **91**, 8102 (2002).

[20] R. Meckenstock, D. Spoddig, Z. Frait, V. Kambersky, J. Pelzla, *Anisotropic Gilbert damping in epitaxial Fe films on InAs(001)*, J. of Magn. and Magn. Materials **272-276**, 1203 (2004).

4.8 Pt thickness dependence of spin pumping in epitaxial Fe/Pt bilayers

S. Keller, L. Mihalceanu, J. Greser, A. Conca, V. Lauer, B. Hillebrands, and E.Th. Papaioannou

In collaboration with Jörg Lösch and Alexander Brodyanski, Institut für Oberflächen- und Schichtanalytik (IFOS), Trippstadter Str. 120, 67663 Kaiserslautern, Germany

Magnetic bilayers composed of a ferromagnetic and a non-magnetic metal are key for the generation and detection of spin currents through spin torque [1] and spin pumping effects [2]. The spin pumping effect allows for the injection of a spin current from a ferromagnetic (FM) layer into an attached non-magnetic metal (NM) layer [3]. This spin current is subsequently transformed into a charge current by the inverse spin Hall effect (ISHE) [4]. Although many aspects of magnetization dynamics in FM/NM bilayers have been investigated by means of spin pumping and the inverse spin Hall effect (ISHE) in different materials [2, 5], to our knowledge no systematic work on epitaxial samples has been performed yet. Epitaxially grown Fe/Pt interfaces can strongly affect the spin pumping effect due to the structural quality of the interface and the induced magnetic anisotropy of the system.

Here, we present our studies on the spin pumping effect in epitaxially grown Fe/Pt bilayers and show new insights into the influence of the Pt thickness on the spin pumping effect.

In a previous publication [6], we have shown that by modifying the structural and interfacial quality of the Fe/Pt bilayers by adjusting the growth temperature to 300 °C, the spin pumping effect can be enhanced. In the previous Annual Report 2014 [7] we first addressed the influence of the platinum thickness on the spin pumping by performing measurements on a few samples.

For this work, bilayers with a constant Fe layer thickness of 12 nm and different Pt layer thicknesses varying from 1 nm to 18 nm were grown on MgO(100) substrates at 300 °C substrate temperature by electron-beam evaporation in an ultrahigh vacuum (UHV) chamber with a base pressure of 5.0×10^{-11} mbar. A reference sample consisting of Fe(12 nm)/MgO(10 nm) was also fabricated at the same experimental conditions as the Fe/Pt samples. With MgO as capping layer it is supposed to eliminate spin pumping.

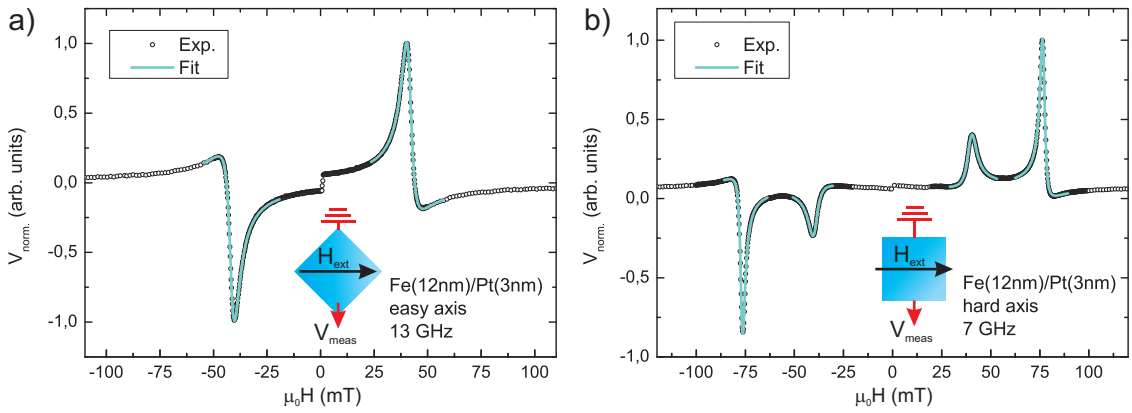

Fig. 1: Spin pumping measurements of the Fe(12nm)/Pt(3nm) sample in a) easy axis configuration with microwave excitation at 13 GHz and b) hard axis configuration with microwave excitation at 7 GHz.

In the spin pumping experiments the magnetization dynamics of the epitaxial Fe/Pt bilayers are excited by a microwave magnetic field generated by a 600 µm Cu microstrip antenna, while an external in-plane magnetizing field is swept. We measure the DC part of the voltage which arises in-plane perpendicular to the external magnetic field due to various effects discussed in Refs. [6,8] by using a lock-in technique. In Fig. 1 the normalized measurement voltage (V_{norm}) as a function of the external magnetic field applied in a) the Fe[100] and b) the Fe[110] direction of the Fe lattice is presented, at the excitation frequencies of 13 GHz and 7 GHz, respectively. With the field reversal a sign change in V_{meas} is observed at the same absolute field values. The field values of the peaks correspond to the ferromagnetic resonance (FMR) condition of the applied frequencies. In the hard axis configuration (Fig. 1b) second peaks with lower voltage amplitudes occur at lower fields (inner peaks). The reason for the presence of the additional FMR peak is the splitting of the Kittel formula along the hard axis of the FMR in two branches due to the pronounced cubic and uniaxial anisotropy terms [6].

The peaks can be fitted individually by symmetrical and antisymmetrical Lorentz functions:

$$V_{meas} = V_{\mathrm{sym}} \frac{(\Delta H)^2}{(H - H_{\mathrm{FMR}})^2 + (\Delta H)^2} + V_{\mathrm{asym}} \frac{-2\Delta H (H - H_{\mathrm{FMR}})}{(H - H_{\mathrm{FMR}})^2 + (\Delta H)^2} \quad , \tag{1}$$

where V_{sym} is the amplitude of the symmetric part, V_{asym} is the amplitude of the antisymmetric part, ΔH is the linewidth, H is the applied external magnetic field, and H_{FMR} is the corresponding FMR field value.

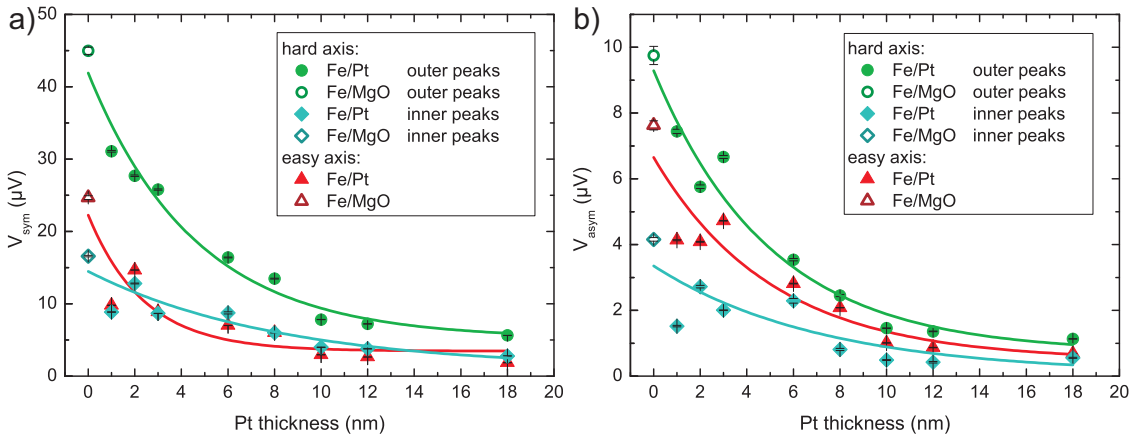

Fig. 2: Voltage amplitudes of the symmetric a) and antisymmetric b) part of the fitting function. The solid lines shows the decay trend of the data points into non-zero saturation.

The symmetrical and antisymmetrical voltage amplitudes of our spin pumping measurements can be seen in Fig. 2. The data points of zero Pt thickness refer to the Fe/MgO reference sample. As one can see, the voltage amplitudes decrease exponentially with rising Pt thickness. The outer peaks of the hard axis configuration exhibit the highest values in our experiments, while the hard axis inner peaks, compared to the peaks of the easy axis configuration, have similar symmetric but different antisymmetric values. The voltage amplitudes of all peaks decrease exponentially down to non-zero saturation values reached for Pt thicknesses above 10 nm. Two alternative and non-mutually excluding explanations can be applied here: First, the measurements are carried out by placing the samples with the Pt side towards the antenna. By this means, the excitation of

the magnetization dynamics in the Fe film is reduced due to the shielding effect by the Pt layer. Reference [13] describes that stripline microwave fields are strongly attenuated inside metal films with reasonable electrical conductivity in the sub-skin-depth regime (i.e. attenuation by a factor of 10 with a metal layer thickness around 10 nm). Therefore an increase in Pt thickness increases the shielding effect as well. In Fig. 3 the relative absorbed microwave power of the spin pumping measurements is plotted. The power is decreasing with increasing Pt thickness. This behaviour shows that the shielding effect of Pt should be taken into consideration.

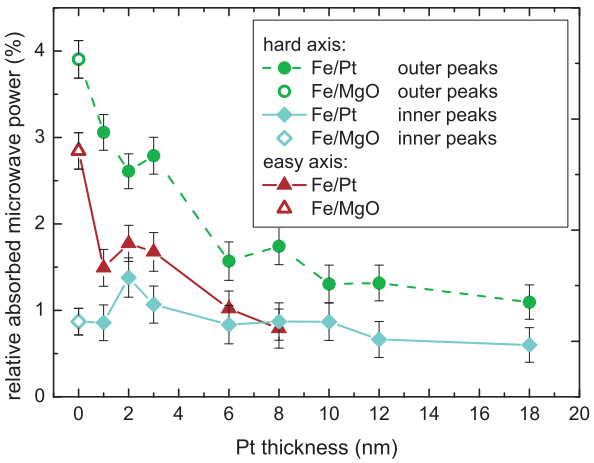

Fig. 3: Relative absorbed microwave power of the spin pumping measurements (absorbed microwave power at FMR relative to the microwave power off the FMR condition).

Second, the spin diffusion length of Pt has been reported to be of the order of 10 nm or less [9–11, 14]. Reference [14] shows, that the ISHE voltage first rises with the Pt layer thickness until reaching its maximum around the spin diffusion length, and then decreases with further increase of the Pt thickness into non-zero saturation. The latter is also observed in our spin pumping measurements. Besides the ISHE other DC effects take place in metallic ferromagnets at FMR [12], which are superimposing with the ISHE and therefore hinder the investigation of the spin pumping effect. These rectification effects are difficult to separate from the ISHE. A spin pumping measurement setup, where the external magnetic field can be rotated, is one possible approach to further elucidate the measured voltages [9].

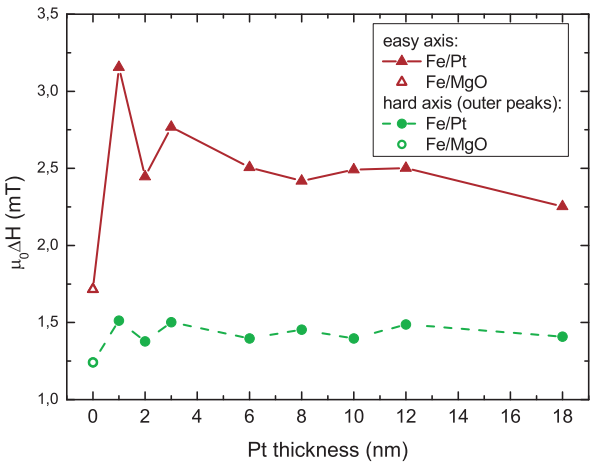

Fig. 4: Linewidths of the spin pumping measurements in the easy and the hard axis configuration.

In Fig. 4 the linewidth of the fits according to Eq. 1 is shown, which is directly correlated to the effective damping of the sample, including the contributions of spin pumping. The damping, and thus, the linewidth increases with the amount of spin pumping, whereas the influence of other effects is assumed to be constant. For easy and hard axis measurement configuration the Fe/MgO reference sample, where no spin pumping is expected to contribute to the damping, exhibits smaller linewidths than the Fe/Pt samples. The difference in linewidth for the easy and hard axis spin pumping measurements is due to the difference in excitation frequency, 13 GHz in easy and 7 GHz in hard axis configuration, respectively. The linewidth of the Fe/Pt samples in hard axis configuration stays almost constant with the varying Pt thickness, while the linewidth in easy axis measurements is decreasing with increasing Pt thickness and has a maximum at very low Pt thicknesses.

Our study shows the impact of epitaxial growth to spin pumping, where a second FMR peak occurs in hard axis measurement configuration. The Fe/MgO reference sample exhibits the highest voltage amplitudes in the spin pumping measurements, while the voltages for the Fe/Pt samples decrease exponentially and the linewidth of the spin pumping measurements in easy axis direction only show a slight decrease with increasing Pt thickness.

The Carl Zeiss Stiftung is gratefully acknowledged for financial support.

References

[1] A. Brataas, A.D. Kent, H. Ohno, *Current-induced torques in magnetic materials*, Nature Mater. **11**, 372 (2012).
[2] A. Hoffmann, *Spin Hall effects in metals*, IEEE Transactions On Magnetics **49**, 5172 (2013).
[3] Y. Tserkovnyak, A. Brataas, G.E.W. Bauer, *Spin pumping and magnetization dynamics in metallic multilayers*, Phys. Rev. B **66**, 224403 (1999).
[4] J.E. Hirsch, *Spin Hall effect*, Phys. Rev. Lett. **83**, 1834 (2002).
[5] D. Czeschka, L. Dreher, M.S. Brandt, M. Weiler, M. Althammer, I.M. Imort, G. Reiss, A. Thomas, W. Schoch, W. Limmer, H. Huebl, R. Gross, S.T.B. Goennenwein, *Scaling behavior of the spin pumping effect in ferromagnet-platinum bilayers*, Phys. Rev. Lett. **107**, 046601 (2011).
[6] E.Th. Papaioannou, P. Fuhrmann, M.B. Jungfleisch, T. Brächer, P. Pirro, V. Lauer, J. Lösch, B. Hillebrands, *Optimizing the spin-pumping induced inverse spin Hall voltage by crystal growth in Fe/Pt bilayers*, Appl. Phys. Lett. **103**, 162401 (2013).
[7] S. Keller, L. Mihalceanu, A. Conca, V. Lauer, B. Hillebrands, E.Th. Papaioannou, *Platinum thickness dependence on the spin pumping in Fe|Pt bilayers*, Annual Report 2014:
http://www.physik.uni-kl.de/hillebrands/publications/annual-reports/annual-report-2014.
[8] M.B. Jungfleisch, V. Lauer, R. Neb, A.V. Chumak, B. Hillebrands, *Improvement of the yttrium iron garnet/platinum interface for spin pumping-based applications*, Appl. Phys. Lett. **103**, 022411 (2013).
[9] O. Mosendz, V. Vlaminck, J.E. Pearson, F.Y. Fradin, G.E.W. Bauer, S.D. Bader, A. Hoffmann, *Detection and quantification of inverse spin Hall effect from spin pumping in permalloy/normal metal bilayers*, Phys. Rev. B **82**, 214403 (2010).
[10] J.-C. Rojas-Sánchez, N. Reyren, P. Laczkowski, W. Savero, J.-P. Attané, C. Deranlot, M. Jamet, *Spin pumping and inverse spin Hall effect in platinum: The essential role of spin-memory loss at metallic interfaces*, Phys. Rev. Lett. **112**, 106602 (2014).
[11] Z. Feng, J. Hu, L. Sun, B. You, D .Wu, J. Du, W. Zhang, A. Hu, Y. Yang, D.M. Tang, B.S. Zhang, H.F. Ding, *Spin Hall angle quantification from spin pumping and microwave photoresistance* Phys. Rev. B **85**, 214423 (2012).
[12] H.J. Juretschke, *Electromagnetic theory of dc effects in ferromagnetic resonance*, J. Appl. Phys. **31**, 1401 (1960).
[13] I.S. Maksymov, M. Kostylev, *Broadband stripline ferromagnetic resonance spectroscopy of ferromagnetic films, multilayers and nanostructures*, Physica E **69**, 253 (2015).
[14] A. Azevedo, L.H. Vilela-Leão, R.L. Rodríguez-Suárez, A.F. Lacerdo Santos, S.M. Rezende, *Spin pumping and anisotropic magnetoresistance voltages in magnetic bilayers: Theory and experiment*, Phys. Rev. B **83**, 144402 (2011).

4.9 Investigation of the influence of a MgO interlayer on spin pumping in epitaxial systems

L. Mihalceanu, S. Keller, A. Conca, B. Hillebrands, and E.Th. Papaioannou

In collaboration with G. Vourlias, K. Symeonidis, Department of Physics, Aristotle University of Thessaloniki, Thessaloniki 54124, Greece

Efficient generation of spin currents belongs to the key aspects of spintronics research aiming at the development of nanoelectronics devices with low power consumption [1]. The spin pumping effect, which is essentially an interfacial effect, is a promising candidate on this route. In this work the spin current gets injected by the spin pumping effect from the ferromagnetic layer into the non magnetic layer at the Fe/MgO and the MgO/Pt interface, and it is detected by measuring the inverse spin Hall effect (ISHE) voltage [1]. The study of Fe/MgO interface is on the focus of research on tunneling based magnetoresistance devices, like in the Fe/MgO/Fe stacks [2] and has already been widely investigated. Here, the influence of an MgO tunneling barrier interlayer on the spin pumping is studied and will be presented for the measurements along the [100] direction of Fe. Suppression of the spin pumping efficiency for Py/MgO/Pt [3], titanium interlayers [4] and nano-oxide interlayers [5] was previously reported. The effect of an MgO interlayer on the crystallographic growth behavior of the material systems is examined as well.

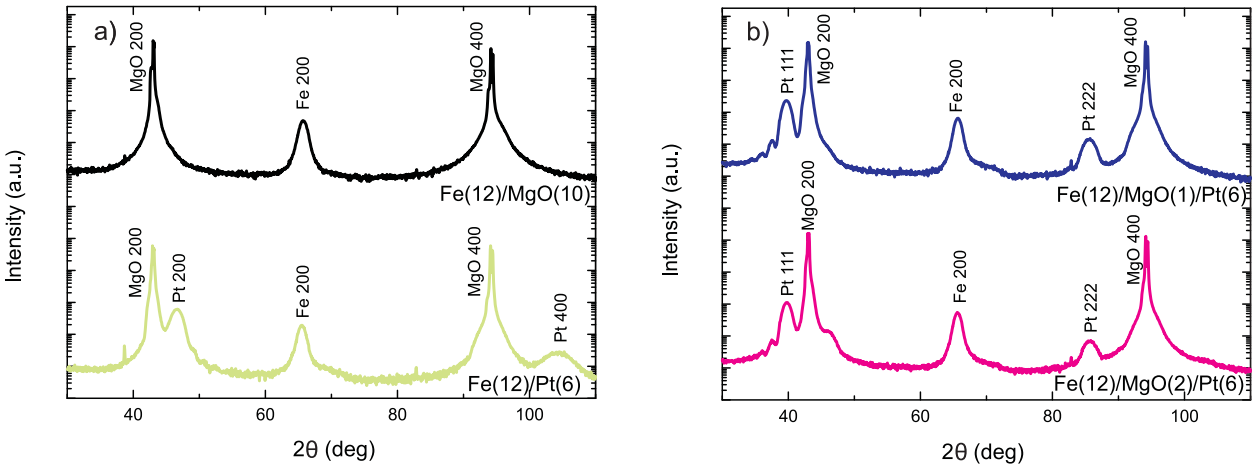

Fig. 1: XRD $\theta - 2\theta$ scans of the Fe/MgO/Pt series showing the crystallographic properties a) for the reference samples and b) for the Fe/MgO/Pt layer system. For better visualization the spectra are shifted along the y-axis.

Spin pumping was investigated on Fe(12 nm)/MgO/Pt(6 nm) samples with varying thickness of the MgO interlayer (0, 1, and 2 nm). This allows for the analysis of the thickness dependence of an MgO interlayer on spin pumping from Fe to Pt. The Fe(12 nm)/MgO(10 nm) sample was used as reference for the spin pumping measurements, as no spin current is generated, while the Fe(12 nm)/Pt(6 nm) sample was taken as a reference allowing for the comparison of spin pumping in systems with and without interlayer. The samples were grown by molecular beam epitaxy on the MgO(100) substrates with the size of 10 x 10 x 0.5 nm.

The crystallographic analysis was performed by standard $\theta - 2\theta$ X-ray diffraction (XRD) scans, which are shown in Fig. 1. The presence of the MgO interlayer has an impact on the crystallographic orientation of Pt.

Fe on MgO grows epitaxially, as well as Pt grows on top of Fe with (200) orientation while Pt on MgO has a textured growth with a (111) orientation. XRD studies also confirm the high quality of the samples. Atomic force microscopy (AFM) provides information about the grain size and morphology of the Pt layer. According to [6] the T_S/T_M ratio with T_S being the temperature of the substrate and T_M the melting temperature of the grown layer can be used to classify the grain size structure of the Pt. This leads for the produced samples to the conclusion that the Pt layer has the same grain size at the interface as well as on the surface. The root mean square (RMS) roughness of the Pt surface was determined to be 0.16 ± 0.03 nm on average.

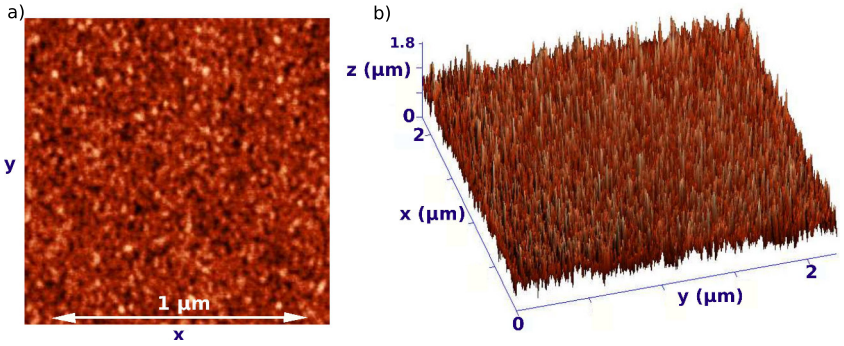

Fig. 2: AFM images of the Fe/MgO/Pt sample with 1 nm nominal MgO interlayer. a) top view, b) surface plot.

In the ferromagnetic resonance (FMR) setup the sample is placed onto a microwave antenna generating a dynamic magnetic Oersted field oriented perpendicularly to an external static magnetic field. Detection of the FMR signal then occurs by using a vector network analyzer (VNA). The Gilbert damping parameter α is obtained by fitting the resonance frequency dependence of the linewidth [7]:

$$\Delta H = \Delta H_0 + \frac{4\pi\alpha f_{\mathrm{FMR}}}{\gamma} \quad , \tag{1}$$

where ΔH_0 is the inhomogeneous broadening, γ is the gyromagnetic ratio and f_{FMR} the FMR frequency.
The interface effects can be quantified by the spin-mixing conductance [8]:

$$g_{\uparrow\downarrow} = \frac{4\pi M_s d_{\mathrm{FM}}}{\gamma \mu_B}(\alpha - \alpha_{\mathrm{ref}}) \quad . \tag{2}$$

where d_{FM} is the thickness of the ferromagnetic layer, M_s is $1750 \pm 1\,\mathrm{kA/m}$ [9] and α_{ref} the Gilbert damping of the Fe(12 nm)/MgO(10 nm) reference sample. The spin-mixing conductance dependence on MgO thickness is illustrated in Fig. 3.

We observe a decrease of the spin-mixing conductance in samples containing an MgO interlayer in consistency with the former results [3–5], as well as a decrease of the Gilbert damping with increasing MgO interlayer. This trend is correlated to a lower spin current injection from the Fe into the Pt due to the MgO barrier layer, provided that other interface effects influencing the damping can be considered to be constant.

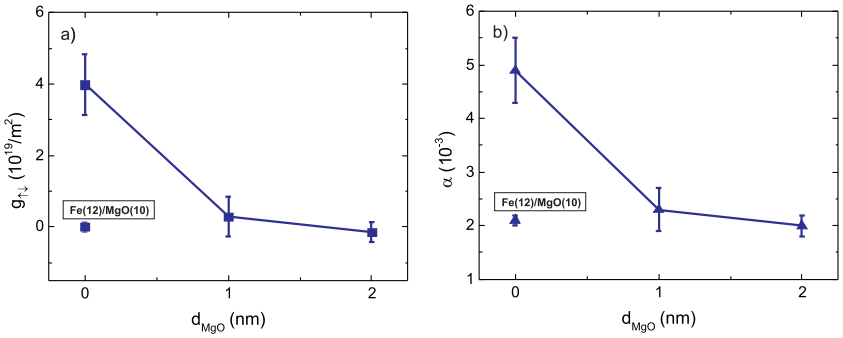

Fig. 3: a) $g_{\uparrow\downarrow}$ and b) α plotted against the nominal d_{MgO} thickness determined by evaporation rate.

Spin pumping was probed by measuring the DC voltage transverse to the external magnetic field. The voltage was recorded by using a lock-in amplifier technique while FMR is excited by a microwave antenna. This DC voltage is assumed to be strongly correlated to the ISHE voltage but at the same time it also contains overlapping contributions of the anisotropic magnetoresistance (AMR) and the anomalous Hall effect (AHE) [11, 12]. While the ISHE voltage is expected to have only symmetric contributions, these rectification effects also contain antisymmetric ones. Thus in order to analyze the DC voltage contributions occurring around the resonance field H_{FMR}, the signal is fitted by an expression containing symmetric and antisymmetric Lorentzian functions [10]:

$$U(H) = U_0 + U_{Sym}\frac{(\Delta H)^2}{(H-H_{\mathrm{FMR}})^2+(\Delta H)^2} - U_{Asym}\frac{\Delta H(H-H_{\mathrm{FMR}})}{(H-H_{\mathrm{FMR}})^2+(\Delta H)^2} \quad , \tag{3}$$

where U_0 is a constant offset, ΔH is the linewidth of the Lorenzian fit curve and H_{FMR} is the magnetic resonance field. The measured voltage together with the fit by Eq. 3 are shown in Fig. 4a.

The obtained linewidth of the detected spin pumping DC voltage is summarized in Fig. 4b and supports the interpretation that with increasing thickness of the MgO layer the spin pumping decreases as also suggested by the decrease of the Gilbert damping parameter with increasing MgO thickness. The reference sample Fe(12 nm)/MgO(10 nm), where no spin pumping is expected, shows the smallest linewidth in the ISHE measurement. The largest linewidth is measured for the Fe(12 nm)/Pt(6 nm) sample with no tunneling barrier. The samples with 1 and 2 nm nominal MgO thickness provide linewidths with values in between the Fe(12 nm)/MgO(10 nm) and Fe(12 nm)/Pt(6 nm) sample, decreasing with MgO thickness.

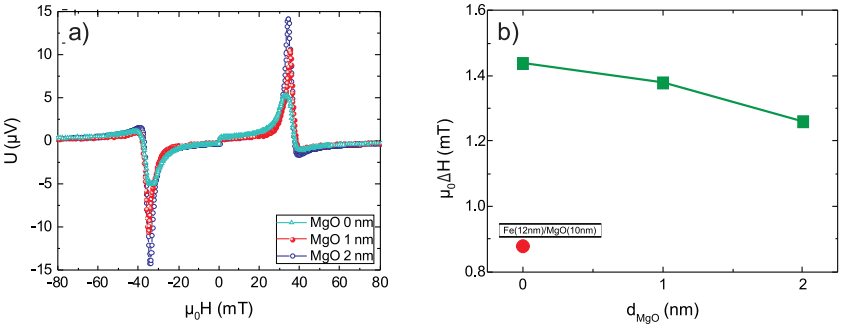

Fig. 4: a) Measurement and fit function of the spin pumping DC voltage plotted against the external applied magnetic field. b) Linewidth of the spin pumping DC voltage peak ΔH plotted against the MgO interlayer thickness.

The symmetric and antisymmetric part of the voltage obtained by the fit function as well as their ratio are summarized in Fig. 5a. The Fe(12 nm)/MgO(10 nm) sample exhibits the largest symmetric and antisymmetric signal. With increasing thickness of the MgO interlayer the signal is also

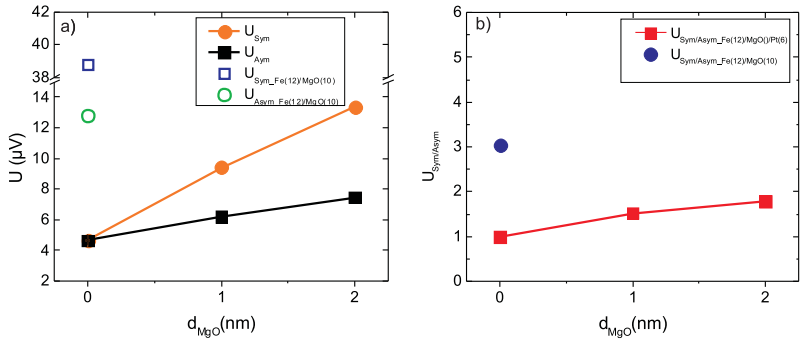

Fig. 5: a) U_{Sym} and U_{Asym} were obtained by fitting and are plotted against the nominal MgO thickness d_{MgO}. b) U_{Sym}/U_{Asym} plotted against the nominal MgO thickness d_{MgO}.

increasing, while the increase in the symmetric signal is more pronounced then the increase in the antisymmetric one. This is approved by the increase of the ratio U_{Sym}/U_{Asym} as shown in Fig. 5b.

In conclusion, we had successfully grown a series of Fe/MgO/Pt samples and characterized the quality of the stacked system by XRD and AFM. We found that Pt orients along a different crystallographic direction when growing on top of MgO instead on top of Fe. By means of the spin pumping FMR measurements we demonstrated that an increasing thickness of the MgO interlayer in Fe/MgO/Pt leads to an increased voltage signal with a more pronounced gain of the symmetric part over the antisymmetric one. One possible interpretation is a decreased rectification contribution, and thus an occurrence of a cleaner injected spin current for the samples containing an MgO barrier, containing less rectification contributions. A more detailed analysis requires additional investigations, particularly angle-resolved measurements.

Financial support from Carl Zeiss Stiftung and from the IKYDA2015 bilateral Greek-German collaboration scheme is gratefully acknowledged.

References

[1] J. Sinova, S.O. Valenzuela, J. Wunderlich, C.H. Back, T. Jungwirth, *Spin Hall effects*, arXiv: 1411.3249, (2014).
[2] W.H. Butler, X.-G. Zhang, T.C. Schulthess, J.M. MacLaren, *Spin-dependent tunneling conductance of Fe|MgO|Fe sandwiches*, Phys. Rev. B **63**, 054416 (2001).
[3] O. Mosendz, J.E. Pearson, F.Y. Fradin, S.D. Bader, A. Hoffmann, *Suppression of spin-pumping by a MgO tunnel-barrier* Appl. Phys. Lett. **96**, 022502 (2010).
[4] H. Nakayama, T. Tashiro, R. Takahashi, Y. Kajiwara, T. Ohtani, K. Ando, R. Iguchi, K. Uchida, T. Yoshino, E. Saitoh, *Suppression of spin pumping in the presence of thin titanium interlayer*, Key Eng. Mater. **508**, 347 (2012).
[5] D.H. Kim, H.H. Kim, C.Y. You, *Suppression of the spin pumping in Pd/$Ni_{81}Fe_{19}$ bilayers with nano-oxide layer*, Appl. Phys. Lett. **99**, 072502 (2011).
[6] M. Oehring *Materials science of thin films*, vol. 2, Academic Press (2002).
[7] A. Conca, J. Greser, T. Sebastian, S. Klingler, B. Obry, B. Leven, B. Hillebrands, *Low spin-wave damping in amorphous CoFeB thin films*, J. Appl. Phys. **113**, 213909 (2013).
[8] K. Carva, I. Turek, *Spin-mixing conductance of thin magnetic films for first principles*, Phys. Rev. B **76**, 104409 (2007).
[9] F. Bonell, S. Andrieu, F. Bertran, P. Lefevre, A.T. Ibrahimi, E. Snoeck, C. Tiusan, F. Montaigne, *MgO-based epitaxial magnetic tunnel junctions using Fe-V electrodes*, IEEE Trans. Magn. **45**, No. 10, 3467 (2009).
[10] J.-C. Rojas-Sánchez, M. Cubukcu, A. Jain, C. Vergnaud, C. Portemont, C. Ducruet, A. Barski, A. Marty, L. Vila, J.-P. Attané, E. Augendre, G. Desfonds, S. Gambarelli, H. Jaffrès, J.-M. George, M. Jamet, *Spin pumping and inverse spin Hall effect in germanium*, Phys. Rev. B **88**, 064403 (2013).
[11] E.Th. Papaioannou, P. Fuhrmann, M.B. Jungfleisch, T. Brächer, P. Pirro, V. Lauer, J. Lösch, B. Hillebrands, *Optimizing the spin-pumping induced inverse spin Hall voltage by crystal growth in Fe/Pt bilayers*, Appl. Phys. Lett. **103**, 162401 (2013).
[12] A. Azevedo, L.H. Vilela-Leão, R.L. Rodríguez-Suárez, A.F. Lacerda Santos, S.M. Rezende, *Spin pumping and anisotropic magnetoresistance voltages in magnetic bilayers: Theory and experiment*, Phys. Rev. B **83**, 1 (2011).

4.10 Phase to amplitude conversion by parallel parametric amplification of spin waves in microstructured waveguides

F. Heussner, T. Brächer, P. Pirro†, T. Meyer, T. Fischer, M. Geilen, B. Heinz, A.A. Serga, and B. Hillebrands*

In collaboration with B. Lägel, Nanostructuring Center (NSC), TU Kaiserslautern, 67663 Kaiserslautern

Current affiliations:
** Univ. Grenoble Alpes, CNRS, CEA, INAC-SPINTEC, 38054 Grenoble, France*
† Institut Jean Lamour, Université Lorraine, CNRS, 54506 Vandœuvre-lès-Nancy, France

In the quest for new efficient methods for information processing, the utilization of spin waves, also referred to as magnons, their quanta, appears as a promising approach [1]. The realization of a XNOR logic gate based on a Mach-Zehnder interferometer [2], the design and the micromagnetic simulation of a spin-wave majority gate [3], the progress towards graded-index magnonics [4], the development of a magnonic beam splitter [5] and a magnon transistor [6] are just a few but instructive examples. Apart from the fact that spin waves can transport information without any charge transfer and, consequently, without Ohmic loss and Joule heating, one major advantage in comparison with today's complementary metal-oxide-semiconductor (CMOS) technology lies in the wave-nature of magnons. Information cannot just be coded in the amplitude but also in the phase of the spin waves, which provides an additional degree of freedom. For instance, the input and the output spin-wave signals of the aforementioned majority gate transport the information in their phase and to realize the date processing, interference effects are exploited. To combine magnon-based data processing with CMOS technology, the transformation of the processed information into an electric signal, which can be used in electronic circuits, is of crucial importance. Since most suitable methods for this purpose like, e.g., the utilization of spin pumping [7] in combination with the inverse spin Hall effect (iSHE) [8], are not sensitive to the spin-wave phases, the electrical readout of the phase information is a challenging task.
In this Report, we experimentally demonstrate a method to convert the phase information of a spin wave into an amplitude information, which can easily be readout by well known spin-wave detection methods like inductive antennas or spin pumping in combination with iSHE. The method is based on the phase-dependent parallel parametric amplification (PPA, also known as parallel parametric pumping) of spin waves in the non-adiabatic regime [9–11].
By utilizing the recently developed localized parametric spin-wave amplifier [12], we have realized this phase-to-amplitude conversion of spin waves in a *microstructured* magnonic waveguide made out of $Ni_{81}Fe_{19}$ (Permalloy, Py), thus, on a length scale that meets the requirements for applications. In addition, due to its easy deposition and structuring with standard methods, Permalloy can be well combined with CMOS technology. In particular, we demonstrate the continuous variation of the parametric amplification gain of a propagating coherent spin wave depending on its phase relation to the pumping field. If the phase of the pumping field is known, this allows to deduce the phase of the signal spin wave based on the detected intensity after passing the amplifier.
Parallel parametric pumping [9–11] describes the splitting of a microwave photon into a pair of magnons at half the pumping frequency, whereby one of them contributes to the formation of the

so called idle spin wave (frequency f_i, wave number k_i) and the other to the amplification of the signal spin wave (frequency f_s, wave number k_s). This process originates from the coupling of an external microwave field, called pumping field (frequency f_p, effective wave number k_p), to the longitudinal component of an already present dynamic magnetization, e.g., in form of an externally excited signal spin wave. The amplification gain of this signal wave is especially strong if the dissipation losses are compensated by the parametrically injected magnons, which is described by the parametric instability threshold. The following conservation laws have to be fulfilled [10]:

$$f_p = f_s + f_i = 2f_s \quad , \quad k_p = k_s + k_i \quad . \tag{1}$$

The momentum of the microwave photon is negligibly small compared to the momentum of the spin waves and, therefore, the effective wave number k_p of the pumping field is primarily determined by its spatial extent. Furthermore, the phases of the signal and idle waves are related to the phase of the pumping field by the following equation [11]:

$$\phi_i + \phi_s = \phi_p + \pi/2 \quad . \tag{2}$$

If a spatially homogeneous pumping field is used, its wave number spectrum contains only $k_p \approx 0$ and, consequently, the signal and idle waves are counterpropagating ($k_i = -k_s$). In this adiabatic regime, the amplification process shows no dependence on the phase difference between the pumping field and the signal wave, since the idle wave with an optimal phase is spontaneously selected from the thermal noise.
In the contrary case of a non-homogeneous pumping field, its wave number spectrum results from the Fourier transform of the spatial extent l_p of the pumping field along the propagation direction of the spin waves. For strongly localized pumping fields in comparison to the wavelength λ of the spin waves to be amplified ($l_p \leq \lambda$) [9–11], this leads to the existence of wave numbers $k_p = 2k_s$. In this non-adiabatic regime, the formation of copropagating signal and idle spin waves can occur in agreement with Eq. (1):

$$k_p = k_s + k_i = 2k_s \quad \rightarrow \quad k_i = k_s \quad . \tag{3}$$

To realize the phase-to-amplitude conversion presented in this Report, the interference of the copropagating idle and signal waves is exploited, which depends on their phase difference $\Delta\phi_{si} = \phi_s - \phi_i$. Therefore, the non-adiabatic regime and, thus, a strong localization of the pumping process is mandatory for the conversion. Using the local parallel parametric amplifier presented in [12] (Fig. 1a), this is achieved by a local enhancement of the external microwave field in combination with the strong dependency of the parametric amplification on exceeding the parametric instability threshold.
Based on these considerations, the investigated device shown in Fig. 1a consists of an Au transmission line (regular width $w_1 = 20\,\mu\text{m}$, thickness $d = 250\,\text{nm}$) conducting a microwave current. The current density is increased when flowing through a narrowed region of the transmission line, where the width is decreased to $w_n = 4\,\mu\text{m}$ on a distance of $l_n = 6\,\mu\text{m}$. This increase in the current density results in a local enhancement of the generated pumping field inside the $Ni_{81}Fe_{19}$ spin-wave waveguide (width $w_s = 4\,\mu\text{m}$, thickness $d_s = 40\,\text{nm}$, length $L_s = 75\,\mu\text{m}$), which is patterned on top and in the center of the Au transmission line and which is transversally magnetized by a static external field of $\mu_0 H_{ext} = 63\,\text{mT}$. The power of the microwave current is chosen in such a way that the instability threshold is only exceeded in the region of the enhanced microwave field, leading to a strong spatial localization of the pumping process. This region is the actual local parallel parametric amplifier. To excite a coherent spin wave in the $Ni_{81}Fe_{19}$ waveguide serving as the signal wave with the information encoded in its phase, a microstructured Cu antenna (width

$w_a = 2\,\mu m$, thickness $d_a = 500\,nm$) is patterned on top of the magnonic waveguide at a distance of $l_1 = 10\,\mu m$ to the local parallel parametric amplifier. To electrically insulate the Cu antenna from the waveguide, a $250\,\mu m$ thick insulation layer made from Hydrosilesquioxane is used.
In the performed experiment, the signal spin wave is excited at the position of the antenna by an alternating Oersted field h_f created by a $t_a = 50\,ns$ long microwave pulse of the frequency $f_s = 7.13\,GHz$ and a power of $P_a = 5\,dBm$ flowing through the antenna. The phase ϕ_s of the signal spin wave is determined by the phase of this microwave pulse. In further experiments not shown here, the wavelength λ of the excited spin wave at the applied field-frequency-combination was determined to be $13.5\,\mu m$. The extent l_p of the localized pumping field is in the range of the spatial extent l_n of the narrowing of the Au transmission line, since only in this region the threshold of parallel parametric pumping is exceeded [13]. Hence, the condition $l_p \leq \lambda$ of the non-adiabatic regime is fulfilled. After the signal wave reaches the amplifier, the pumping field h_{2f} is created by a second pulsed microwave current with a duration of $t_p = 50\,ns$ and a power of $P_p = 22\,dBm$ flowing through the Au transmission line. Both microwave pulses are generated by the same microwave source. The pumping pulse with twice the frequency $f_p = 2f_s = 14.26\,GHz$ is created using a frequency doubler. Therefore, the phase difference $\Delta\phi_{sp} = 2\phi_s - \phi_p$ between the pumping field and the signal wave is stable and can be controlled by a phase shifter located in the microwave setup in the branch of the pumping pulse. The aim of the experiment is to prove that the amplitude of the signal wave after passing the amplifier depends on the phase difference $\Delta\phi_{sp}$. If this is the case, the potentially unknown phase of the signal wave can be converted into an amplitude signal by using a pumping field with known phase as a reference. By utilizing Brillouin light scattering microscopy [14] the spin wave (SW) intensity is measured at a distance of $3.5\,\mu m$ behind the amplifier in the middle of the magnonic waveguide, as indicated in the sketch in Fig. 1a.

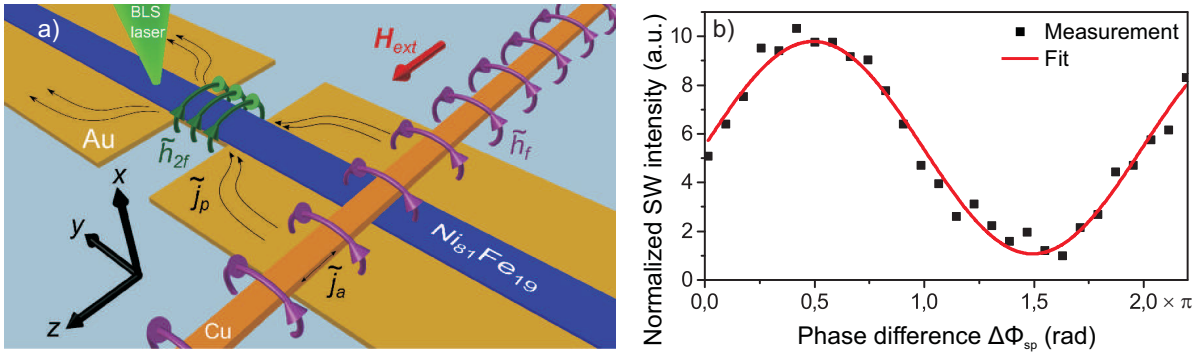

Fig. 1: a) Sketch of the investigated device. b) Modulation of the intensity of the signal spin wave excited at the antenna after passing the amplifier depending on the phase difference $\Delta\phi_{sp}$ between the pumping field and the signal spin wave.

The squares in Fig. 1b show the detected spin wave intensity in dependence on the phase difference $\Delta\phi_{sp}$. It can clearly be seen that the intensity of the signal wave can be modulated by a factor of 10. Thus, this phenomenon can be used to convert distinct phase shifts of the signal spin wave into an amplitude variation after passing the amplifier by keeping the initial phase of the pumping field unchanged.
The origin of this phase-dependent amplification can be explained by interference effects of the involved spin waves. Adjusting the phase shift of the pumping field results in a change of the phase difference $\Delta\phi_{sp}$ and, consequently, also in a change of the phase difference between the signal and the idle wave $\Delta\phi_{si}$. Following Eq. (2), this results in: $\Delta\phi_{si} = \phi_s - \phi_i = 2\phi_s - \phi_p - \pi/2 = \Delta\phi_{sp} - \pi/2$.

This explains the observed intensity modulation in a vivid manner: In the maximum of Fig. 1b the signal and idle waves interfere constructively, resulting in the maximum amplification. In the opposite case of the minimum in Fig. 1b, the signal and the idle waves interfere destructively and extinguish each other. Hence, the measured intensity behind the amplifier is caused solely by the unamplified input signal wave. The sinusoidal fit in Fig. 1b depicted by the solid line reveals the continuous modulation of the intensity resulting from the phase-dependent interference of the involved spin waves.

To conclude, we have experimentally proven the possibility to realize a phase-dependent amplification of a coherent spin wave propagating in a microstructured Py waveguide by employing localized parallel parametric pumping in the non-adiabatic regime. For the purpose of information processing, this can be used to convert phase information into amplitude information in devices with length scales and with materials that meet the requirements for applications. If the phase shift of the pumping field is kept fixed and only the phase shift of the signal wave varies due to information processing steps performed beforehand, the intensity level of the signal wave after passing the amplifier reflects the information encoded in the phase of the signal wave. This amplitude information can be readout by spin-wave detection techniques which themselves are not sensitive to the spin-wave phase. The strong variation by a factor of 10 between maximal and minimal amplification of the signal wave ensures a high reliability of the readout process and increases the sensitivity of detection of small signals.

The authors thank the Nano Structuring Center of the Technische Universität Kaiserslautern for their assistance in sample preparation. Financial support by the DFG (TRR49) is gratefully acknowledged.

References

[1] A.V. Chumak, V.I. Vasyuchka, A.A. Serga, B. Hillebrands, *Magnon spintronics*, Nat. Phys. **11**, 453-461 (2015).
[2] T. Schneider, A.A. Serga, B. Leven, B. Hillebrands, R.L. Stamps, M.P. Kostylev, *Realization of spin-wave logic gates*, Appl. Phys. Lett. **92**, 022505 (2008).
[3] S. Klingler, P. Pirro, T. Brächer, B. Leven, B. Hillebrands, A.V. Chumak, *Design of a spin-wave majority gate employing mode selection*, Appl. Phys. Lett. **105**, 152410 (2014).
[4] C.S. Davies, A. Francis, A.V. Sadovnikov, S.V. Chertopalov, M.T. Bryan, S.V. Grishin, D.A. Allwood, Y.P. Sharaevskii, S.A. Nikitov, V.V. Kruglyak, *Towards graded-index magnonics: Steering spin waves in magnonic networks*, Phys. Rev. B **92**, 020408(R) (2015).
[5] A.V. Sadovnikov, C.S. Davies, S.V. Grishin, V.V. Kruglyak, D.V. Romanenko, Yu.P. Sharaevskii, S.A. Nikitov, *Magnonic beam splitter: The building block of parallel magnonic circuitry*, Appl. Phys. Lett. **106**, 192406 (2015).
[6] A.V. Chumak, A.A. Serga, B. Hillebrands, *Magnon transistor for all-magnon data processing*, Nat. Commun. **5**, 4700 (2014).
[7] Y. Tserkovnyak, A. Brataas, G.E.W. Bauer, *Spin pumping and magnetization dynamics in metallic multilayers*, Phys. Rev. B **66**, 224403 (2002).
[8] J.E. Hirsch, *Spin Hall effect*, Phys. Rev. Lett. **83**, 1834-1837 (1999).
[9] G.A. Melkov, A.A. Serga, V.S. Tiberkevich, Yu.V. Kobljanskij, A.N. Slavin, *Nonadiabatic interaction of a propagating wave packet with localized parametric pumping*, Phys. Rev. E **63**, 066607 (2001).
[10] G.A. Melkov, A.A. Serga, A.N. Slavin, V.S. Tiberkevich, A.N. Oleinik, A.V. Bagada, *Parametric interaction of magnetostatic waves with a nonstationary local pump*, JETP **89**, 1189-1199 (1999).
[11] A.A. Serga, S.O. Demokritov, B. Hillebrands, S.-G. Min, A.N. Slavin, *Phase control of nonadiabatic parametric amplification of spin wave packets*, J. Appl. Phys. **93**, 8585-8587 (2003).
[12] T. Brächer, F. Heussner, P. Pirro, T. Fischer, M. Geilen, B. Heinz, B. Lägel, A.A. Serga, B. Hillebrands, *Time- and power-dependent operation of a parametric spin-wave amplifier*, Appl. Phys. Lett. **105**, 232409 (2014).
[13] T. Brächer, P. Pirro, F. Heussner, A.A. Serga, B. Hillebrands, *Localized parallel parametric generation of spin waves in a $Ni_{81}Fe_{19}$ waveguide by spatial variation of the pumping field*, Appl. Phys. Lett. **104**, 092418 (2014).
[14] V.E. Demidov, S.O. Demokritov, B. Hillebrands, M. Laufenberg, P.P. Freitas, *Radiation of spin waves by a single micrometer-sized magnetic element*, Appl. Phys. Lett. **85**, 2866-2868 (2004).

D. Spin Caloric Transport

Spin Caloric Transport is a dynamically growing field of research, which investigates the interplay between spin- and heat-based transport phenomena. The observation of the spin Seebeck effect (SSE) in a magnetic insulator demonstrates the crucial role of collective magnetization excitations, i.e. spin waves and their quanta, magnons, in spin caloric transport processes, and illustrates the conceptual distinction between this phenomenon and conventional thermoelectric generation. Most interesting and important is the conversion of a heat gradient into a magnon current and vice versa in a magnetic insulator. On a long time scale this may lead to the utilization of heat currents to support the transfer and processing of spin information.

In Report 4.11 we present our findings on the impact of temperature and thermal gradients on parametric pumping processes in YIG/Pt bilayers in a wide wavevector range. It has been shown, that the threshold pumping power, and corresponding spin-wave damping, strongly depend on the mean temperature of the YIG/Pt sample, whereas a temperature gradient without change in mean temperature does not change the threshold. This tendency is visible throughout the whole measured range of magnetic fields, in the low-field regime where parallel parametric pumping occurs as well as in the high-field regime where perpendicular pumping takes place. It has been confirmed that the longitudinal spin Seebeck effect is present, but finally its influence on the spin-wave damping is too weak for the temperature gradients applied in our experiment.

In Report 4.12 we demonstrate the influence of the magnetic insulator thickness in YIG/Pt bilayers on the temporal dynamics of the longitudinal spin Seebeck effect (LSSE). A microwave-induced heating technique has been used to generate a thermal gradient across the bilayer interface. The experiment demonstrates a strong dependence of the time evolution of the LSSE signal on the magnetic layer thickness. An increase of the YIG thickness from 1.26 µm to 30 µm leads to an increase of the rise time of the detected LSSE voltage by 7 times. The experimental data have been fitted with a previously developed model of the thermal magnon diffusion in thermal gradients. The optimal fitting results in the YIG thickness dependent magnon diffusion length, that implies the necessity to improve the used model.

D. Spin-kalorischer Transport

Der spin-kalorische Transport ist ein rasant wachsendes Forschungsfeld, welches das Zusammenspiel zwischen spin- und wärmebasierten Transportphänomenen untersucht. Die Untersuchungen des Spin-Seebeck-Effekts (SSE) in magnetischen Isolatoren zeigen dabei die wichtige Rolle auf, welche die kollektiven Anregungen des magnetischen Systems - also Spinwellen - in spin-kalorischen Transportprozessen spielen. Weiterhin verdeutlichen diese Beobachtungen die konzeptuelle Unterscheidung zwischen diesen Phänomenen auf der einen sowie den konventionellen thermoelektrischen Effekten auf der anderen Seite. Von größtem Interesse und von größter Wichtigkeit in diesem Forschungsgebiet ist die Untersuchung der Umwandlung von Temperaturgradienten in reine Spinströme in Isolatoren. Perspektivisch kann das Verständnis dieser Prozesse zur Nutzung von Wärmeströmen für den Transport sowie die Verarbeitung von Spin-Information beitragen.

Im Bericht 4.11 stellen wir unsere Erkenntnisse vor, wie sich Temperatur und Wärmegradienten auf den Prozess des parametrischen Pumpens in YIG/Pt Zweischichtstrukturen in einem großen Wellenvektorbereich auswirken. Es wird gezeigt, dass die Schwellleistung und die damit ver-

bundene Spinwellendämpfung stark von der mittleren Temperatur der YIG/Pt Probe abhängen, wohingegen ein Temperaturgradient ohne Veränderung der mittleren Temperatur den Schwellwert nicht ändert. Dieses Verhalten ist innerhalb des gesamten vermessenen Magnetfeldbereiches sichtbar, sowohl im Bereich kleiner Magnetfelder, der Bereich des parallelen parametrischen Pumpens, als auch im Bereich hoher Magnetfelder, indem ein senkrechtes Pumpen stattfindet. Die Existenz des Spin-Seebeck-Effekts ist nachgewiesen worden, jedoch ist sein Einfluss auf die Spinwellendämpfung zu schwach um bei den im Experiment angelegten Temperaturgradienten einen sichtbaren Effekt hervorzurufen.

Im Bericht 4.12 zeigen wir den Einfluss der Schichtdicke des magnetischen Isolators in YIG/Pt-Zweischichtsystemen auf die zeitliche Entwicklung des longitudinalen Spin-Seebeck-Effekts (LSSE). Mithilfe einer mikrowellenassistierten Heiztechnik wird ein Wärmegradient durch die Schichtgrenzfläche erzeugt. Das Experiment offenbart eine starke Abhängigkeit der Zeitentwicklung des LSSE Signals von der Dicke der magnetischen Schicht. Ein Zunahme der YIG Dicke von $1,26\,\mu m$ bis hin zu $30\,\mu m$ führt zu einer Zunahme der Anstiegszeiten der gemessenen LSSE Spannung um den Faktor 7. Die experimentellen Daten werden mit einem bereits zuvor entwickelten Modell der thermischen Magnonendiffusion in thermischen Gradienten gefittet. Die optimierten Fitparameter liefern eine Aussage über die Abhängigkeit der Magnonendiffusionslänge von der YIG Schichtdicke, die die Notwendigkeit einer Weiterentwicklung des verwendeten Modells aufzeigt.

4.11 Pumping threshold of dipolar-exchange magnons in thermal gradients

T. Langner, A.A. Serga, B. Hillebrands, and V.I. Vasyuchka

In collaboration with A. Kirihara, Smart Energy Research Laboratories, NEC Corporation, Tsukuba 305-8501, Japan

Magnons, the fundamental excitations of the electron spin system in a ferromagnet and quanta of a spin wave, have attracted a lot of interest in recent research in view of their application for data transfer and information processing [1]. Parallel parametric pumping is a powerful tool to create and amplify magnons in the dipolar and in the dipolar-exchange areas of a spin-wave spectrum [2–4]. Hereby a dynamic magnetic field with twice the magnon frequency is applied parallel to the longitudinal component of the dynamic magnetization of a ferromagnet. A microwave frequency photon converts into two magnons with half its frequency and opposite wavevectors. This technique is characterized by a wavevector dependent threshold process caused by spin-wave damping. If the energy parametrically transferred to the spin system overcomes the spin-wave losses parametric instability occurs and the magnon density increases exponentially with time. Recent developments have shown that intrinsic magnetic damping can be influenced by the spin Seebeck effect [5]. It has been reported that a temperature gradient applied across the interface between a bilayer of a magnetic material and a nonmagnetic metal establishes an additional spin pumping channel to the ferromagnet. If the temperature of the non-magnetic metal layer is higher than the temperature of the ferromagnetic material a spin angular momentum is transferred into the ferromagnet and reduces the damping. In the opposite case it is absorbed and thus the magnetic damping is enhanced. Using the spin Seebeck effect an amplification of dipolar spin waves has recently been reported [6].
In this Report we show the investigation of the influence of the spin Seebeck effect on the parametric pumping threshold for a wide wavevector range. It is shown that a possible effect in our system is weak and cannot be detected within the error bars. Unlike a temperature gradient a homogeneous variation in temperature leads to a pronounced damping variation instead.

An image of the experimental setup configuration is shown in Fig. 1. A pumping microwave Oersted field is induced by a stripline antenna of 50 µm width that is structured on an aluminum

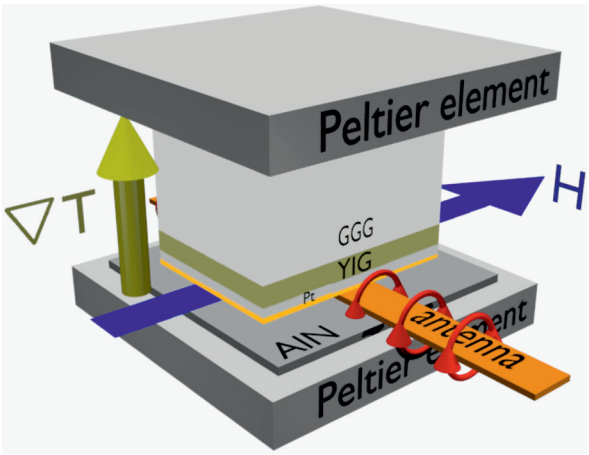

Fig. 1: Scheme of the experimental setup. The Pt/YIG/GGG/YIG multilayer is clamped between two separately controlled Peltier elements that create a thermal gradient along the thickness of the sample. The Pt layer is electrically isolated from the antenna by a thin PMMA coating. The whole setup is mounted in a heat sink. A microwave current applied to the antenna creates a dynamic Oersted field with its main component parallel to the static magnetization of the sample. The reflected signal from the antenna delivers information about the creation of magnons. The resistance of the Pt layer is measured to control the layer temperature.

nitride (AlN) substrate. AlN is used due to its high thermal conductivity at room temperature (285 W/m·K, [7]). The investigated sample is a multilayer of 5 nm Platinum (Pt), 6.7 µm Yttrium Iron Garnet (YIG), 500 µm Gallium Gadolinium Garnet (GGG) and again 6.7 µm YIG. The YIG layers are grown on the GGG substrate by liquid phase epitaxy. Afterwards platinum was sputtered on one YIG side. The sample is placed on top of the antenna with the platinum layer at the bottom. A thin layer of coated Polymethyl Methacrylate (PMMA) electrically isolates the Pt layer from the antenna. Two separately controlled Peltier elements, one below the AlN substrate and one directly on top of the multilayer sample, are used to create a temperature gradient transversal to the sample plane. The back sides of the Peltier elements are connected to heat sinks that are clamped between the poles of an electromagnet. In order to control the temperature stability of the Pt layer, its electrical resistance is measured over the time of the experiment. The externally applied bias magnetic field is oriented in plane of the experimental sample and perpendicular to the long axis of the microwave antenna.
10 µs long microwave current pulses with a carrier frequency of 14 GHz and a repetition time of 10 ms applied to the antenna create an alternating Oersted field around the microstrip. A stub tuner connected to the antenna creates a tunable microwave resonator. The reflected microwave signal from this resonator is detected by a semiconductor diode and shown on an oscilloscope (350 MHz bandwidth). The microwave power applied to the antenna is set to exactly that level where the reflected pulse starts showing a kink at the end of the pulse shape. This kink appears as a result of a change in the quality factor of the tuned resonator due to excitation of magnons and thus is the test for the appearance of the parametric instability [8, 9]. The applied microwave power level in this case is considered here as threshold power.

In our experiments the parametric pumping threshold powers were determined for a wide range of magnon wavevectors (see Fig. 2a). For this the threshold power is measured in a wide range of bias magnetic field values. In each case we see the typical dependence (see Fig. 2b). One can see that parametric magnon excitation strongly depends on the bias magnetic field. Close to the ferromagnetic resonance (FMR) with $\mathbf{k} = 0$, at the critical field H_C, the excitation is most efficient and, thus, the applied pumping field is minimal. With decreasing external magnetic field in the range below the critical field ($H < H_C$) the threshold power increases slowly due to a decrease in the ellipticity of the excited spin waves (see Ref. [10]). For magnetic fields little below the FMR condition a peak can be seen. It appears because of an increase of the threshold power due to interaction of the magnons with a transversal phonon mode. With increasing external magnetic fields above the critical field the threshold power increases sharply and transforms into a modified perpendicular pumping excitation scheme that becomes more efficient than parallel pumping, see Ref. [9] for a detailed description.

In a first set of experiments, the temperature of the YIG/Pt bilayer was changed homogeneously in 20 °C steps. The results are shown in Fig. 2b. Beside a shift of the whole curve to higher bias magnetic fields, which is a consequence of the temperature-dependent decrease in the saturation magnetization, a continuous increase in the threshold power is obvious. For each temperature step we observe a difference of approximately 1 dB in applied microwave power to reach the threshold value. According to Ref. [11] the intrinsic damping in YIG is closely connected to the absolute temperature. A higher damping leads to a higher threshold power since it has to be overcome by a higher pumping field.

In a second step inhomogeneous temperature configurations were created across the sample thickness. The temperature of the sample top is 20 °C or 52 °C depending of the direction of the gradient. The bottom Peltier element has been adapted so that we obtain a mean temperature of the YIG film

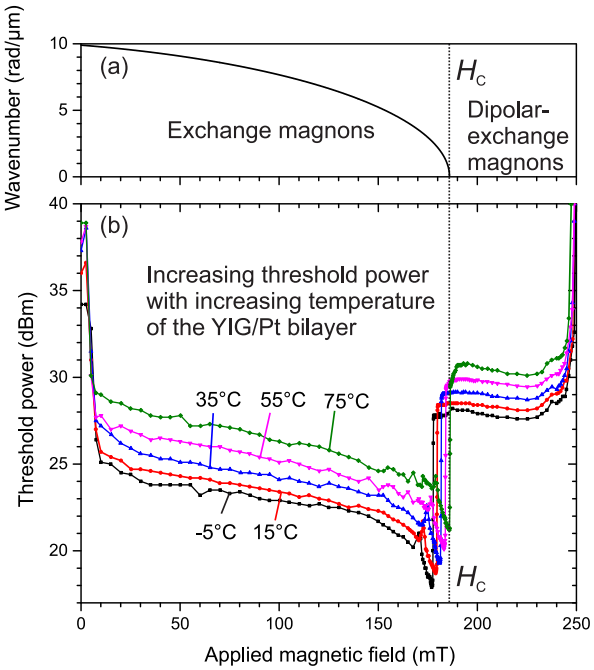

Fig. 2: (a) Applied wavevector spectrum for $T = 75\,^{\circ}\mathrm{C}$ with respect to the externally applied magnetic field. The spectrum was determined using the theory in Ref. [3] (b) Measured dependencies of the threshold power on the externally applied magnetic field for constant temperatures of the sample.

of 35 °C in every case. This mean temperature has been fixed by the electrical resistance of the Pt layer and by an additional precise tuning of the FMR threshold minimum to the same magnetic field value in every case.
A temperature gradient across the multilayer interface leads to the longitudinal spin Seebeck effect (LSSE). Its existence in our system has been proven in direct measurements of the LSSE voltage between the lateral edges of the Pt layer, see the inset in Fig 3. For different directions of the temperature gradient the measured voltages have opposite signs with a sign change at zero field.
For a homogeneous temperature of the sample of 35 °C no inverse spin Hall voltage due to the spin Seebeck effect is detected. At the same time the measurements of the threshold powers in the parametric pumping process reveal that there is no measurable influence of the longitudinal spin Seebeck effect on the spin-wave damping parameter, see Fig. 3. All three curves shown are on the same level within an uncertainty of 0.1 dB of applied microwave power.

In summary, the threshold powers for the parallel parametric pumping process in YIG/Pt bilayers in a wide wavevector range have been investigated for different thermal configurations. It has

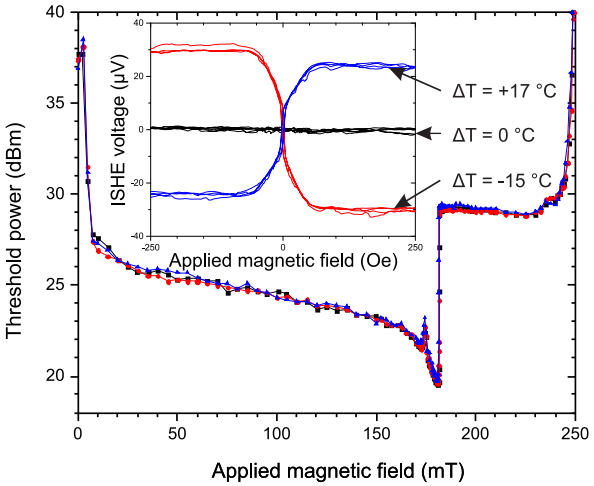

Fig. 3: Measured dependencies of the threshold power on the externally applied magnetic field for different temperature gradients perpendicular to the sample plane. The mean temperature of $T = 35\,^{\circ}\mathrm{C}$ of the sample is the same for all three curves. The inset shows a LSSE voltage measurement depending on the externally applied magnetic field for the same applied temperature gradients.

been shown, that the threshold power strongly depends on the mean temperature of the YIG layer, whereas a temperature gradient without change in the mean temperature of a YIG film does not change the threshold power. These tendencies are visible throughout the entire measured range, in the low-field regime where parallel parametric pumping occurs as well as in the higher-field regime where perpendicular pumping occurs. It has been confirmed that the longitudinal spin Seebeck effect is present, but finally its influence on the magnetic damping is too weak to be determined in our experiments. Thus we can conclude that the spin Seebeck effect has only small influence on the parametric pumping process for the temperature gradients applied in our experiment.

We gratefully acknowledge financial support by Deutsche Forschungsgemeinschaft (DFG) within priority program SPP1538 “Spin Caloric Transport”.

References

[1] A.V. Chumak, V.I. Vasyuchka, A.A. Serga, B. Hillebrands, *Magnon spintronics*, Nat. Phys. **11**, 453-461 (2015).
[2] E. Schlömann, J.J. Green, U. Milano, *Recent developments in ferromagnetic resonance at high power levels*, J. Appl. Phys. **31**, 386S (1960).
[3] A.G. Gurevich, G.A. Melkov, *Magnetization oscillations and waves*, CRC, New York (1996).
[4] V.E. Zakharov, V.S. L’vov, S.S. Starobinets, *Stationary nonlinear theory of parametric excitation of waves*, Sov. Phys. JETP **32**, 656 (1971).
[5] M.B. Jungfleisch, T. An, K. Ando, Y. Kajiwara, K. Uchida, V.I. Vasyuchka, A.V. Chumak, A.A. Serga, E. Saitoh, B. Hillebrands, *Heat induced damping modification in yttrium iron garnet/platinum hetero-structures*, Appl. Phys. Lett. **102**, 062417 (2013).
[6] E. Padrón-Hernández, A. Azevedo, S.M. Rezende, *Amplification of spin waves by the spin Seebeck effect*, J. Appl. Phys. **111**, 07D504 (2012).
[7] G.A. Slack, R.A. Tanzilli, R.O. Pohl, J.W. Vandersande, *The intrinsic thermal-conductivity of AlN*, J. Phys. Chem. Solids **48**, 7 , 641-647 (1987).
[8] C.W. Sandweg, Y. Kajiwara, A.V. Chumak, A.A. Serga, V.I. Vasyuchka, M.B. Jungfleisch, E. Saitoh, B. Hillebrands, *Spin pumping by parametrically excited exchange magnons*, Phys. Rev. Lett. **106**, 216601 (2011).
[9] T. Neumann, A.A. Serga, V.I. Vasyuchka, B. Hillebrands, *Field-induced transition from parallel to perpendicular parametric pumping for a microstrip transducer*, Appl. Phys. Lett. **94**, 192502 (2009).
[10] A.A. Serga, C.W. Sandweg, V.I. Vasyuchka, M.B. Jungfleisch, B. Hillebrands, A. Kreisel, P. Kopietz, M.P. Kostylev, *Brillouin light scattering spectroscopy of parametrically excited dipole-exchange magnons*, Phys. Rev. B **86**, 134403 (2012).
[11] V. Cherepanov, I. Kolokolov, V. L’vov, *The saga of YIG: spectra, thermodynamics, interaction and relaxation of magnons in a complex magnet*, Physics Reports **229**, No. 3, 81-144 (1993).

4.12 Thickness dependent temporal evolution of the spin Seebeck effect in YIG|Pt bilayers

T. Noack, T. Langner, F. Heussner, V. Lauer, A.A. Serga, B. Hillebrands, and V.I. Vasyuchka

There is a rising tendency in the importance of spin currents as an alternative to charge currents for logic devices [1]. This is due to the lower generated Joule heating and many different opportunities to manipulate and generate spin currents. A spin current relates to a charge current with opposite flow directions for spin up and spin down carriers or it can consist of magnons - the quanta of collective spin excitations [2]. Among other methods, the magnon current can be excited by creation of a thermal gradient through a ferromagnet. Experiments have shown that due to the strong phonon-magnon interaction the effective temperature of magnons is very close to the temperature of phonons [3]. In temperature gradient this leads to spatial differences in the density of thermally excited magnons. This non-equilibrium state results in a diffusion of the thermally excited magnons along the gradient direction - the longitudinal spin Seebeck effect (LSSE). However, the exact microscopic mechanism responsible for the magnon mediated spin Seebeck effect is not completely understood yet. Especially the timescale of the spin Seebeck effect, which is an important factor for usage of spin Seebeck measurements in temperature and temperature gradient sensing, must be clarified both experimentally and theoretically.
Recently the first results on time dependence of the longitudinal spin Seebeck effect in a single Platinum|Yttrium Iron Garnet bilayer (Pt|YIG) have been reported [4]. A rise time of the longitudinal spin Seebeck voltage (V_{LSSE}) of a few hundred nanoseconds was observed. For thermally excited magnons a finite magnon propagation length around 500 nm in YIG was found in Ref. [5]. In this Report we reveal the influence of the YIG thickness on the magnon propagation length and therefore on the time dependent behaviour of the longitudinal spin Seebeck voltage. Our results show that the magnon propagation length determined from a previously proposed simplified model [5], is not a constant but increases with the increasing YIG thickness.

The scheme of the experimental setup, which was used for our research, is shown in Fig. 1a. In this experiment microwave induced heating of the Pt layer was used for the creation of the thermal gradient in Pt|YIG bilayers. The Pt film is heated by eddy currents induced in the metal by a microwave Oersted field excited around a 600 µm wide microstrip transmission line placed below the Pt|YIG sample. The microstrip is driven with a microwave generator that produces microwave currents at a fixed frequency of 6.875 GHz in all measurements. This frequency value was chosen after we observed the transmission spectrum of the used microstrip circuit and the minimal transmission losses were found. Microwave heating pulses of duration of 10 µs with 3 ns long edges were applied with a repetition frequency of 1 kHz to allow the system to cool down after every heating cycle. The applied microwave power was set at +30 dBm using an amplifier. To avoid possible reflections of microwave energy a matched load (50 Ω) is connected at the end of the microstrip. The samples were placed on top of the microwave antenna with the platinum layer disposed close to the antenna. All samples used in the experiments have the same structure: a 10 nm-thick Pt layer was deposited on top of a YIG layer with a different thickness for every sample. The YIG films were grown by liquid phase epitaxy on a 500 µm thick Gadolinium Gallium Garnet substrate. The platinum film was deposited using sputter deposition on top of the YIG layer.

The thermal gradient generates a spin current across the Pt|YIG interface, which can be measured

using the inverse spin Hall effect (ISHE). Due to spin-dependent scattering of spin polarized conducting electrons in the Pt layer the spin current across the Pt|YIG interface is converted into a charge current in-plane of the metal layer. It can be easily measured as a corresponding voltage: $V_{\mathrm{ISHE}} \propto \Theta_{\mathrm{SHE}}(\mathbf{J_S} \times \sigma) \cdot \boldsymbol{l}$, where Θ_{SHE} is the spin Hall angle, which gives the efficiency of the SHE in platinum, $\mathbf{J_S}$ is the spin current, σ is the spin polarization and $\boldsymbol{l} = 3\,\mathrm{mm}$ is the distance between the contacts in Fig. 1b.

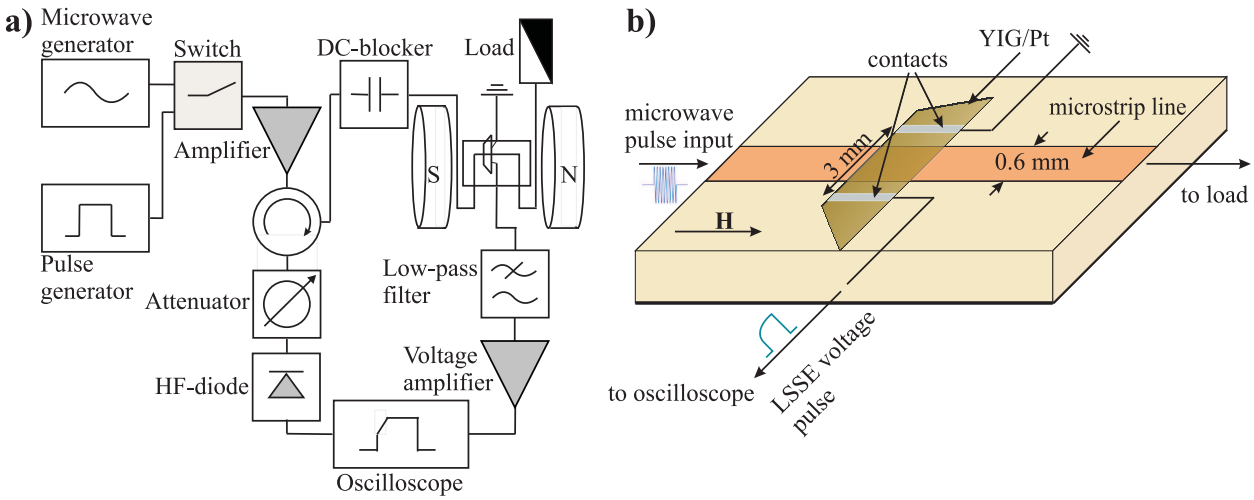

Fig. 1: a) Scheme of the experimental setup used for the investigation of the temporal evolution of the LSSE voltage using microwave-induced heating. b) Sketch of the sample holder with the mounted sample.

The amplitude of the inverse spin Hall effect is proportional to the amplitude of the longitudinal spin Seebeck effect. For further discussion in this Report we will use the nomenclature V_{LSSE} for the detected voltage as the LSSE is the origin of the measured ISHE voltage.

The observed pulsed DC signal was filtered by a low-pass filter (DC-400 MHz) to avoid a possible disturbance by strong microwave pulses. Due to the small magnitude of the ISHE voltage of several microvolts we had to amplify our signal 1000 times by using a voltage amplifier. Finally, the detected signal was displayed at the oscilloscope together with the reflected microwave pulse, which was directed by a microwave circulator to a HF-diode detector (see Fig. 1a). Figure 1b shows the geometry of the sample holder. The magnetic field $\mathbf{H}$ was oriented in the sample plane along the microstrip. The magnetic field strength was $H = 250\,\mathrm{Oe}$ for all measurements. This small value of the applied magnetic field was chosen to avoid possible resonant and parametric excitations of spin-waves in the YIG film by the microwave magnetic field. The absence of such excitation processes is evidenced by the fact that the shape of the LSSE pulse was the same for 250 Oe and for over 2500 Oe where the spin-wave spectrum is shifted so high in frequency that there are no parametric effects.

Our intention was to investigate the time dependent behaviour of the spin Seebeck voltage for different YIG thicknesses. The experiment has been carried out for five different samples with YIG thicknesses of 1.26 µm, 2.1 µm, 4.1 µm, 6.7 µm and 30 µm. For every sample we applied a 10 µs long heating pulse and analysed the difference in the evolution of the V_{LSSE} voltage. In order to eliminate nonmagnetic thermoelectric contributions to V_{LSSE} we subtracted $V_{\mathrm{LSSE}}^{+\mathrm{H}}$ - $V_{\mathrm{LSSE}}^{-\mathrm{H}}$. The rise time of the LSSE signal increases with increase of the YIG thickness. The normalized time profiles for 3 YIG thicknesses are shown in Fig. 2a. A strong influence of the YIG thickness on the rise time of the V_{LSSE} voltage was observed.

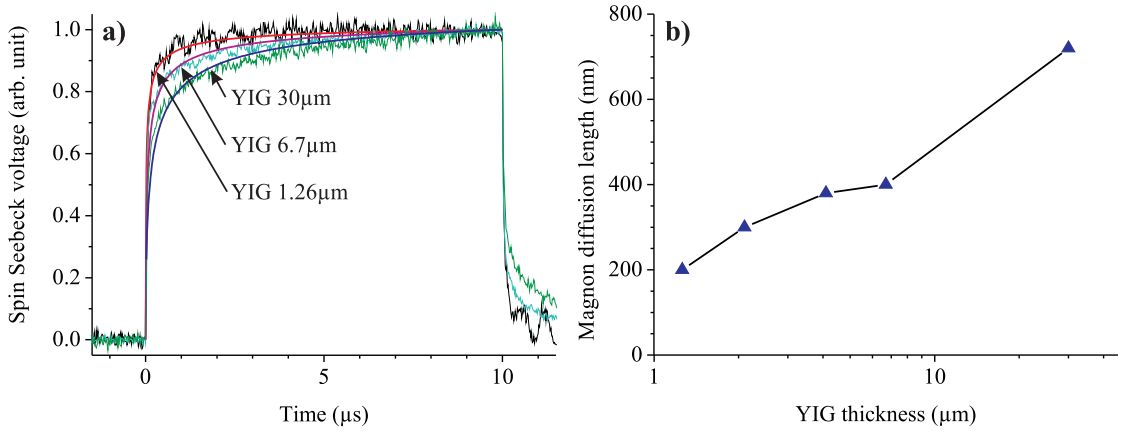

Fig. 2: a) Measured profiles of the LSSE voltage for the 1.26 µm, 6.7 µm and 30 µm thick YIG samples with the simulated fitting curves for different magnon diffusion lengths. The best matching fitting curve was chosen by the method of least squares. b) Dependence of the calculated magnon diffusion lengths on the YIG film thickness.

To obtain a more specific prediction about the time dependence and the magnon diffusion lengths we performed a simulation using the software COMSOL. As in Ref. [5] we consider the spin Seebeck voltage as a combination of an interface effect and a bulk effect:

$$V_{\mathrm{LSSE}}(t) \propto \alpha \int_{-\delta d}^{0} \nabla T_y(y,t)dy + \beta \int_{0}^{l} \nabla T_y(y,t)\exp(-y/L)dy \quad , \tag{1}$$

where L is the thermal magnon diffusion length, y is the direction across the sample. α and β are coupling parameters, α defines the coupling between the electron bath in the normal metal and the phonon bath in the magnetic material while β defines the magnon-magnon interaction within the magnetic material. It was shown in Ref. [5, 6] that the rise time of the thermal gradient at the interface is much faster than the observed rise time of the spin Seebeck effect. Therefore we do not consider the first term in our simulations and use only the bulk term for the fitting of the measured data. For our fittings we simulated the temporal dynamics of the thermal gradient and calculated the bulk term for different magnon diffusion lengths L. Finally we used the method of least squares to calculate a simulation that fits best to the different samples. After normalization of the measured dynamics of the spin Seebeck voltage it was plotted together with the simulated bulk terms in Fig. 2a.

By using this fitting procedure we could determine the effective magnon propagation length for every YIG thickness with an accuracy of 20 nm. The obtained diffusion lengths are shown in Fig. 2b. It displays a distinct increase with the increase of the investigated YIG thickness. At this stage of the research, we see that the effective magnon diffusion length is changing. This change could be associated with a regular spin-wave damping if one assumes that this damping monotonically increases with the increase in the YIG-film thickness. However, we do not have sufficient grounds for such a statement. Moreover, from our point of view this statement can even not be verified by conventional measurements of the damping parameter of coherently excited spin-wave excitations. That is because the damping can significantly differ for thermally excited short-wavelength high-energy magnons (which are distinguished as the main contribution to the SSE) and for relatively long-wavelength and low-energy magnons accessible for a direct excitation in microwave experiments. At the same time, we believe that a further improvement of the utilized

theoretical model can help to understand the time-dependent LSSE dynamics. An important factor, which is not implemented in the used model yet, is the dynamic of the magnons. In fact, in the model, it is supposed that the magnons that are driven somewhere in the sample by a local temperature gradient are immediately detected at the interface and participate to the ISHE. To improve the model we need to involve the propagation time of the magnons to the interface and to take into account their sequential transport through spatially varying temperature gradients.

In this Report we demonstrated the influence of the magnetic insulator thickness in YIG|Pt bilayers on the temporal dynamics of the longitudinal spin Seebeck effect (LSSE). A microwave-induced heating technique has been used to generate a thermal gradient across the bilayer interface. The experiment demonstrates a strong dependence of the time evolution of the LSSE signal on the magnetic layer thickness. An increase of the YIG thickness from 1.26 µm to 30 µm leads to an increase of the rise time of the detected LSSE voltage by 7 times. The experimental data have been fitted with a previously developed model of the thermal magnon diffusion in thermal gradients. The optimal fitting results in the YIG thickness dependent magnon diffusion length, that implies the necessity to improve the used model.

We gratefully acknowledge financial support by Deutsche Forschungsgemeinschaft (DFG) within priority program 1538 “Spin Caloric Transport”, and technical support from the Nano Structuring Center, TU Kaiserslautern.

References

[1] C.-F. Pai, L. Liu, Y. Li, H. Tseng, D. Ralph, R. Buhrman, *Spin transfer torque devices utilizing the giant spin Hall effect of tungsten*, Appl. Phys. Lett. **101**, 122404 (2012).

[2] A.V. Chumak, V.I. Vasyuchka, A.A. Serga, B. Hillebrands, *Magnon spintronics*, Nat. Phys. **11**, 453-461 (2015).

[3] M. Agrawal, V.I. Vasyuchka, A.A. Serga, A.D. Karenowska, G.A. Melkov, B. Hillebrands, *Direct measurement of magnon temperature: New insight into magnon-phonon coupling in magnetic insulators*, Phys. Rev. Lett. **111**, 107204 (2013).

[4] N. Roschewsky, M. Schreier, A. Kamra, F. Schade, K. Ganzhorn, S. Meyer, H. Huebl, S. Geprägs, R. Gross, S.T.B. Goennenwein, *Time resolved spin Seebeck effect experiments*, Appl. Phys. Lett. **104**, 202410 (2014).

[5] M. Agrawal, V.I. Vasyuchka, A.A. Serga, A. Kirihara, P. Pirro, T. Langner, M.B. Jungfleisch, A.V. Chumak, E.Th. Papaioannou, B. Hillebrands, *Role of bulk-magnon transport in the temporal evolution of the longitudinal spin-Seebeck effect*, Phys. Rev. B **89**, 224414 (2014).

[6] M. Agrawal, A.A. Serga, V. Lauer, E.Th. Papaioannou, B. Hillebrands, V.I. Vasyuchka, *Microwave-induced spin currents in ferromagnetic-insulator|normal-metal bilayer system*, Appl. Phys. Lett. **105**, 092404 (2014).

E. New Materials and Heusler Compounds

The material class of Heusler compounds contains several promising candidates regarding their utilization in the field of *spintronics* and in particular *magnon spintronics*. The major reasons for the interest in Heusler compounds are their high Curie temperature, their high spin polarization, and their low magnetic Gilbert damping.

Spintronics can be regarded as an extension of conventional electronics by using the electrons' spin as an additional degree of freedom for applications in data storage and sensing. Spintronic devices mainly rely on magneto-resistive effects such as the giant magneto resistance and tunneling magneto resistance. For the optimization of these effects, it is crucial to find materials with a high spin polarization such as the Heusler compounds. The field of magnon spintronics can largely benefit from the low Gilbert damping in some of the Heusler compounds. The major motivation behind magnon spintronics is an energy-efficient information transport and processing that is purely based on magnons, which are the fundamental excitations in a magnetic material. A major challenge in magnon spintronics is the identification and development of suitable low-damping materials for the realization of magnon conduits on the microscale. This challenge can be addressed by the utilization of Heusler compounds.

Heusler compounds have the general composition X_2YZ or XYZ, where X and Y are transition metals, and Z is an element out of the main groups III-V. One of the most promising classes of Heusler materials is given by the cobalt-based compounds with the composition Co_2YZ. The reason for both, the high spin polarization as well as the low Gilbert damping, is the half-metallic character of Heusler compounds. Half metallicity describes the different features in the band structure of minority and majority electrons close to the Fermi energy. For the minority electrons, a band gap can be found at the Fermi energy. In contrast to this, the majority spin channel exhibits a finite density of states at the Fermi level and, thus, metallic character.

Our group was a part of the joint Japanese-German research unit *Advanced Spintronic Materials and Transport Phenomena* (ASPIMATT) that successfully ended this year. The research initiative has addressed the development, the characterization, and the optimization of Heusler materials for the utilization in spintronics and magnon spintronics. The work package addressed by our group covers *nonlinear spin-wave dynamics and radiation properties of small Heusler devices* in the field of magnon spintronics.

Our recent experiments reported in Report 4.13 using the Heusler compound $Co_2Mn_{0.6}Fe_{0.4}Si$ (CMFS) focus on the manipulation of the effective magnon damping by utilising the spin Hall effect (SHE) and spin transfer torque (STT) effects. The measurements have revealed a large increase of the thermally activated magnon intensity via the SHE and STT by more than a factor of 30 in a wide spin-wave waveguide. Our results offer another way for intensity and frequency controlled magnonic devices regulated via a DC current.

In Report 4.14 we investigate the material $Co_{40}Fe_{40}B_{20}$ as a candidate material for the production of spin-wave waveguides. This material has been reported to show a low Gilbert damping parameter and, due to its high saturation magnetization, it features a high spin wave group velocity. The application of different annealing temperatures and capping layers was investigated in order to preserve the low Gilbert damping parameter of the spin-wave waveguides from $Co_{40}Fe_{40}B_{20}$ in the micro-structuring process.

In Report 4.15 we present the design of new materials via the control of the growth parameters. We have successfully managed to grow epitaxially Pt on top of Fe in spite of the large lattice

mismatch of both elements. We show the growth evolution of Pt on Fe with respect to the growth parameters and the subsequent large influence on the magnetic properties. The optimization of the epitaxial evaporation process paves the way of investigating spin dependent phenomena on perfect interfaces.

E. Neue Materialien und Heusler-Legierungen

In der Materialklasse der Heusler-Verbindungen finden sich zahlreiche vielversprechende Kandidaten hinsichtlich der Verwendung in den Feldern der *Spintronik* und der *Magnon-Spintronik*. Die Hauptgründe für das Interesse an den Heusler-Materialien sind ihre hohe Curie-Temperatur, ihre hohe Spinpolarisation und ihre niedrige magnetische Gilbert-Dämpfung.

Die Spintronik stellt eine Erweiterung konventioneller Elektronik dar, die durch die Nutzung des Elektronenspins als zusätzlichen Freiheitsgrad zur Datenspeicherung und in der Sensorik realisiert wird. Spintronische Bauelemente stützen sich hauptsächlich auf Effekte wie den Riesenmagnetowiderstand oder den Tunnelmagnetowiderstand. Die Optimierung dieser Effekte setzt Materialien mit einer hohen Spinpolarisation wie die Heusler-Verbindungen voraus. Das Feld der Magnon-Spintronik kann wiederum hauptsächlich von der niedrigen Gilbert-Dämpfung in Heusler-Materialien profitieren. Die Hauptmotivation hinter der Magnon-Spintronik ist eine energieeffiziente Datenverarbeitung auf Basis von Magnonen, welche die fundamentalen Anregungen in einem magnetischen Festkörper sind. Eine der großen Herausforderungen der Magnon-Spintronik ist die Identifizierung und die Entwicklung von geeigneten Materialen für die Realisierung von magnonischen Wellenleitern auf der Mikrometerskala. Diese Herausforderung kann durch die Verwendung von Heusler-Materialien angegangen werden.

Heusler-Materialien zeigen eine generelle Zusammensetzung der Form X_2YZ oder XYZ. Hierbei sind X und Y Übergangsmetalle, während Z eine Element aus den Hauptgruppen III-V ist. Eine der interessantesten Untergruppen von möglichen Heusler-Verbindungen ist die Gruppe der Kobaltbasierten Materialien der Form Co_2YZ. Der Grund für die hohe Spinpolarisation sowie auch die geringe Gilbert-Dämpfung liegt in der halbmetallischen Natur der Heusler-Verbindungen. Dieser halbmetallische Charakter beschreibt die Unterschiede in der Bandstruktur der Majoritäts- und Minoritätsladungsträger insbesondere nahe der Fermi-Energie. Für die Minoritätselektronen lässt sich eine Bandlücke an der Fermi-Kante beobachten, während die Bandstruktur der Majoritätselektronen dort eine endliche Zustandsdichte, und damit metallischen Charakter, aufweist.

Unsere Gruppe war Teil der japanisch-deutschen Forschungsinitiative *Advanced Spintronic Materials and Transport Phenomena* (ASPIMATT), die dieses Jahr erfolgreich endete. Diese Initiative hatte die Entwicklung, Charakterisierung und Optimierung von Heusler-Materialien für die Verwendung in Spintronik und Magnon-Spintronik zum Ziel. Das Arbeitspaket, das in unserer Gruppe bearbeitet wurde, trägt den Titel *Nonlinear spin-wave dynamics and radiation properties of small Heusler devices* und befasste sich mit dem Gebiet der Magnon-Spintronik.

Unsere in Bericht 4.13 dargestellten kürzlich erfolgten Experimente an der Heusler-Verbindung $Co_2Mn_{0.6}Fe_{0.4}Si$ (CMFS) konzentrieren sich auf die Manipulation der effektiven Magnon-Dämpfung durch Verwendung des Spin-Hall-Effekts (SHE) und des Spin-Transfer-Torque (STT) Effekts. Die Messungen offenbarten eine starken Anstieg der thermisch aktivierten Magnonenintensität durch SHE und STT durch einen Faktor größer als 30 in einem weiten Spinwellen-Wellenleiter. Unsere Ergebnisse bieten einen Alternativ-Weg für die Ansteuerung Intensitäts- und Frequenzkontrollierter magnonischer Hardware durch Gleichströme.

In Bericht 4.14 untersuchen wir das Material $Co_{40}Fe_{40}B_{20}$ als Kandidaten für die Produktion von Spinwellen-Wellenleitern. Es wurde berichtet, dass es einen geringen Gilbert-Dämpfungsparameter und aufgrund seiner hohen Sättigungsmagnetisierung eine große Spinwellen-Gruppengeschwindigkeit besitzt. Die Anwendung verschiedener Ausheiztemperaturen und unterschiedlicher Deckschichten wurde hinsichtlich der Erzielung eines geringen Gilbert-Dämpfungsparameter der Spinwellen-Wellenleiter aus $Co_{40}Fe_{40}B_{20}$ im Mikrostrukturierungsprozess untersucht.

In Bericht 4.15 zeigen wir eine alternative Herangehensweise in dem Design-Prozess neuer Materialien: durch die verbesserte Kontrolle der Wachstumsparameter. Wir haben erfolgreich epitaktisch Pt auf Fe gewachsen, trotz der großen Gitterfehlanpassung beider Elemente. Wir zeigen die Wachstumsentwicklung von Pt auf Fe mit Bezug auf die Wachstumsparameter und den daraus resultierenden großen Einfluss auf die magnetischen Eigenschaften. Die Optimierung des epitaktischen Aufdampfprozesses ebnet den Weg für die Untersuchung Spin-korrelierter Phänomene an perfekten Grenzflächen.

4.13 Control of the effective spin-wave damping in Heusler-Pt waveguides via the spin-transfer torque effect

T. Meyer, T. Brächer, P. Pirro†, T. Fischer, A.A. Serga, and B. Hillebrands*

In collaboration with H. Naganuma, K. Mukaiyama, M. Oogane, and Y. Ando
Department of Applied Physics, Graduate School of Engineering, Tohoku University, Sendai 980-8579, Japan

Current affiliations:
** Université Grenoble Alpes, CNRS, CEA, INAC-SPINTEC, 38054 Grenoble, France*
† Institut Jean Lamour, Université Lorraine, CNRS, 54506 Vandœuvre-lès-Nancy, France

In the field of magnonics, the value of the Gilbert damping parameter is one of the most crucial parameters. It limits any possible application utilizing magnons, the quanta of spin waves, for information processing. Therefore, in the last years the development of new materials with a low Gilbert damping such as Cobalt-based Heusler compounds have paved the way for future magnon spintronic devices [1]. Moreover, utilizing the spin-Hall effect (SHE) [2] to generate pure spin currents in a normal metal, the spin-transfer torque effect (STT) [3] possesses great potential to modify the effective magnon damping in spatially extended magnon devices.

However, up to this time, most of the investigations have been performed in systems where either the current density [4] or the magnetic system itself [5,6] were spatially confined or they show only comparably small changes in the spin-wave intensities [7–9]. In contrast, in this Report, we present a strong increase of the thermally activated magnon intensity via the SHE and STT in a spin-wave waveguide patterned from the low-damping $Co_2Mn_{0.6}Fe_{0.4}Si$ (CMFS) Heusler compound.

Figure 1 shows the investigated sample. A 5 nm thick CMFS layer was grown on a Cr buffer layer of the same thickness and, after annealing, a 2 nm thick Pt layer was deposited on top of the stack. Subsequently, the patterning into waveguides with a width of 7 µm and a length of 70 µm was performed. In order to apply electric currents, Au contacts are patterned onto both ends of the waveguide. Thus, an applied DC current flows through the whole microstructure including the Pt layer. Via the SHE, an applied DC charge current in the Pt layer generates a pure spin current flowing into the CMFS layer. This pure spin current exerts a torque on the magnetization via the STT effect. It is worth to note that the DC current will not only flow in the Pt layer but also in the CMFS and Cr layers since all layers are metallic. This gives rise to an additional pure spin current

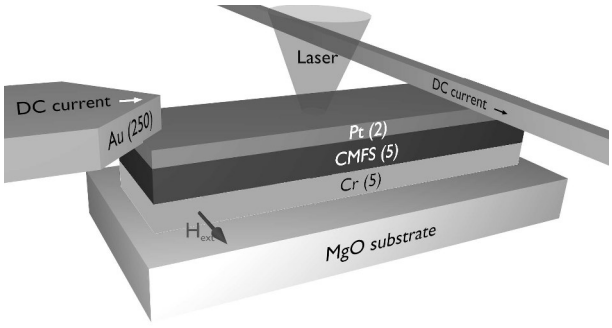

Fig. 1: Schematic sample setup with the corresponding layer thicknesses in nanometer in brackets and the direction of the externally applied magnetic field. For all measurements the BLS laser was positioned in the center of the waveguide.

from the Cr layer into the CMFS layer, causing an additional torque on the magnetization. Here, one has to consider that the sign of the spin-Hall angle θ_{SH} of Pt is positive $\theta_{SH}^{Pt} > 0$ [10] and the spin-Hall angle of Cr is reported to be negative $\theta_{SH}^{Cr} < 0$ [11]. Due to this fact and since the spin currents emerging from the Pt and Cr layers enter the CMFS layer from opposite surfaces, both currents add up, resulting in an increased torque in the CMFS layer.

In this Report, the intensities of thermally activated spin waves and their dependence on an applied DC current are measured using Brillouin light scattering (BLS) microscopy [12]. The black squares (grey circles) in Fig. 2a show the normalized total spin-wave intensity depending on the DC current for a magnetic field of $+50\,\mathrm{mT}$ ($-50\,\mathrm{mT}$). For a positive (negative) magnetic field and positive (negative) applied currents the intensity increases by a factor of 2. This increase in intensity originates from a decreased effective spin-wave damping due to the injected spin current which changes its sign if the direction of the magnetic field or of the DC current is inverted.

Since the applied DC current is accompanied by Joule heating, a further increase of the electric current can damage the microstructures. Thus, in order to minimize the spurious heating, in the following, all DC currents are applied in 50 ns long pulses with a repetition time of 500 ns. All results presented in the following were obtained for an externally applied magnetic field of $+70\,\mathrm{mT}$. Utilizing time-resolved BLS, this gives access to the spin-wave intensity during the DC pulse as well as in the currentless state between two pulses. The black squares in Fig. 2b show

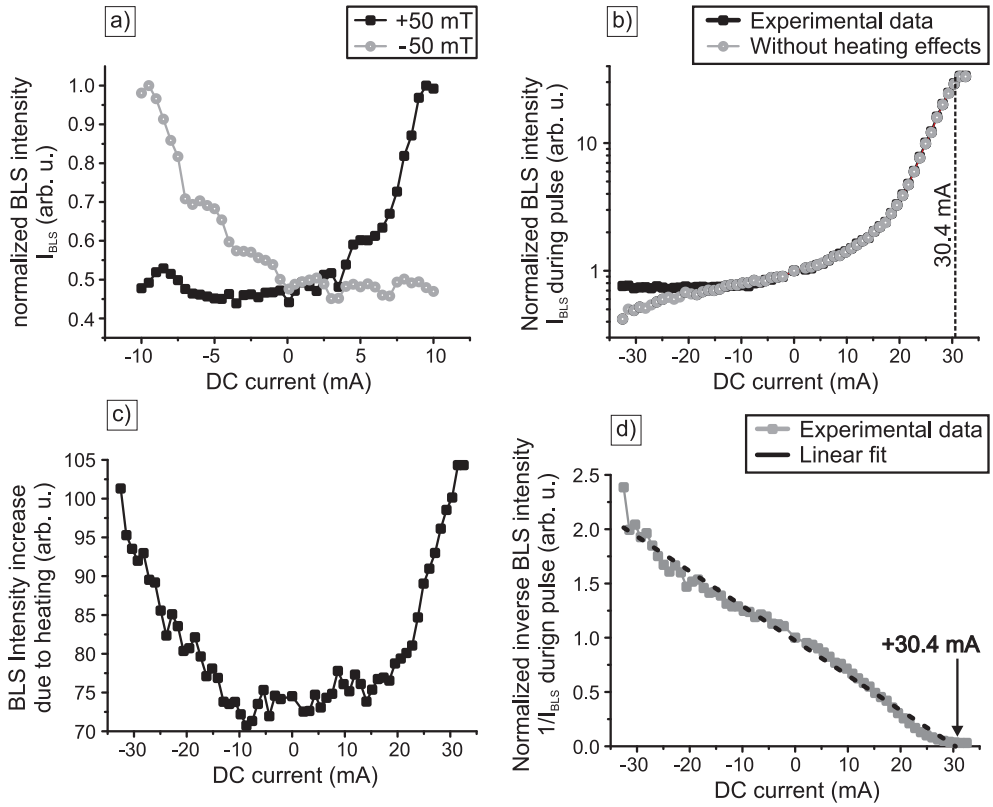

Fig. 2: Experimental results. a) Normalized total BLS intensity I_{BLS} depending on the DC current for a magnetic field of $+50\,\mathrm{mT}$ (black squares) and $-50\,\mathrm{mT}$ (grey circles). b) From the time-resolved measurements extracted normalized total BLS intensity I_{BLS} during the DC pulses (black squares). The grey circles show the corrected data with the thermal contribution substracted. Please note the logarithmic scale. c) Thermally increased total spin-wave intensity in the time between two DC pulses. d) Normalized inverse total BLS intensity $1/I_{BLS}$. The data is the same as shown in b) with the heating effects taken into account. The dashed line shows a linear fit yielding a threshold current of $+30.4\,\mathrm{mA}$.

the spin-wave intensity during the current pulses measured by time-resolved BLS (please note the log-scale). In contrast to the rather small intensity increase shown in Fig. 2a, an increase of up to a factor of 32 can be observed. Further, the data shows a saturation of the spin-wave intensity for applied currents larger than +30 mA. This saturation can be related to the onset of strong nonlinear magnon-magnon scattering processes in the presence of high magnon densities. As already mentioned, the time-resolved BLS measurements give not only access to the spin-wave intensity while the DC pulse is applied but also to the spin-wave intensity before and after the DC pulse. Here, an increased thermal spin-wave signal could be observed as shown in Fig. 2c. This increase is comparably small and, more important, independent of the current polarity but only on the absolute current value. Thus, this increase of the thermal signal in the currentless state can be assigned to residual Joule heating of the sample, and, thus, must be substracted. The grey circles in Fig. 2b show the corrected data. For negative applied currents the heating contribution has a large impact as the total intensity is small and the corrections are more significant.

To further analyze the results, the threshold current value under the investigated conditions is determined, which describes the point where the spin-wave damping is completely compensated. Figure 2d shows the dependence of the inverse BLS intensity with the heating effects substracted. Here, the expected linear dependence of the inverse BLS intensity on the applied current [6] can clearly be seen. A linear fit yields a threshold value of +30.4 mA. Hence, this shows that for the largest applied current the threshold is exceeded in the experiments. However, even if the spin-wave damping is completely compensated, in contrast to other reports [4], no onset of an auto-oscillation is observed. In the case of an auto-oscillation, the energy in the magnonic system would be concentrated in one certain spin-wave mode. However, the data shows no appearance of a distinct mode but a comparable spin-wave frequency spectrum shifted to lower frequencies and the intensity saturates for currents above 30 mA (see Fig. 2b) due to increased nonlinear magnon-magnon interactions.

So far only the spin-wave intensities were discussed. However, at large positive applied currents, i.e. when the effective damping is reduced, an additional frequency shift of the spin-wave spectrum can be observed [6]. Figures 3a,b show the spin-wave spectra and the frequency of the maximum during the DC pulse for different applied currents, respectively. Here, a large shift of more than 2 GHz is observed. However, the spin-wave frequencies stay constant for currents below +18 mA. As no shift is observed for negative currents, heating effects can be eliminated as origin for this effect. Also simulations of the Oersted-field inside the CMFS layer originating from the DC current show that these fields are small and can be neglected. As the spin-wave spectra shift to lower

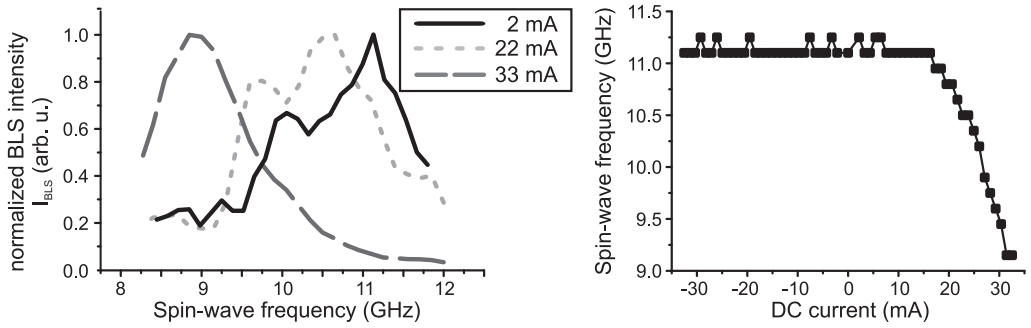

Fig. 3: Frequency shift of the spin-wave spectrum. a) Spin-wave spectra extracted from the time-resolved measurements during the DC pulses are applied for different applied current values. b) Spin-wave frequency at which the maximum BLS intensity is detected depending on the DC current.

frequencies, the origin of this shift can be contributed to a reduction of the effective magnetization along the external field by a drastic increase of the number of magnons. This reduction of the effective magnetization will cause a shift of the spin-wave spectrum to lower frequencies.

In conclusion, we have shown that by using the SHE and STT effect the effective spin-wave damping in the Cobalt-based Heusler compound CMFS can be modified in a wide range and even be completely compensated. This shows the feasibility of CMFS for being used in future magnonic logic devices and controlling these devices by a DC current. Furthermore, by using time-resolved BLS measurements, heating effects due to Joule heating by the DC currents could be determined and taken into account. We show that in the presented geometry, without any localization of the magnetic system or the DC current density, no auto-oscillation occurs. The observed large frequency shift of the spin-wave spectrum can be attributed to a strongly increased number of magnons in the magnetic system. This result offers another way for intensity- and frequency-controlled magnonic devices via a DC current.

We gratefully acknowledge financial support by the DFG Research Unit 1464 and the Strategic Japanese-German Joint Research Program from JST: ASPIMATT.

References

[1] T. Sebastian, Y. Ohdaira, T. Kubota, P. Pirro, T. Brächer, K. Vogt, A.A. Serga, H. Naganuma, M. Oogane, Y. Ando, B. Hillebrands, *Low-damping spin-wave propagation in a micro-structured $Co_2Mn_{0.6}Fe_{0.4}Si$ Heusler waveguide*, Appl. Phys. Lett. **100**, 112402 (2012).

[2] J.E. Hirsch, *Spin Hall effect*, Phys. Rev. Lett. **83**, 1834 (1999).

[3] J.C. Slonczewski, *Current-driven excitation of magnetic multilayers*, J. Magn. Magn. Mater. **159** (1996).

[4] V.E. Demidov, S. Urazhdin, H. Ulrichs, V. Tiberkevich, A. Slavin, D. Baither, G. Schmitz, S.O. Demokritov, *Magnetic nano-oscillator driven by pure spin current*, Nat. mater. **11** (2012).

[5] V.E. Demidov, S. Urazhdin, E.R.J. Edwards, S.O. Demokritov, *Wide-range control of ferromagnetic resonance by spin Hall effect*, Appl. Phys. Lett. **99**, 172501 (2011).

[6] V.E. Demidov, S. Urazhdin, E.R.J. Edwards, M.D. Stiles, R.D. McMichael, S.O. Demokritov, *Control of magnetic fluctuations by spin current*, Phys. Rev. Lett. **107**, 107204 (2011).

[7] K. Ando, S. Takahashi, K. Harii, K. Sasage, J. Ieda, S. Maekawa, E. Saitoh, *Electric manipulation of spin relaxation using the spin Hall effect*, Phys. Rev. Lett. **101**, 036601 (2008).

[8] V.E. Demidov, S. Urazhdin, A.B. Rinkevich, G. Reiss, S.O. Demokritov, *Spin Hall controlled magnonic microwaveguides*, Appl. Phys. Lett. **104**, 152402 (2014).

[9] K. An, D.R. Birt, C.-F. Pai, K. Olsson, D.C. Ralph, R.A. Buhrmann, X. Li, *Control of propagating spin waves via spin transfer torque in a metallic bilayer waveguide*, Phys. Rev. B **89**, 140405 (2014).

[10] M. Schreier, G.E.W. Bauer, V. Vasyuchka, J. Flipse, K. Uchida, J. Lotze, V. Lauer, A. Chumak, A.A. Serga, S. Daimon, T. Kikkawa, E. Saitoh, B.J. van Wees, B. Hillebrands, R. Gross, S.T.B. Goennenwein, *Sign of inverse spin Hall voltages generated by ferromagnetic resonance and temperature gradients in yttrium iron garnet platinum bilayers*, J. Phys. D **48**, 025001 (2014).

[11] C. Du, H. Wang, F. Yang, P.C. Hammel, *Systematic variation of spin-orbit coupling with d-orbital filling: Large inverse spin Hall effect in 3d transition metals*, Phys. Rev. B **90**, 140407 (2014).

[12] V.E. Demidov, S.O. Demokritov, B. Hillebrands, M. Laufenberg, P.P. Freitas, *Radiation of spin waves by a single micrometer-sized magnetic element*, Appl. Phys. Lett. **85**, 2866 (2004).

4.14 Investigation of $Co_{40}Fe_{40}B_{20}$ spin wave waveguides

T. Fischer, T. Brächer, T. Meyer, B. Heinz, M. Geilen, B. Hillebrands, and A. Conca*

**Current affiliation:*
Univ. Grenoble Alpes, CNRS, CEA, INAC-SPINTEC, 38054 Grenoble, France

With continuous miniaturization of devices, adequate dissipation of the generated Joule heat becomes more and more difficult. For this reason, the clock speed of modern CMOS-based CPUs is limited and an increase of data processing speeds can only be achieved by employing multi-core CPUs [1]. However, this will not suffice to satisfy Moore's law [2] in the next decade.
Spin waves and their application in logic devices are of high interest since they represent a possible solution to this issue. In contrast to electric currents experiencing Ohmic losses and, therefore, generating waste heat, spin waves promise to drastically reduce the heat generated in logic devices. A major step into this direction was the development and the realization of a magnon transistor [3] as well as the numerical simulation of a spin-wave majority logic gate [4]. However, the successful establishment of computational devices based on spin-wave logic elements still lacks for suitable materials which can be deposited and structured easily and, furthermore, exhibit a low Gilbert damping parameter in order to enable large spin-wave propagation lengths.
In this Report, we present the investigation of the material $Co_{40}Fe_{40}B_{20}$ as a candidate material for the fabrication of spin-wave conduits. This material has been reported to show a low Gilbert damping parameter [5, 6] and, due to its high saturation magnetization [7], features a high spin-wave group velocity.
In order to investigate the properties of spin waves in $Co_{40}Fe_{40}B_{20}$, thin films with a nominal thickness of 40 nm have been sputter-deposited. Following the deposition of the magnetic material, a set of samples was treated with an *in situ* annealing step at 350 °C for a period of 90 minutes. Subsequently, either a layer of Al (7 nm) or a double layer of MgO (7 nm) and Pt (7 nm) was deposited on top of the magnetic layer. To prevent any diffusion of boron into the MgO layer [8], the capping was deposited after performing the annealing step.
AFM measurements reveal a smooth topography of all samples and hence, a closed capping layer (RMS value of 0.3 nm) preventing the underlying magnetic layer from oxidation was produced in all cases.

In the following, the results obtained from the sample that was treated with an annealing step and capped with MgO and Pt shall be presented. FMR measurements performed with this sample are shown in Fig. 1. The Kittel fit [9] leads to an effective magnetization value of $M_{\mathrm{eff}} = 1157.7 \pm 0.1\,\mathrm{kAm^{-1}}$ and the dependence of the absorption linewidth on the resonance frequency results in a comparably low Gilbert damping parameter $\alpha = (5.6 \pm 0.5) \times 10^{-3}$.
In order to investigate the spin-wave propagation, the plain films were structured into spin-wave waveguides employing electron beam lithography and ion beam etching. Subsequently, to allow for the excitation of spin waves, a shunt coplanar Au waveguide of width $w_{\mathrm{a}} = 1\,\mu\mathrm{m}$ was patterned on top of the waveguides acting as an excitation antenna for spin waves. Spin-wave propagation occured with the external magnetic field applied parallel to the short axis of the waveguides, also referred to as the Damon-Eshbach mode geometry.
A preservation of the Gilbert damping parameter α of the spin-wave propagation in these waveguides is of particular interest. In order to determine α in the microstructured waveguides, the antenna structure is designed in a way such that spin waves can be excited on both ends of the

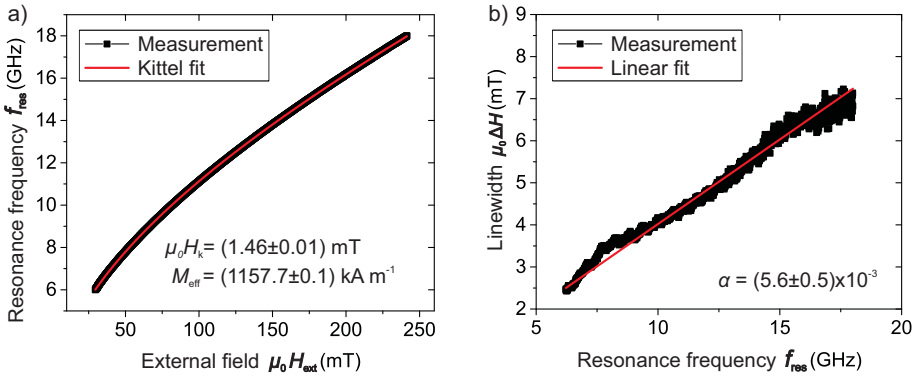

Fig. 1: Results of the FMR measurements performed with a plain $Co_{40}Fe_{40}B_{20}$ film with an MgO|Pt capping layer. a) Resonance frequency in dependence on the externally applied magnetic field and Kittel fit [9]. The anisotropy field is described by $\mu_0 H_k$. b) Linewidth of the absorption peak at the FMR frequency in dependence on the resonance frequency and linear fit for the estimation of the Gilbert damping parameter α.

waveguides. The counterpropagating and interfering waves create a stationary interference pattern, whose spatial periodity enables the determination of the corresponding wave vector and the decay length of the spin wave excited with a particular frequency. Hence, the dispersion relation can be identified. The spin-wave intensity is measured by means of microfocussed Brillouin light scattering spectroscopy (μBLS). The black squares in Fig. 2 show the BLS intensity measured centrally along the waveguide with a width of $w = 3.5\,\mu$m for an excitation frequency of $f_{SW} = 5.4\,$GHz and $f_{SW} = 7.6\,$GHz, respectively, and an external field of $\mu_0 H_{ext,eff} = 25\,$mT. Following the approach introduced in [10], α can be calculated according to the relation

$$\alpha \cdot (\omega_0 + \frac{\omega_M}{2}) = \frac{v_g}{\delta} \quad . \tag{1}$$

Here, $\omega_0 = \gamma\mu_0 H_{ext,eff}$ denotes the bulk FMR frequency in the effective external field, $\omega_m = \gamma\mu_0 M_{eff}$ the precessional frequency in the field evoked by the effective magnetization of the material, v_g the group velocity, and δ the amplitude decay length.

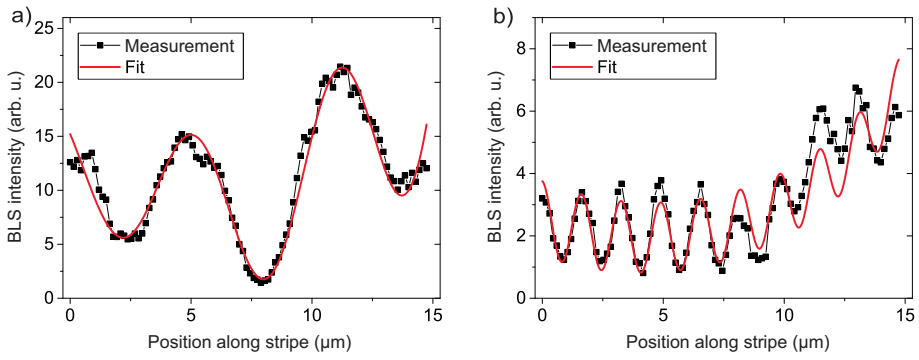

Fig. 2: Spin-wave intensity along the waveguide for excitation frequencies of a) $f_{SW} = 5.4\,$GHz and b) $f_{SW} = 7.6\,$GHz, respectively, and fit of theoretical intensity patterns to the measured values (solid lines). The waveguide has a width of $w = 3.5\,\mu$m.

Fitting the theoretically predicted interference pattern for the first width mode of the waveguide to the measured data leads to a wave vector of $k_{SW} = 0.52\,\mu\text{m}^{-1}$ and $k_{SW} = 1.92\,\mu\text{m}^{-1}$, respectively.

The resulting amplitude decay lengths lie in the range of $\delta = 8\,\mu\text{m}$. The dispersion relation is shown by the black squares in Fig. 3 and shows a nearly linear trend. Therefore, a linear curve is fitted to the experimental values with its slope representing the group velocity.

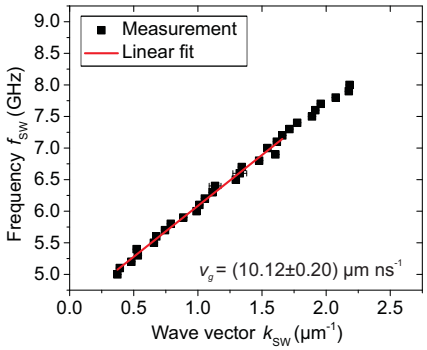

Fig. 3: Dispersion relation for the sample with a layer system of $Co_{40}Fe_{40}B_{20}(40)|MgO(7)|Pt(7)$ and linear approximation. The linear fit leads to a group velocity of $v_g = 10.12\,\mu\text{m}\cdot\text{ns}^{-1}$.

Here, this linear approximation results in a group velocity of $v_g = (10.12 \pm 0.20)\,\mu\text{m/ns}$. With $\mu_0 H_{\text{ext,eff}} = 25\text{mT}$ and $M_{\text{eff}} = 1157.7\,\text{kA}\,\text{m}^{-1}$ from the FMR measurements, a Gilbert damping parameter of $\alpha = (9.5 \pm 0.5) \times 10^{-3}$ is obtained. This value drastically differs from the one found from FMR measurements performed with the plain film of the same material composition and layer system.

To further investigate this large discrepancy, another plain film was structured into an array of stripes with a width of $10\,\mu\text{m}$ and a length of $100\,\mu\text{m}$. With this microstructured sample, FMR measurements were performed with the external field applied parallel to the long axis of the stripes as well as with the external field applied perpendicular to the long axis of the stripes (backward-volume mode geometry). The results of these measurements are shown in Fig. 4.

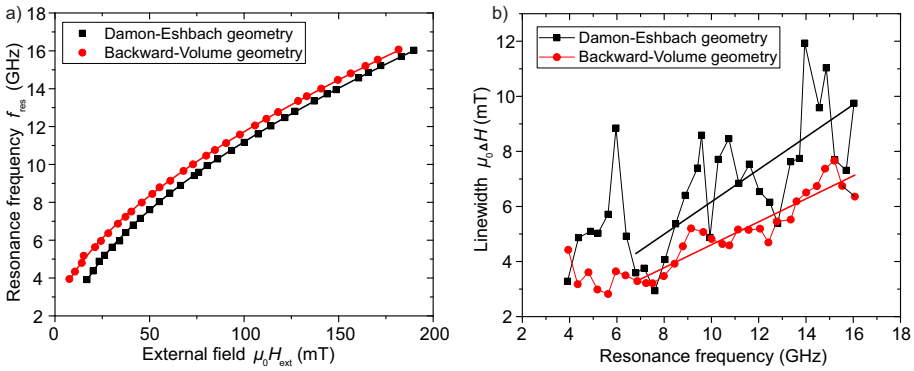

Fig. 4: Results of the measurements of the FMR performed with the stripe array. a) Resonance frequency in dependence on the externally applied field and Kittel fit including the modification due to the shape anisotropy. b) Linewidth of the absorption in dependence on the resonance frequency. The Gilbert damping parameter α can be determined from the slope of the linear fits shown as solid lines. In both the diagrams, squares represent the data obtained in Damon-Eshbach mode geometry and circles represent the data measured in backward-volume mode geometry, respectively.

In this case, the Kittel formula has to be modified to account for the shape anisotropy of the stripes. This approach is introduced e.g. in [9] and [11]. The value obtained for the saturation magnetization is $M_{\text{eff}} = 1255.2\,\text{kA}\,\text{m}^{-1}$ in Damon-Eshbach mode geometry and $M_{\text{eff}} = 1248.0\,\text{kA}\,\text{m}^{-1}$ in backward-volume mode geometry. For the anisotropy field, values of $\mu_0 H_{\text{k}} = 4.86\,\text{mT}$ and

$\mu_0 H_k = 4.69\,\mathrm{mT}$ are found, respectively. This result justifies the approach describing the FMR in these stripes by a simple modification of Kittel's formula to account for the shape anisotropy.
Surprisingly, the value of $\alpha = (6.4 \pm 0.5) \times 10^{-3}$ for the Gilbert damping parameter in backward-volume mode geometry agrees well with the one found for the plain film while the value of $\alpha = (9.0 \pm 0.5) \times 10^{-3}$ found in the Damon-Eshbach mode geometry is closer to the one estimated from the dispersion relation. In contrast, no significant difference of the properties of annealed samples and the ones which had not been treated with an annealing step has been found. Also, we did not encounter any differences between the different cappings on top of the magnetic layers. Overall, the large discrepancy of the Gilbert damping parameter of the waveguides and the plain films can have different reasons: Possible explanations for these results could be the degradation of the magnetic material properties during the structuring process or the influence of the heat amount transferred by the laser to the sample during the BLS measurements. However, a large influence of these two effects is unlikely since this degradation would also have been observed in the FMR measurements performed with the stripe array. Hence, the presence of an inhomogeneous magnetization state in the Damon-Eshbach mode geometry giving rise to increased losses due to magnon-magnon interaction appears to be the most reasonable explanation for the observed propagation characteristics.
In conclusion, this work revealed certain unexpected hurdles in the establishment of spin-wave waveguides from $Co_{40}Fe_{40}B_{20}$. These obstacles have to be overcome in order to enable the application of this material in future spin-logic devices. Therefore, a further understanding of the properties of spin-wave waveguides manufactured from this material is needed. Future micromagnetic simulations or an investigation of the spin-wave propagation in backward-volume mode geometry will address these questions.
We wish to thank the team of the Nano Structuring Center at the University of Kaiserslautern for their support in sample preparation. Financial support by the state of Rhineland-Palatinate (MB-WWK and MWKEL) and by the European Regional Development Fund (ERDF) in the frame of the Spintronic Technology Platform (STeP) is acknowledged.

References

[1] C. Mims, *Why CPUs Aren't Getting Any Faster*, MIT Tech. Rev. (2012).
[2] G.E. Moore, Cramming More Components onto Integrated Circuits, Electronics **38**, 114 (1965).
[3] A.V. Chumak, A.A. Serga, B. Hillebrands, *Magnon transistor for all-magnon data processing*, Nat. Comm. **5** (2014).
[4] S. Klingler, P. Pirro, T. Brächer, B. Leven, B. Hillebrands, A.V. Chumak, *Design of a spin-wave majority gate employing mode selection*, Appl. Phys. Lett. **105**, 152410 (2014).
[5] A. Conca, J. Greser, T. Sebastian, S. Klingler, B. Obry, B. Leven, B. Hillebrands, *Low spin-wave damping in amorphous $Co_{40}Fe_{40}B_{20}$ thin films*, J. Appl. Phys. **113**, 2011 (2013).
[6] A. Conca, E.Th. Papaioannou, S. Klingler, J. Greser, T. Sebastian, B. Leven, J. Lösch, B. Hillebrands, *Annealing influence on the Gilbert damping parameter and the exchange constant of CoFeB thin films*, Appl. Phys. Lett. **104**, 182407 (2014).
[7] T. Schwarze, D. Grundler, *Magnonic crystal wave guide with large spin-wave propagation velocity in CoFeB*, Appl. Phys. Lett. **102**, 222412 (2013).
[8] H.K. Chandra, P. Mahadevan, *Boron diffusion in MgO and emergence of magnetic ground states: A first-principles study*, Phys. Rev. B **89**, 144412 (2014).
[9] C. Kittel, *On the theory of ferromagnetic resonance absorption*, Phys. Rev. **73**, 155 (1948).
[10] D.D. Stancil, A. Prabhakar, *Spin waves: Theory and Applications*, Springer US, 1st ed. (2009).
[11] S.S. Kalarickal, P. Krivosik, M. Wu, C.E. Patton, M.L. Schneider, P. Kabos, T.J. Silva, J.P. Nibarger, *Ferromagnetic resonance linewidth in metallic thin films: Comparison of measurement methods*, J. Appl. Phys. **99**, 093909 (2006).

4.15 Study of the magnetic properties of epitaxial Fe/Pt bilayers for spin pumping measurements

S. Keller, J. Greser, A. Conca, P. Fuhrmann, B. Hillebrands, and E.Th. Papaioannou

In collaboration with Jörg Lösch and Alexander Brodyanski, Institut für Oberflächen- und Schichtanalytik (IFOS), Trippstadter Str. 120, 67663 Kaiserslautern, Germany

Magnetic bilayers composed of a ferromagnetic and a non-magnetic metal are of great interest in research activities concerning the detection of spin currents through spin torque and spin pumping effects [1–3]. However, the structural quality and the presence of magnetic anisotropies are often neglected in most of the studies, since they are carried out on polycrystalline samples. Here, we show the influence of high epitaxial quality on the magnetization reversal in Fe/Pt bilayers in perspective of the usage in spin pumping measurements. The used bilayers have identical layer thicknesses but are grown at different substrate temperatures (30 °C, 150 °C, 300 °C, and 450 °C). Kerr effect measurements reveal the presence of a small uniaxial anisotropy superimposed on a cubic magneto-crystalline anisotropy. That strongly influences the magnetization reversal process resulting in one and two step hysteresis loops.

The bilayers were grown on MgO(100) substrates consisting of a Fe layer of 12 nm thickness and a Pt layer of 10 nm thickness by electron-beam evaporation in an ultrahigh vacuum (UHV) chamber with a base pressure of 5.0×10^{-11} mbar.

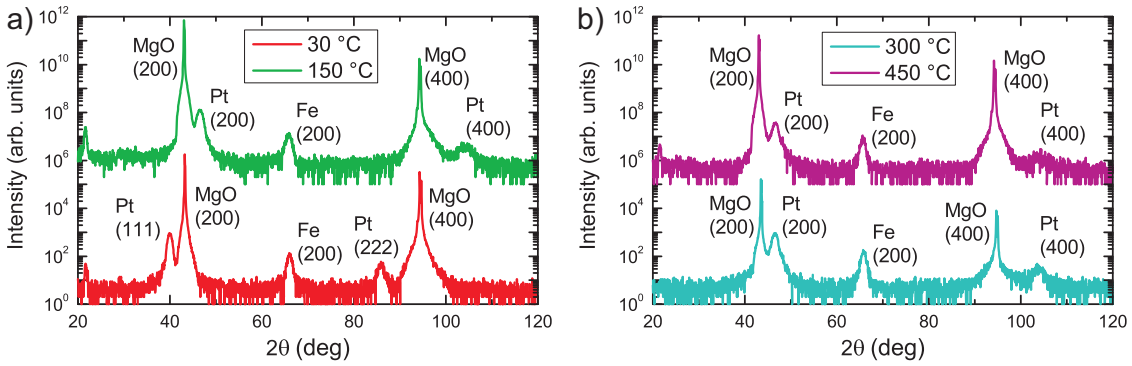

Fig. 1: XRD Θ/2Θ-scans from the samples grown at a) 30 °C and 150 °C, b) 300 °C and 450 °C. The plots for the 150° and 450° samples have been shifted upwards by a factor of 10^6 for clarity.

X-ray diffraction (XRD) measurements (shown in Fig. 1) show the presence of Fe(200) diffraction peaks proving the epitaxy of the Fe layer on top of the MgO substrate. The growth of Pt exhibits interesting properties. For the sample grown at 30 °C the Pt on top of Fe has a preferred grain orientation of (111). In contrast, diffraction peaks of Pt(200) and Pt(400) arising from the Pt top layer parallel to the Fe (200) planes were observed for all samples grown above 150 °C. The growth of the fcc Pt layer on bcc Fe along the [100] plane direction can be correlated to the epitaxial Bain path [4] where the Pt cell is 45° rotated with respect to the Fe lattice (see also Fig. 2c).

The structural quality of the growth of Fe was further investigated by performing XRD azimuthal-scans. Figure 2a nicely shows the in-plane properties of the 300 °C sample: It exhibits 45° in-plane epitaxial relation (Fe[100] ∥ MgO[110], Fe[110] ∥ MgO[010]) between the substrate and the

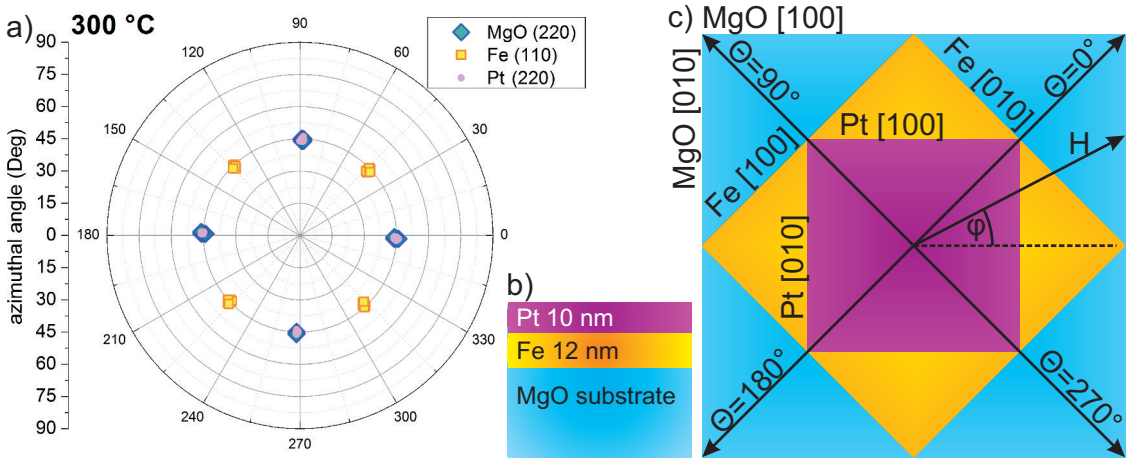

Fig. 2: a) XRD azimuthal-scan from the sample grown at 300 °C. The Pt(220) peaks are on top of the MgO(220). b) Layer thickness scheme of the Fe/Pt samples. c) Scheme of the crystal orientations of the samples relative to the MgO substrate and scheme of the angles ϕ and Θ between the Fe[100] and the magnetization, respectively between the MgO[100] and the external magnetic field.

Fe film. Furthermore Fig. 2a shows the epitaxial growth of Pt on Fe: 4 peaks of Pt(220), each rotated by 90° to each other, are tilted from the Fe(110) peaks by 45°. This confirms the 45° rotation of the Pt lattice on top of Fe. For the 150 °C and 450 °C samples the in-plane orientation of Fe is distorted in some areas and deviates from the 45 ° relationship. In particular an angle of 30° between (Fe[100] || MgO[110]) and (Pt[100] || Fe[110]) is observed.

STM images taken *in-situ* after the growth of Fe and of Pt elucidate further the structural quality of the samples. The growth of Fe at different temperatures leads to significant changes in grain shape, size and flatness. By increasing the temperature the mean size of the crystallites significantly increases from 5 nm at room temperature to 15 nm at 450 °C. Rounded islands with narrow size distribution can be observed for the 30 °C sample. Furthermore, a dramatic change in the islands shape from small rounded grains to almost squared like crystallites for the 300°C and 450°C samples occurs. Especially square type islands with big flat terraces appear above 300°C. The Pt evaporation on top of Fe maintains the surface characteristics of the samples and the differences between the samples.

In order to correlate the structural with the magnetic properties we have studied the magnetization revearsal process in our Fe/Pt films using the longitudinal magneto-optical Kerr effect. The 45° epitaxial relation (Fe[100] || MgO[110], Fe[110] || MgO[010]) (see Fig. 2c) between the substrate MgO and the Fe layer is reflected in the magnetic measurements by the Fe[100] direction to be the easy magnetic axis with a four-fold symmetry. The Pt overlayer does not break the four-fold symmetry. Furthermore, by varying the in-plane angle from 0° to 360° with a stepsize of 2° in the longitudinal geometry, we observe one-step and two-step loops with characteristic coercivity values for the first (H_{C1}) and for the second (H_{C2}) step as shown in Fig. 3a.

We have measured the switching fields H_{C1} and H_{C2} and plot them exemplarily for the sample grown at 300°C in Fig. 3b with respect to the angle ϕ of the applied magnetic field (illustrated in Fig. 2c). For hysteresis loops, where two steps occur, the magnetization switches by 90° each step, while for hysteresis loops with only a single step, the expected 180° domain wall nucleation does not fit. In fact, the single step switch consists of two consecutive switches by 90° as described in Ref. [5].

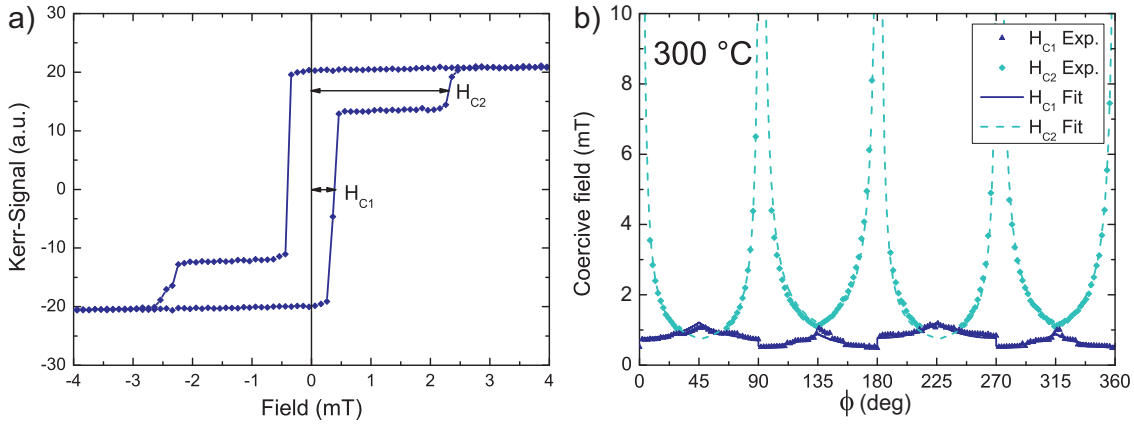

Fig. 3: a) Typical hysteresis loop of the Fe/Pt samples with two coercive field steps. b) Plot of the coercive field steps in dependence of the angle between the external magnetic field and the MgO[100] direction. Around 45° and 225° only one-step field switching occurs.

This behaviour can be quantified in terms of the total energy E, which is a function of the intrinsic cubic anisotropy, K_1, and the superimposing uniaxial magnetic anisotropy term, K_u [6]:

$$E = K_u \sin^2\theta + \frac{K_1}{4}\sin^2 2\theta - M\,H\,\cos(\theta-\phi) \quad , \tag{1}$$

where θ is the angle between the Fe[100] axis and the magnetization and ϕ the angle between the Fe[100] axis and the external magnetic field. With the assumption of single domain states with minimal energy (this means in particular low external field and Θ = 0°, 90°, 180°, and 270°) and 90° domain wall nucleation, we solve the equation for the coercive field steps [6]:

$$H_{C1,2} = \frac{\varepsilon_{90°}/M \pm K_u/M}{\pm\cos(\phi)\pm\sin(\phi)} + H_{off} \quad , \tag{2}$$

where $\varepsilon_{90°}$ is the 90° domain wall nucleation energy, K_u is the uniaxial anisotropy constant, M is the magnetization, and ϕ is the angle of the external field. The signs "±" in this formula change in intervals of 45° as listed in Ref. [6].

In contrast to Cowburn et al. [6], an additional offset field H_{off} is required in Eq. 2 for the 300 °C and 450 °C samples and the parameters for the two coercive steps start to differ for the same sample (Fig. 4). While for the 30 °C and the 150 °C samples the fitting parameters for the coercive steps H_{C1} and H_{C2} are the same and the coercive offset fields H_{off} are zero, for samples grown at temperatures of 300 °C and higher the parameters for the fitting split up for the two steps and the offset becomes non-zero. For the 450 °C sample the splitting as well as the 90° domain wall nucleation energy and the offset fields are strongly increased. The offsets for H_{C1} and H_{C2} thus have opposite signs. According to Fig. 4b the uniaxial anisotropy constant over magnetization for the 30 °C sample is almost zero and for the 300 °C sample it is at maximum.

In conclusion, this report shows the epitaxial growth of Fe/Pt bilayers with 45° rotation of the Pt lattice on top of Fe. Even a small uniaxial anisotropy imposed on a cubic anisotropy can strongly influence the magnetization reversal process measured by longitudinal magneto-optical Kerr effect resulting in one and two step hysteresis loops. With increasing growth temperature a splitting in the coercive field step parameters occurs.

The Carl Zeiss Stiftung is gratefully acknowledged for financial support.

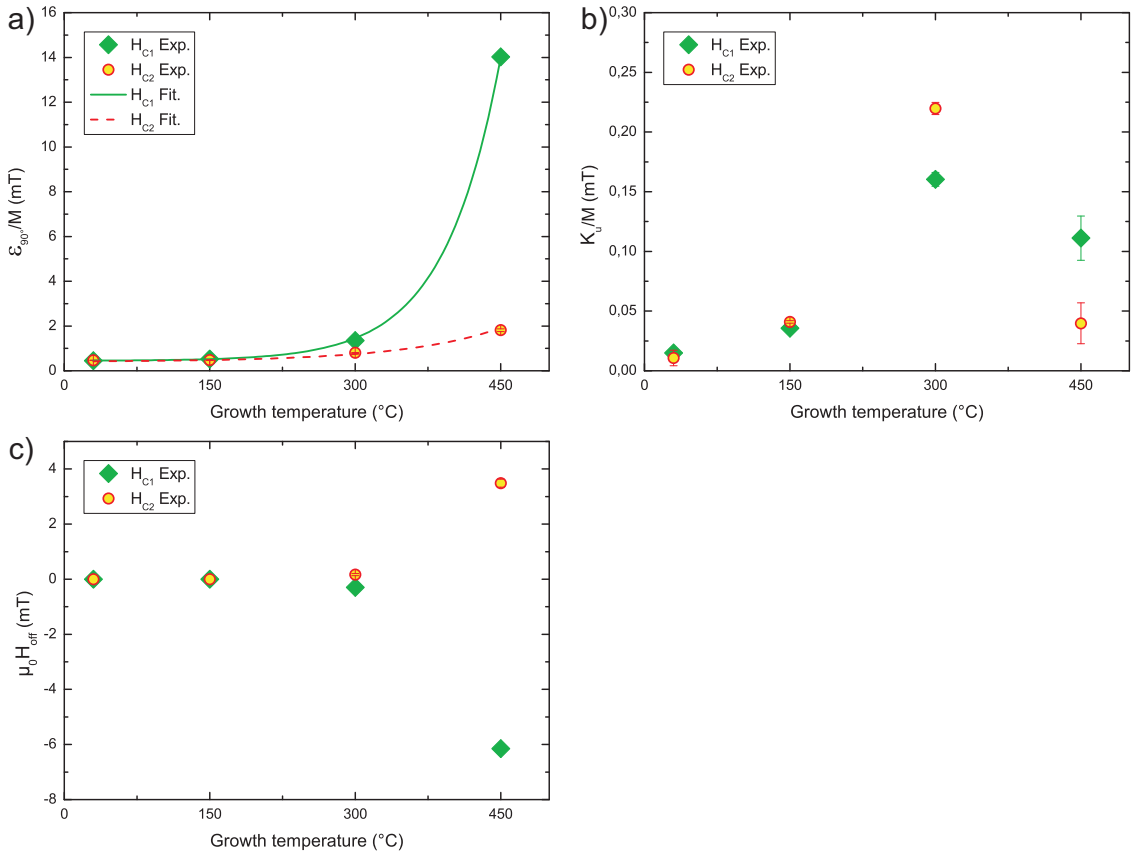

Fig. 4: Plots of the fitting parameter of the Fe/Pt samples according to equation 2: a) 90 °C domain wall nucleation energy divided by magnetization, b) uniaxial anisotropy constant divided by magnetization and c) coercive offset field.

References

[1] E.Th. Papaioannou, P. Fuhrmann, M.B. Jungfleisch, T. Brächer, P. Pirro, V. Lauer, J. Lösch, B. Hillebrands, *Optimizing the spin-pumping induced inverse spin Hall voltage by crystal growth in Fe/Pt bilayers*, Appl. Phys. Lett. **103**, 162401 (2013).

[2] A. Brataas, A.D. Kent, H. Ohno, *Current-induced torques in magnetic materials*, Nature Mater. **11**, 372 (2012).

[3] A. Hoffmann, *Spin Hall effects in metals*, IEEE Transactions On Magnetics **49**, 5172 (2013).

[4] B. Daniels, W. Nix, B. Clemens, *Enhanced mechanical hardness in compositionally modulated Fe(001)Pt(001) and Fe(001)Cr(001) epitaxial thin films*, Thin Solid Films **253**, 218 (1994).

[5] Q.F. Zhan, S. Vandezande, K. Temst, C. Van Haesendonck, *Magnetic anisotropies of epitaxial Fe/MgO(001) films with varying thickness and grown under different conditions*, New J. Phys. **11** 063003 (2009).

[6] R.P. Cowburn, S.J. Gray, J. Ferré, J.A.C. Bland, J. Miltat, *Magnetic switching and in-plane uniaxial anisotropy in ultrathin Ag/Fe/Ag(100) epitaxial films*, J. Appl. Phys. **78** 7210 (1995).

F. Applied Spintronics

A substantial part of our research is devoted to fields that have a close relation to applications. Our group is aiming to intensify the communication flow between the academic and the industrial world in order to promote the necessary transfer of technology and *know-how*. This year we successfully concluded our project "Spintronics Technology Platform in Rhineland-Palatinate - STeP". There we performed a Europe-wide unique type of direct transfer of *know-how* and technology, jointly with the University of Mainz, within the collaboration with the company Sensitec GmbH, Mainz. This was funded by the Ministerium für Bildung, Wissenschaft, Weiterbildung und Kultur in Rhineland-Palatinate in the frame of the European EFRE program. Among the main goals we name the construction of a R&D infrastructure directed to small and medium enterprises in Rhineland-Palatinate together with the innovation in GMR and TMR technologies with a strong emphasis on the use of industrial production lines for the creation and testing of new sensor concepts. In this project we contributed to the design and testing of new sensor concepts, the material characterization, especially of Heusler thin films, and in other subjects.

In this summer we also concluded a very fruitful collaboration within the joint inter-regional team of the Greater Region Magnetism Network (GRMN) which had been established in the year 2012 in the framework of the University of the Greater Region. Here, the universities of Lorraine, Saarbrücken and Kaiserslautern joined their forces to explore magnetic phenomena and their novel application potential. As main aim of the GRMN the synergy of expertise and activities to develop concerted teaching strategies as well as highly innovative technology transfer concepts has been identified.

In Report 4.16 a retrospect is given on the aims, joint efforts and main achievements of the STeP project. A short review on the conclusion meeting is given, which took place under participation of Mrs. Vera Reiß, the Minister of Research and Education of Rhineland-Palatinate.

In Report 4.17 two new concept developments of AMR demonstrators for automotive applications are presented. Those works have been carried out in the form of two Master of Education theses in the framework of the Greater Region Magnetism Network.

F. Angewandte Spintronik

Ein Teil unserer Aktivitäten ist auf anwendungsorientierte Forschung gerichtet. Ziel unserer Gruppe ist es hierbei, Brücken zwischen der akademischen und der industriellen Welt zu bauen, um den Technologietransfer und den Ideenaustausch zu fördern. Im Februar 2015 haben wir erfolgreich unser industrielles Kooperationsprojekt Spintronik-Technologie-Plattform (STeP) abgeschlossen, das seit 2012 vom Ministerium für Bildung, Wissenschaft, Weiterbildung und Kultur in Rheinland-Pfalz im Rahmen des europäischen EFRE-Programms finanziert wurde. Dieses Projekt war eine Zusammenarbeit zwischen der TU Kaiserslautern, der Universität Mainz und dem Industriepartner Sensitec, der große Erfahrung in der Sensorik und in den praktischen Anwendungen der Spintronik gesammelt hat. Hauptziele der Plattform waren insbesondere eine Bereitstellung von Forschungsinfrastruktur und anwendungsorientiertem universitären Know-How besonders für kleine und mittlere Unternehmen (KMU) in Rheinland-Pfalz und die Förderung von Innovation im Bereich der GMR und TMR-Technologien. Unsere Aufgabe bestand unter anderen darin, das Design neuer Sensoren mit mikromagnetischen Simulationen zu unterstützen und die Charakterisierung von Heusler-Dünnschichtsystemen vorzunehmen.

Als weitere prominente Initiative auf dem Gebiet der anwendungsorientierten Forschung wurde ebenfalls in diesem Jahr nach einer dreijährigen Förderung das Magnetismusnetzwerk der Großregion (GRMN) im Rahmen der Universität der Großregion erfolgreich abgeschlossen. Hier bündelten die Universitäten von Lothringen, Saarbrücken und Kaiserslautern ihr Know-how und ihre Netzwerkstrukturen, um magnetische Phänomene und ihr Anwendungspotential auszuloten. Ein Hauptziel dieser Initiative war es, die Synergie der Expertisen und Aktivitäten zu nutzen um ein konzertiertes Lehrkonzept auf dem Gebiet des Magnetismus und innovative Technologietransfer-Konzepte zu entwickeln.

In Bericht 4.16 wird eine Retrospektive der Ziele und Erfolge des STeP-Projektes gegeben. Er schließt mit einer kurzen Zusammenfassung der Abschlusskonferenz, auf der im Februar 2015 unter Beteiligung der Rheinland-Pfälzischen Wissenschaftsministerin Vera Reiß die Ergebnisse und Erfolge der Initiative diskutiert wurden.

In Bericht 4.17 werden zwei neue Konzeptentwicklungen für AMR-Demonstratoren für die Automotive Industrie vorgestellt. Diese Konzepte wurden in zwei Lehramts-Masterarbeiten im Rahmen des Magnetismus-Netzwerkes der Großregion entwickelt.

4.16 Successful conclusion of the Spintronics Technology Platform in Rhineland-Palatinate STeP

B. Leven, A. Conca, A. Ruiz Calaforra, and B. Hillebrands*

In collaboration with F. Casper, G. Jakob, and M. Kläui, Fachbereich Physik, Johannes Gutenberg Universität Mainz, Staudinger Weg 9, Mainz, Germany;
J. Paul, R. Lehndorff, M. Doms, J. Hölzl, and R. Slatter, Sensitec GmbH, Mainz, Germany

**Current affiliation:*
SPINTEC, CEA 1005 building, 17 rue des Martyrs, 38054 GRENOBLE Cedex 9, France

In a collaboration between the Universities of Kaiserslautern and Mainz, the Spintronics Technology Platform in Rhineland-Palatinate (STeP) was installed in the year 2012 in order to develop new concepts and measurement methods in the field of magnetic sensor technology and to promote those to the industrial economics. The aim of the STeP project was the sustainable establishment of a technology platform in the field of spintronics providing competences as well as infrastructure especially for small and medium sized enterprizes (SMEs). Within this initiative the main goal was to bring together industry-oriented research infrastructure and university know-how for a direct and fast transfer of technology with a special focus on regional partners. As a cornerstone, Sensitec GmbH (Mainz) as the technological leader in the field of magnetic sensors, was gained as a collaboration partner. To the public, Sensitec is well known for supplying the Mars rover Curiosity with the most recent sensor technology. All together, the STeP consortium comprised the team of Britta Leven and Burkard Hillebrands at the University of Kaiserslautern and the team of Gerhard Jakob and Matthias Kläui at the University of Mainz. The Spintronics Technology platform itself consists of an industrial sputter deposition facility including all necessary patterning tools established in the clean room environment of the Sensitec company in Mainz. In addition to the industrial infrastructure, which was partly used for the STeP project, Sensitec also supplied the STeP consortium with the necessary know-how for industrial application requirements. Thus, the gap between university research and industrial application needs in the field of spintronics could be bridged directly.

Those processes realized in the framework of the Spintronics Technology Platform in Rhineland-Palatinate followed a Europe-wide unique approach. The transfer of basic know-how from university XMR research to industrially specified process lines in the field of magnetic multilayers and sensors was at the core to establish a novel and manifold pool of competences. One of the central technological aims was the direct translation of the highly sensitive magnesium oxide-based process to DIN specified industry process lines for the realization of high quality TMR junctions. This was a particular challenge as the scientific research-derived processes were characterized only for small substrates up to diameters of 80 mm and therefore needed drastic upscaling for a large wafer fab fabrication (five inch wafer fab) without loss of high quality, homogeneity and reproducibility of the few nm thick layer. Another aim of the STeP project was to further develop a tool box system including novel Heusler-based GMR and TMR devices to open up the field for flexible applications adjustable to various functional and technological requirements. One example is a highly specialized 360°sensor based on complex spin valve pinning concepts. Furthermore, the STeP consortium demonstrated that not only technologically established materials such as NiFe

and CoFeB are suitable candidates for TMR devices in mass production, but that Heusler compounds such as CFAS are also well suited. The latter can also be implemented in industrial Silicon technology process lines to realize TMR sensor devices for specialized requirements. The first tests of wafer fabricated Heusler-TMR sensors revealed satisfactory TMR-values successfully providing a proof of concept. A special outcome of the STeP project was the development of a new XMR reliability test integrated on-chip thus allowing in future for a direct and especially space-saving sensor quality validation, and consequently, more efficient and reliable sensor production in the future. These results are the basis for a joint patent application of the STeP consortium partners.

The above results show that with the strategic concept of STeP and the composition of the team it was possible to directly bridge the gap between university research and industrial application in the field of spintronics. The novel approach of direct and fast transfer of technology from the universities to the industrial processing technology is an important prerequisite for the subsequent integration of research results in conventional production technology lines of the semiconductor industry. In an exemplary way STeP initialized a prompt implementation of basic research results in industrial wafer processing. Usually, this translation from ideas in university environment into product realization takes many years.

Fig. 1: STeP consortium jointly with the Minister of Research and Education of Rhineland-Palatinate, Mrs. Vera Reiß, during the conclusion meeting of the STeP project on 12.2.2015 : Dr. Frederick Casper (JGU Mainz), Dr. Ronald Lehndorff (Sensitec), Dr. Marco Doms (Sensitec), Prof. Dr. Mathias Kläui (JGU Mainz), Minister Mrs. Vera Reiß, Dr. Andres Conca (TU Kaiserslautern), Jürgen Rühl (LTI Drives), Dr. Britta Leven (TU Kaiserslautern), Prof. Dr. Burkard Hillebrands (TU Kaiserslautern), Dr. Jürgen Gerber (INNOMAG), Dr. Rolf Slatter (Sensitec, CEO); left to right.

In order to integrate the STeP consortium into a wider network of important players in the market of magnetic sensor technology it was closely connected to the network of innovation *Magnetische Mikrosysteme InnoMag e.V.*. This platform headquartered in Mainz is operating all over Germany and opens the field of innovative magnetic microsystems for new applications in the areas of automotive industries, automation, bioanalytics and safety engineering. Concerning scientific research, STeP is associated to the Graduate School of Excellence *Materials Science IN MainZ* (MAINZ) and the State Research Center OPTIMAS. Both University partners of STeP additionally closely collaborated with the Center for Technology Transfer for New Materials (TT-DINEMA) of the University of Mainz and the Nano Structuring Center (NSC) of the University of Kaiserslautern.

In February 2015 STeP was successfully concluded after three years of funding. The final meeting was held with participation of Mrs. Vera Reiß, Minister of Education, Science, Further Education and Culture of the State of Rhineland-Palatinate. Reiß expressed her special acknowlegdement on the remarkable results of the project: “The Spintronics Platform of Technology - the STeP project - is a Europe-wide unique success in the cooperation between excellent research and industry. In record time the project partners, the Technische Universität Kaiserslautern and the Johannes Gutenberg-Universität Mainz in cooperation with the Sensitec company, managed to build a bridge between basic research in the laboratories and industrial feasibility. The STeP project combined the research excellence available at the Universities in Rhineland-Palatinate with the innovative capacity of the local companies in an outstanding way”, she pointed out and added: “The transfer of knowledge from the universities towards the small and medium sized enterprises is an essential prerequisite for the success of the economic systems in Rhineland-Palatinate in a globalized world. To support this is an important goal of the government of Rhineland-Palatinate.”

The establishment of the Spintronics Technology Platform in Rhineland-Palatinate (STeP) was supported by the program “*Wachstum durch Innovation*” with about 1.4 Mio. Euro by Funds of the European Fonds of Regional Developments (ERDF) and the ministry for Education, Science, Further Education and Culture (MBWWK) and the ministry for Economic Affairs, Climate Protection, Energy and Regional Planning (MWKEL) of the state Rhineland-Palatinate.

4.17 New spintronics demonstrators for automotive applications

B. Leven, O. Nick, M. Hutzel, D. Weller, E.Th. Papaioannou, A. Conca, and B. Hillebrands

In collaboration with J. Kuhn, Arbeitsgruppe Didaktik der Physik, Fachbereich Physik, TU Kaiserslautern, Germany

In the framework of the Greater Region Magnetism Network GRMN, which was a joint European initiative with the Universities of Sarrebruck and Lothringen in connection with the University of the Greater Region, the promotion of magnetism and its application fields has been of major interest. Here, the local economy, the educational community and environment as well as the open public was in the focus of the teams to stimulate people's interest and awareness. One possible route to follow is to use technical demonstrators giving insight into typical examples of technological applications of magnetism in everyday's life and to present those e.g. on fairs, open days of institutes or even any event aiming at creating contact between people and technology. Important is that the demonstrator itself is an eye-catcher, plausible and easy to understand, robust to use and last but not least well sized and thus transportable. Following these requests, two Master of Education students of the University of Kaiserslautern, Martin Hutzel und Oliver Nick, designed new demonstrators for magnetic sensors in collaboration with Sensitec GmbH, Mainz, one of the members of the industrial advisory board of the GRMN network. They joined the magnetism group from December 2014 until April 2015 to prepare their Master theses. The topics of their theses were each related to the conceptual design of demonstrators for magnetoresistive sensors in automotive applications. Both demonstrators are aimed for exhibitions and fair expositions and interactive usage to bring recent magnetism technology to people's notice. The addresses are the general public spanning from younger pupils up to experienced interested persons.

Magnetoresistive sensors are applied in many devices of modern technology, mostly without our recognition. They represent an integral part in motor vehicles, for the detection of axial positions, the determination of the given values in ABS and ESP, or the acquisition of steering angles. Here, the daily experience shows that especially the last point is commonly unknown to most people. This fact defined the starting point for the thesis of Martin Hutzel. Using AMR sensors built by Sensitec GmbH, he realized a demonstrator concept for the today's steering mechanism in cars, which in general people's mind wrongly still is working on a simple mechanical basis. The most important criteria for the development of a demonstrator are a clear visibility, the restriction to the essential parts, to accentuate the important components, and having a well thought and concise construction. Figure 1 shows the design of the main part of the steering demonstrator consisting of a rotating axis with a steering wheel on one end and a fixed permanent magnet on the other end. The magnetic sensor unit is mounted *contactless* in front of the rotating permanent sensor and connected to a micro-controller unit and a PC. Here, the interested visitor can read some information about the principle and about magnetoresistive sensors in the info box and observe in-situ the sensor read-out signal as well as the orientation of the permanent magnet.

The demonstrator is built in a very robust way, so that any interested visitor can test the angle positioning and sensing her-/himself. The used visualization program based on LabView directly shows the readout signal (voltage) of the sensor and the corresponding angle orientation of the permanent magnet. Additionally, the visitor can get some important information in an information

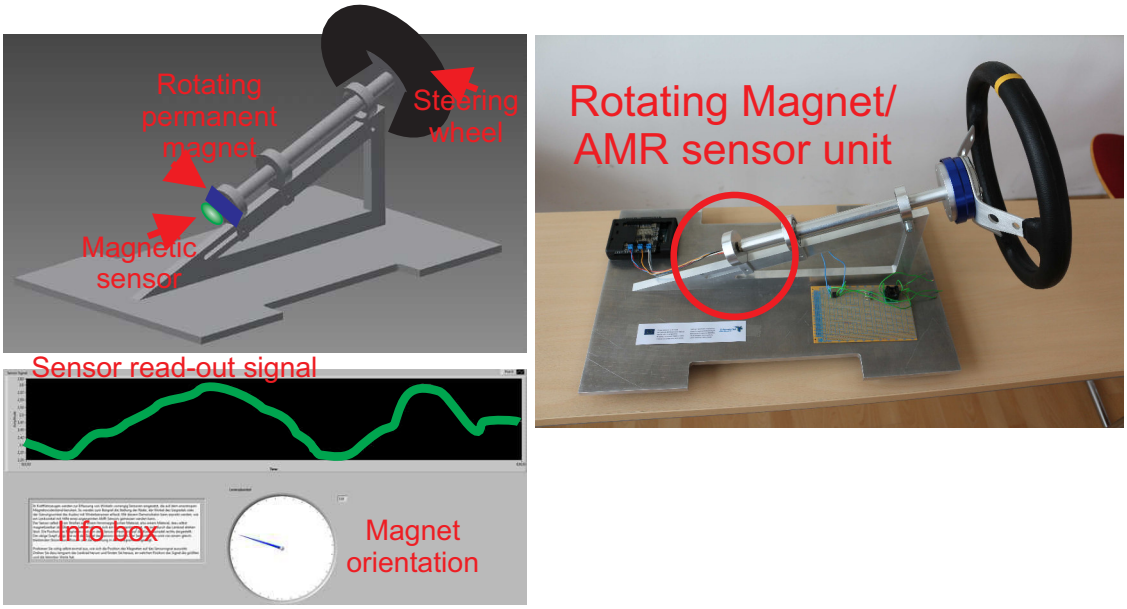

Fig. 1: Sketch and photo of the steering wheel demonstrator and its interactive PC visualization program developed in the frame of the Master of education thesis of Martin Hutzel, TU Kaiserslautern 2015. The most important area is the contactless AMR angle sensing area, which is freely visible.

box displayed on the screen. For a complete simplified recognition it is planned to extend this demonstrator by a model axis with small wheels so that the real steering can be understood while testing this demonstrator.

In the second master of education thesis, Oliver Nick developed a demonstrator for the technique of detection of the revolutions per minute in automotive applications. The demonstrator concept followed the well defined criteria of clear visibility, self-restriction to essential parts with the necessary accentuation and robust usability. A metal table top construction was designed containing stainless steel as well as aluminum parts, a crank handle for hands-on experiments and two pairs of permanent magnets fixed to the axis and a non-contact AMR sensor to detect the position of the magnet. One magnet/sensor unit is mounted at the very end of the rotating axis, and acting as angle detector unit, the second pair is mounted at a position at the axis shell to act simultaneously as rotating clock counter unit. The design can be seen in Fig. 2.

In the final demonstration unit the sensor signal will be displayed on a laptop screen. The demon-

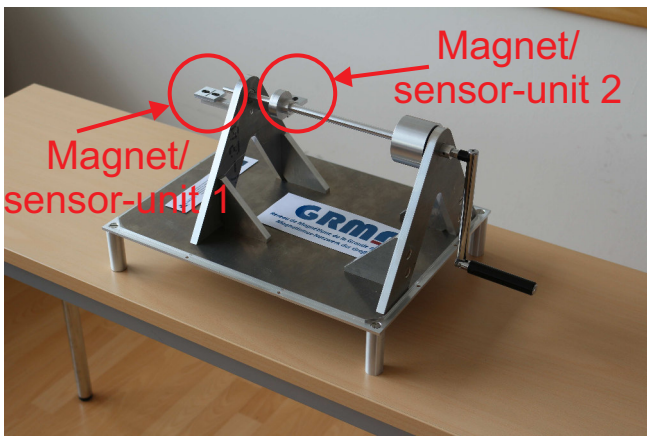

Fig. 2: Photo of the revolutions per minute demonstrator in the frame of the Master of education thesis of Oliver Nick, TU Kaiserslautern 2015.

strator is aimed to be used interactively by interested visitors. Thus, following the guidelines of the GRMN network, the didactic concept to attract attention, to overcome possible prejudices against technology as a whole and to make today's technological applications of magnetism in particular visible can be fulfilled with the help of those new developed demonstrators.

Financial support by the European Regional Development Fund (ERDF) in the framework of the INTERREG IVA Greater region in case of GRMN is gratefully acknowledged.

Chapter 5: Publications

Most publications can be downloaded from http://www.physik.uni-kl.de/hillebrands.

5.1 submitted

1. *Magnon supercurrent in a magnon Bose-Einstein condensate subject to a thermal gradient*
   P. Clausen, D.A. Bozhko, V.I. Vasyuchka, G.A. Melkov, B. Hillebrands, A.A. Serga
   submitted, arXiv:1503.00482

2. *Spin-transfer torque based damping control of parametrically excited spin waves in a magnetic insulator*
   V. Lauer, D.A. Bozhko, T. Brächer, P. Pirro, V.I. Vasyuchka, A.A. Serga, M.B. Jungfleisch, M. Agrawal, Yu.V. Kobljanskyj, G.A. Melkov, C. Dubs, B. Hillebrands, A.V. Chumak
   submitted, arXiv:1508.07517

5.2 published

1. *Formation of Bose-Einstein magnon condensate via dipolar and exchange thermalization channels*
   D.A. Bozhko, P. Clausen, A.V. Chumak, Yu.V. Kobljanskyj, B. Hillebrands, A.A. Serga
   Low Temperature Physics/Fizika Nizkikh Temperatur, **41**, 10 (2015)

2. *Thermal conductance of thin film YIG determined using Bayesian statistics*
   C. Euler, P. Hołuj, T. Langner, A. Kehlberger, V.I. Vasyuchka, M. Kläui, G. Jakob
   Phys. Rev. B **92**, 094406 (2015)

3. *Magnetische Materialien nach Maß für die Spintronik*
   M. Vogel, A.V. Chumak, B. Hillebrands, G. von Freymann
   Physik in unserer Zeit **46**, 218 (2015)

4. *Experimental observation of the interaction of propagating spin waves with Néel domain walls in a Landau domain structure*
   P. Pirro, T. Koyama, T. Brächer, T. Sebastian, B. Leven, B. Hillebrands
   Appl. Phys. Lett. **106**, 232405 (2015)

5. *Length scale of the spin Seebeck effect*
   A. Kehlberger, U. Ritzmann, D. Hinzke, E.-J. Guo, J. Cramer, G. Jakob, M.C. Onbasli, D.H. Kim, C.A. Ross, M.B. Jungfleisch, B. Hillebrands, U. Nowak, M. Kläui
   Phys. Rev. Lett. **115**, 096602 (2015)

6. *Detection of spin waves in permalloy using planar Hall effect*
   Y.V. Kobljanskyj, G.A. Melkov, A.A. Serga, A.N. Slavin, B. Hillebrands
   Physical Review Applied **4**, 014014 (2015)

7. *Micro-focused Brillouin light scattering: imaging spin waves at the nanoscale (Review paper)*
   T. Sebastian, K. Schultheiss, B. Obry, B. Hillebrands, H. Schultheiss
   Frontiers in Physics **3**, 35 (2015)

8. *Stimulated thermalization of a parametrically driven magnon gas as a prerequisite for Bose-Einstein magnon condensation*
   P. Clausen, D.A. Bozhko, V.I. Vasyuchka, B. Hillebrands, G.A. Melkov, A.A. Serga
   Phys. Rev. B **91**, 220402(R) (2015)

9. *Magnon spintronics (Invited Review)*
   A.V. Chumak, V.I. Vasyuchka, A.A. Serga, B. Hillebrands,
   Nature Physics **11**, 453 (2015)

10. *Spin-wave logic devices based on isotropic forward volume magneto-static waves*
    S. Klingler, P. Pirro, T. Brächer, B. Leven, B. Hillebrands, A.V. Chumak
    Appl. Phys. Lett. **106**, 212406 (2015)

11. *Optically-reconfigurable magnetic materials*
    M. Vogel, A.V. Chumak, E.H. Waller, T. Langner, V.I. Vasyuchka, B. Hillebrands, G. von Freymann
    Nature Physics **11**, 487 (2015)

12. *The role of the non-magnetic material in spin pumping and magnetization dynamics in NiFe and CoFeB multilayer systems*
    A. Ruiz-Calaforra, T. Brächer, V. Lauer, P. Pirro, B. Heinz, M. Geilen, A. Chumak, A. Conca, B. Leven, B. Hillebrands
    J. Appl. Phys. **106**, 163901 (2015)

13. *Thickness and power dependence of the spin-pumping effect in $Y_3Fe_5O_{12}$/Pt heterostructures measured by the inverse spin Hall effect*
    M.B. Jungfleisch, A.V. Chumak, A. Kehlberger, V. Lauer, D.H. Kim, M.C. Onbasli, C.A. Ross, M. Kläui, B. Hillebrands
    Phys. Rev. B **91**, 134407 (2015)

14. *Observation of a hole-size-dependent energy shift of the surface-plasmon resonance in Ni antidot thin films*
    H. Fang, B. Caballero, E.M. Akinoglu, E.Th. Papaioannou, A. García-Martín, J.C. Cuevas, M. Giersig, P. Fumagalli
    J. Appl. Phys. **117**, 153104 (2015)

15. *Advancement in Heusler compounds and other spintronics material designs and applications*
    S. Mizukami, A.A. Serga
    J. Phys. D: Appl. Phys. **48**, 160301 (2015)

16. *All-optical characterisation of the spintronic Heusler compound $Co_2Mn_{0.6}Fe_{0.4}Si$*
    T. Sebastian, Y. Kawada, B. Obry, T. Brächer, P. Pirro, D.A. Bozhko, A.A. Serga, H. Naganuma, M. Oogane, Y. Ando, B. Hillebrands
    J. Phys. D: Appl. Phys. **48**, 164015 (2015)

17. *A spin-wave logic gate based on a width-modulated dynamic magnonic crystal*
    A.A. Nikitin, A.B. Ustinov, A.A. Semenov, A.V. Chumak, A.A. Serga, V.I. Vasyuchka, E. Lähderanta, B.A. Kalinikos, B. Hillebrands
    Appl. Phys. Lett. **106**, 102405 (2015)

18. *Magnonen für den Computer von Übermorgen*
B. Leven, A.V. Chumak, B. Hillebrands
Physik in unserer Zeit **46** 34 (2015)

19. *Sign of inverse spin Hall voltages generated by ferromagnetic resonance and temperature gradients in yttrium iron garnet | platinum bilayers*
M. Schreier, G.E.W. Bauer, V.I. Vasyuchka, J. Flipse, K. Uchida, J. Lotze, V. Lauer, A.V. Chumak, A.A. Serga, S. Daimon, T. Kikkawa, E. Saitoh, B.J. van Wees, B. Hillebrands, R. Gross, S.T.B. Goennenwein
J. Phys. D: Appl. Phys. **48**, 025001 (2015)

20. *Measurements of the exchange stiffness of YIG films using broadband ferromagnetic resonance techniques*
S. Klingler, A.V. Chumak, T. Mewes, B. Khodadadi, C. Mewes, C. Dubs, O. Surzhenko, B. Hillebrands, A. Conca
J. Phys. D: Appl. Phys. **48**, 015001 (2015)

21. *Time- and power-dependent operation of a parametric spin-wave amplifier*
T. Brächer, F. Heussner, P. Pirro, T. Fischer, M. Geilen, B. Heinz, B. Lägel, A.A. Serga, B. Hillebrands
Appl. Phys. Lett. **105**, 232409 (2014)

22. *Non-Gilbert-damping mechanism in a ferromagnetic Heusler compound probed by nonlinear spin dynamics*
P. Pirro, T. Sebastian, T. Brächer, A.A. Serga, T. Kubota, H. Naganuma, M. Oogane, Y. Ando, B. Hillebrands
Phys. Rev. Lett. **113**, 227601 (2014)

5.3 Further publications

1. *Description of research of our group in the daily newspaper "Die Welt": Ein neues Superhirn für künftige Supercomputer*
http://www.welt.de/wissenschaft/article143823535/Ein-neues-Superhirn-fuer-kuenftige-Supercomputer.html
Die Welt, issue July 10, 2015

5.4 Ph.D. theses

1. *Thermalisierung und Kondensation parametrisch gepumpter Magnonengase*
Peter Clausen, TU Kaiserslautern, July 2015

2. *Thin magnetic layer elements for applications in spintronics*
Ana Ruiz-Calaforra, TU Kaiserslautern, March 2015

3. *Parallel parametric amplification of spin waves in microstructures*
Thomas Brächer, TU Kaiserslautern, March 2015

5.5 Diploma theses

1. *Interface engineering of Fe/Pt and Fe/MgO/Pt multilayersystems in relation to spin pumping*
   Laura Mihalceanu, TU Kaiserslautern, July 2015

2. *Herstellung, Charakterisierung und Spinwelleneigenschaften mikrostrukturierter $Co_{40}Fe_{40}B_{20}$-Spinwellen-Wellenleiter*
   Tobias Fischer, TU Kaiserslautern, May 2015

3. *Lokalisierte parallele parametrische Verstärkung von kohärent angeregten Spinwellen in $Ni_{81}Fe_{19}$-Mikrostreifen*
   Frank Heussner, TU Kaiserslautern, January 2015

4. *Spinwellendynamik in mikrostrukturiertem Yttrium-Eisen-Granat*
   Stefan Klingler, TU Kaiserslautern, November 2014

5.6 Master theses (Master of education)

1. *Erarbeitung eines Konzeptes zu einem Anfängerpraktikumsversuch zum Thema "Grundlagen des Magnetismus und Elektromagnetismus" und dessen Realisierung*
   Manuela Kratz, TU Kaiserslautern, September 2015

2. *Erstellung eines Konzeptes für einen Praktikumsversuch zum Thema Anwendung des Elektromagnetismus und dessen Realisierung*
   Matthias Monzel, TU Kaiserslautern, September 2015

3. *Erstellung eines Messe-Demonstrators zur Darstellung der Winkelübertragung einer Lenksäule unter Verwendung magnetresistiver Sensoren*
   Martin Hutzel, TU Kaiserslautern, May 2015

4. *Konzeptionelle Entwicklung und Realisierung eines Demonstrators zur Drehzahlmessung mittels magnetresistiver Sensoren für die Öffentlichkeitsarbeit*
   Oliver Nick, TU Kaiserslautern, May 2015

Chapter 6: Conferences, Workshops, Schools, Seminars

(shown in chronological order)

6.1 Invited talks

6.1.1 International conferences and workshops

A.V. Chumak:
Magnonics in view of applications in logic
580. Wilhelm und Else-Heraeus-Seminar "Oxide Spintronics: Novel Materials, Transport and Emerging Phenomena", Bad Honnef, Germany, January 2015

B. Hillebrands:
Magnonics: Trends and challenges
The AIMR International Symposium 2015 (AMIS 2015) "A new horizon for materials science with mathematics collaboration", Sendai, Japan, February 2015

B. Leven:
Magnon spintronics - Future potential of spintronics for sensor applications
13th MR-Symposium "Magnetoresistive Sensors and Magnetic Systems", Wetzlar, Germany, March 2015

B. Hillebrands:
Currents of Bose-Einstein magnon condensates
IEEE International Magnetics Conference INTERMAG 2015, Beijing, China, May 2015

A.V. Chumak:
Magnonics in view of applications in logic
IEEE International Magnetics Conference INTERMAG 2015, Beijing, China, May 2015

B. Hillebrands:
Magnon transport using macroscopic quantum states
York-Tohoku-Kaiserslautern Research Symposium on "New-Concept Spintronics Devices", York, United Kingdom, June 2015

B. Hillebrands:
Optically reconfigurable magnetic materials
Spin Mechanics 3, Munich, Germany, June 2015

B. Hillebrands:
Spin transport using magnon gases
2nd International Conference "Recent Trends in Nanomagnetism, Spintronics and their Applications" (RTNSA-2015), Ordizia, Spain, June 2015

A.A. Serga:
Influence of spin waves on electrical currents in ferromagnets
2nd International Conference "Recent Trends in Nanomagnetism, Spintronics and their Applications" (RTNSA-2015), Ordizia, Spain, June 2015

B. Hillebrands:
Transport with Bose-Einstein magnon condensates
20th International Conference on Magnetism (ICM 2015), Barcelona, Spain, July 2015

A.V. Chumak:
Spin-wave logic devices
20th International Conference on Magnetism (ICM 2015), Barcelona, Spain, July 2015

A.V. Chumak:
Spin pumping and spin transfer torque in YIG/Pt bilayers
Magnonics 2015, Seeon, Germany, August 2015

B. Hillebrands:
Magnon supercurrents
Quantum Magnets 2015 Workshop, Kolymbari, Crete, Greece, September 2015

A.A. Serga:
Thermally induced magnon supercurrents
Workshop on Non-linear spin-heat interactions, Columbus, Ohio, USA, September 2015

B. Hillebrands:
Spin transport using magnon gases
The 29th REIMEI and ERATO-SQR workshop on "Spin orbit coupling and spin mechanics", Mainz, Germany, October 2015

6.1.2 Invited seminar talks and colloquia

B. Hillebrands:
Magnonics: Trends and challenges
Physics and Astronomy Colloquium, University of Exeter, United Kingdom, January 2015

B. Hillebrands:
Magnonics: Trends and challenges
Condensed Matter Physics Seminar, Department of Physics, The University of Oxford, United Kingdom, March 2015

B. Leven:
Spinwellen und Domänenwände - Grundlagenexperimente und Anwendungspotential
Physikalisches Kolloquium, Fachbereich Physik, TU Kaiserslautern, June 2015

B. Hillebrands:
Novel transport phenomena using magnonic Bose-Einstein condensates
Half-day symposium at Seagate, USA, June 2015

B. Hillebrands:
Transport in magnonic Bose-Einstein condensates
Materials Science Seminar, Argonne National Laboratory, Michigan, USA, June 2015

A.A. Serga:

Condensed magnon phases in Yttrium Iron Garnet films
Group seminar, Physical Department, Oakland University, Rochester, Michigan, USA, September 2015

B. Hillebrands:
Spin-wave logic devices: state of the art, perspectives, and limitations
Intel company, USA, September 2015

6.1.3 Lectures at summer schools

B. Hillebrands:
Magnetization Dynamics I - Fundamentals
Magnetization Dynamics II - Magnonics: Trends and challenges
IEEE Magnetics Society Summer School 2015, Minneapolis, Minnesota, USA, June 2015

B. Hillebrands:
Fundamentals of magnonics (Keynote lecture)
Gordon Research Seminar "Spin Dynamics in Nanostructures", Hong Kong, China, July 2015

B. Hillebrands:
Magnonics: Trends and Challenges
SpinIcur Summer School 2015, Braga, Portugal, September 2015

6.2 Contributed talks and posters

6.2.1 Conferences and workshops

D.A. Bozhko, A. Kirihara, A.V. Chumak, B. Hillebrands, A.A. Serga:

Spin pumping by Bose-Einstein condensate of magnons in YIG/Pt bilayers
59th Conference on Magnetism and Magnetic Materials (MMM) 2014, Honolulu, Hawaii, USA, November 2014

V. Lauer, T. Brächer, C. Dubs, B. Hillebrands, A. Chumak:

Spin pumping by magnetization precession in a wide frequency range
580. Wilhelm und Else-Heraeus-Seminar "Oxide Spintronics: Novel Materials, Transport and Emerging Phenomena", Bad Honnef, Germany, January 2015

M. Vogel, A.V. Chumak, E.H. Waller, T. Langner, V.I. Vasyuchka, B. Hillebrands, G. von Freymann:

An optically-reconfigurable dynamic magnetic material for the control of spin waves
580. Wilhelm und Else-Heraeus-Seminar "Oxide Spintronics: Novel Materials, Transport and Emerging Phenomena", Bad Honnef, Germany, January 2015

S. Klingler, P. Pirro, T. Brächer, B. Leven, B. Hillebrands, A.V. Chumak:

Design of a fully functional spin-wave majority gate
580. Wilhelm und Else-Heraeus-Seminar "Oxide Spintronics: Novel Materials, Transport and Emerging Phenomena", Bad Honnef, Germany, January 2015

M. Agrawal, V.I. Vasyuchka, A.A. Serga, A. Kirihara, P. Pirro, T. Langner, M.B. Jungfleisch, A.V. Chumak, E.Th. Papaioannou, B. Hillebrands:

Temporal evolution of the longitudinal spin Seebeck effect
Spin Caloric Transport (SPP 1538) Kolloquium, Bad Honnef, Germany, February 2015

M. Vogel, A.V. Chumak, E.H. Waller, T. Langner, V.I. Vasyuchka, B. Hillebrands, G. von Freymann:

An optically-reconfigurable magnetic material for the control of spin waves
Spin Caloric Transport (SPP 1538) Kolloquium, Bad Honnef, Germany, February 2015

V.I. Vasyuchka:

Magnon mediated heat and spin transport in magnetic insulators
Spin Caloric Transport (SPP 1538) Kolloquium, Bad Honnef, Germany, February 2015

A.A. Serga:

Magnon Seebeck effect
Spin Caloric Transport (SPP 1538) Kolloquium, Bad Honnef, Germany, February 2015

S. Keller, L. Mihalceanu, A. Conca, J. Greser, J. Lösch, B. Hillebrands, E.Th. Papaioannou:

Platinum thickness dependence on the spin pumping in Fe\Pt bilayers
International Magnetics Conference INTERMAG 2015, Beijing, China, May 2015

A.A. Serga, Yu.V. Kobljanskyj, G.A. Melkov, A. Slavin, B. Hillebrands:

Control of electric resistance of a ferromagnetic metal by parametric excitation of microwave magnons
International Magnetics Conference INTERMAG 2015, Beijing, China, May 2015

E.Th. Papaioannou, E. Melander, E. Östman, V. Kapaklis, B. Hjörvarsson:

Thickness dependence of the magneto-optic enhancement in Co sub-wavelength anti-dot arrays
International Magnetics Conference INTERMAG 2015, Beijing, China, May 2015

T. Langner, A.V. Chumak, A.A. Serga, B. Hillebrands, V.I. Vasyuchka:

Spin waves and magnonic crystals influenced by thermal gradients
SpinCaT PhD workshop 2015, Garching, Germany, June 2015

T. Langner, M. Agrawal, T. Noack, A.A. Serga, A. Kirihara, M.B. Jungfleisch, P. Pirro, A.V. Chumak, E.Th. Papaioannou, B. Hillebrands, V.I. Vasyuchka:

Temporal evolution of the longitudinal spin Seebeck effect
Spin Mechanics 3, Munich, Germany, June 2015

D.A. Bozhko, A. Kirihara, Y. Tserkovnyak, A.V. Chumak, B. Hillebrands, A.A. Serga:

Full electric detection of a Bose-Einstein condensate via the spin-pumping effect
2nd International Conference "Recent Trends in Nanomagnetism, Spintronics and their Applications" (RTNSA-2015), Ordizia, Spain, June 2015

T. Meyer, T. Sebastian, P. Pirro, T. Brächer, T. Fischer, A.A. Serga, T. Kubota, Y. Ohdaira, H. Naganuma, K. Mukaiyama, M. Oogane, Y. Ando, B. Hillebrands:

Magnonics in Heusler compounds
York-Tohoku-Kaiserslautern core-to-core symposium, York, United Kingdom, June 2015

V. Lauer, D.A. Bozhko, T. Brächer, P. Pirro, V.I. Vasyuchka, A.A. Serga, M.B. Jungfleisch, M. Agrawal, Yu.V. Kobljanskyj, G.A. Melkov, C. Dubs, B. Hillebrands, A.V. Chumak:

Control of the spin-wave relaxation in a magnetic insulator of macroscopic dimensions via spin-transfer torque
20th International Conference on Magnetism (ICM 2015), Barcelona, Spain, July 2015

A. Conca, S. Keller, L. Mihalceanu, J. Greser, E.Th. Papaioannou, B. Hillebrands:

Study of the ferromagnetic resonance properties in epitaxial FePt samples
20th International Conference on Magnetism (ICM 2015), Barcelona, Spain, July 2015

D.A. Bozhko, P. Clausen, V.I. Vasyuchka, B. Hillebrands, G.A. Melkov, A.A. Serga:

Stimulated thermalization of a parametrically driven magnon gas as a prerequisite for Bose-Einstein magnon condensation
20th International Conference on Magnetism (ICM 2015), Barcelona, Spain, July 2015

M. Vogel, A.V. Chumak, E.H. Waller, T. Langner, V.I. Vasyuchka, B. Hillebrands, G. von Freymann:

Optically-reconfigurable magnetic materials for the control of spin waves
20th International Conference on Magnetism (ICM 2015), Barcelona, Spain, July 2015

E.Th. Papaioannou, M. Rollinger, E. Melander, P. Thielen, E. Ístman, V. Kapaklis, M. Cinchetti, A. Garcia-Martin, M. Aeschlimann:

Light localization and magneto-optic enhancement in Ni and Co anti-dot arrays
20th International Conference on Magnetism (ICM 2015), Barcelona, Spain, July 2015

A. Ruiz Calaforra, T. Brächer, V. Lauer, P. Pirro, B. Heinz, M. Geilen, A.V. Chumak, A. Conca, B. Leven, B. Hillebrands:

Influence of the non-magnetic material on the magnetization dynamics and spin pumping in NiFe and CoFeB multilayer systems
20th International Conference on Magnetism (ICM 2015), Barcelona, Spain, July 2015

V.I. Vasyuchka, M. Agrawal, A. Serga, V. Lauer, E.Th. Papaioannou, B. Hillebrands:

Microwave-induced spin currents in ferromagnetic-insulator | normal-metal bilayer system
20th International Conference on Magnetism (ICM 2015), Barcelona, Spain, July 2015

B. Leven, F. Ciubotaru, V.I. Vasyuchka, A.V. Chumak, A.A. Serga, B. Hillebrands:

Unidirectional spin-wave edge modes in perpendicularly magnetized permalloy structures
20th International Conference on Magnetism (ICM 2015), Barcelona, Spain, July 2015

A.A. Serga, M. Agrawal, V.I. Vasyuchka, B. Hillebrands:
Effective way of spin-wave excitation in YIG-Pt structures
20th International Conference on Magnetism (ICM 2015), Barcelona, Spain, July 2015

T. Meyer, T. Brächer, P. Pirro, T. Fischer, A.A. Serga, H. Naganuma, K. Mukaiyama, M. Oogane, Y. Ando, B. Hillebrands:
Control of the effective spin-wave damping in Heusler/Pt waveguides via the spin-transfer torque effect
Gordon Research Conference "Spindynamics in Nanostructures", Hong Kong, China, July 2015

V.I. Vasyuchka, T. Langner, M. Agrawal, A.A. Serga, V. Lauer, E.Th. Papaioannou, B. Hillebrands:
Microwave-induced spin currents in ferromagnetic-insulator|normal-metal bilayers
Magnonics 2015, Seeon, Germany, August 2015

A.A. Serga, M. Agrawal, V.I. Vasyuchka, B. Hillebrands:
Spin-wave excitation in YIG-Pt bilayers
Magnonics 2015, Seeon, Germany, August 2015

V. Lauer, D.A. Bozhko, T. Brächer, P. Pirro, V.I. Vasyuchka, A.A. Serga, M.B. Jungfleisch, M. Agrawal, Yu.V. Kobljanskyj, G.A. Melkov, C. Dubs, B. Hillebrands, A.V. Chumak:
Control of the spin-wave relaxation in a magnetic insulator of macroscopic dimensions via spin-transfer torque
Magnonics 2015, Seeon, Germany, August 2015

D.A. Bozhko, P. Clausen, A.V. Chumak, B. Hillebrands, A.A. Serga:
Formation of Bose-Einstein magnon condensate via dipolar and exchange thermalization channels
6th MAINZ Student Seminar, Lisbon, Portugal, October 2015

D.A. Bozhko, P. Clausen, A.V. Chumak, B. Hillebrands, A.A. Serga:
Formation of Bose-Einstein magnon condensate via dipolar and exchange thermalization channels
SFB/Transregio 49 Student Seminar Winter Term 2015/16, Cologne, Germany, October 2015

D.A. Bozhko, P. Clausen, A.V. Chumak, B. Hillebrands, A.A. Serga:
Formation of Bose-Einstein magnon condensate via dipolar and exchange thermalization channels
XI International Scientific Conference «Electronics and Applied Physics», Kyiv, Ukraine, October 2015

6.2.2 Contributions to the DPG Frühjahrstagung

13 contributions: DPG Frühjahrstagung, Berlin, Germany, March 2015

6.2.3 Seminars

S. Klingler, P. Pirro, T. Brächer, B. Leven, B. Hillebrands, A.V. Chumak:

Design and application of spin-wave majority gates
Walther-Meißner-Seminar on topical issues of low temperature solid state physics WS 2014/15, Garching, Germany, January 2015

D.A. Bozhko:

Bose-Einstein condensation of magnons
Scientific Seminar, Melkov Laboratory, Faculty of Radiophysics, Taras Shevchenko National University of Kyiv, Ukraine, October 2015

6.2.4 Schools

D.A. Bozhko, A. Kirihara, A.V. Chumak, B. Hillebrands, A.A. Serga:

Spin pumping by Bose-Einstein condensate of magnons in YIG/Pt bilayers
IEEE Magnetics Society Summer School 2015, Minneapolis, Minnesota, USA, June 2015

V. Lauer, D.A. Bozhko, T. Brächer, P. Pirro, V.I. Vasyuchka, A.A. Serga, M.B. Jungfleisch, M. Agrawal, Yu.V. Kobljanskyj, G.A. Melkov, C. Dubs, B. Hillebrands, A.V. Chumak:

Control of the spin-wave relaxation in a magnetic insulator of macroscopic dimensions via spin-transfer torque
European School of Magnetism (ESM) 2015, Cluj-Napoca, Romania, Aug-Sep 2015

L. Mihalceanu, S. Keller, J. Greser, V. Lauer, A. Conca, T. Brächer, B. Hillebrands, E.Th. Papaioannou:

Spin pumping in epitaxially grown Fe/Pt system with MgO interlayer
European School of Magnetism (ESM) 2015, Cluj-Napoca, Romania, Aug-Sep 2015

6.3 Annual group retreat

In 2015 our group organized a three-day retreat at the Kurhaus am Trifels, Annweiler. We had two days of intense scientific discussion and 26 presentations by our group members. Prof. Dr. Claus Fieker from the University of Kaiserslautern gave a fascinating evening talk on the mathematical basics of cryptography and its application in information technology. On the first day, the group members participated in a soft skill seminar on “Vortragspräsentation auf wissenschaftlichen Konferenzen (Presentations at scientific conferences) ”held by Andrea Stasche.

6.4 Other meetings and trade fairs

A. Conca:

Reliability measurements: results of the STEP project
Final Meeting STEP Project, Mainz, Germany, February 2015

A.V. Chumak, T. Meyer, T. Fischer, S. Keller:

Magnon transistor
CeBiT (at Rhineland-Palatinate stand), Hannover, Germany, March 2015

A. Conca, T. Langner:
STeP, TT-DINEMA (RLP stand)
Hannover Messe (at Rhineland-Palatinate stand), Hannover, Germany, April 2015

V. Lauer:
Scientific progress report: Kaiserslautern
InSpin meeting, Amsterdam, Netherlands, September 2015

A.A. Serga:
Scientific progress report: Kaiserslautern
InSpin meeting, Amsterdam, Netherlands, September 2015

A.A. Serga:
Magnon supercurrents in thermal gradients
TRR49 Annual Retreat, Langenselbold, Germany, September 2015

D.A. Bozhko, P. Clausen, V.I. Vasyuchka, B. Hillebrands, G.A. Melkov, A.A. Serga:
Stimulated thermalization of a parametrically driven magnon gas as a prerequisite for Bose-Einstein magnon condensation
TRR49 Annual Retreat, Langenselbold, Germany, September 2015

B. Hillebrands:
Magnonics and ultrafast physics in Kaiserslautern
One-day conference on magnetism in the Greater Region, Nancy, France, October 2015

6.5 Awards, Fellowships, and others

D.A. Bozhko:
Gold Poster Award for "Spin pumping by Bose-Einstein condensate of magnons in YIG/Pt bilayers"
IEEE Magnetics Society Summer School 2015, Minneapolis, Minnesota, USA, June 2015

P. Pirro:
Preis des Freundeskreises
TU Kaiserslautern, Germany, June 2015

D.A. Bozhko:
Best Poster Award for "Stimulated thermalization of a parametrically driven magnon gas as a prerequisite for Bose-Einstein magnon condensation"
20th International Conference on Magnetism (ICM 2015), Barcelona, Spain, July 2015

B. Hillebrands:
Discussion leader "Quantum Spintronics"
Gordon Research Conference "Spin Dynamics in Nanostructures", Hong Kong, China, July 2015

Appendix: Impressions from 2015

Ph.D. defense Dr. Thomas Brächer, 09.03.2015

DPG Spring Meeting in Berlin, 15.-20.03.2015

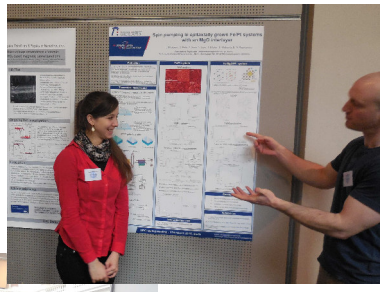

CeBIT, 16.-20.03.2015

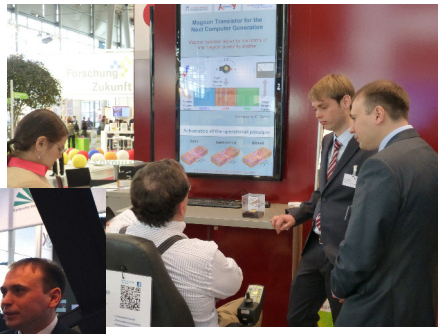

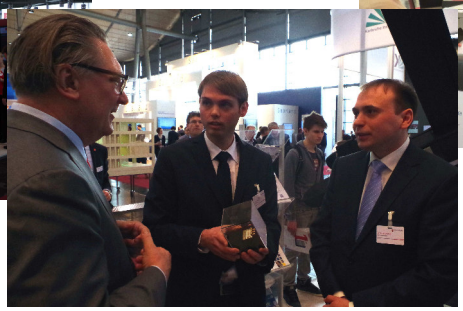

Ph.D. defense Dr. Ana Ruiz-Calaforra, 24.03.2015

20 years celebration AG Magnetismus, 10.04.2015

Hannover Messe, 13-17.04.2015

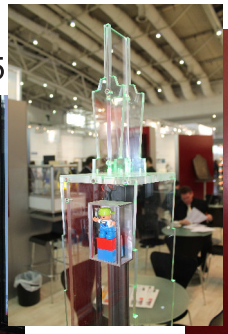

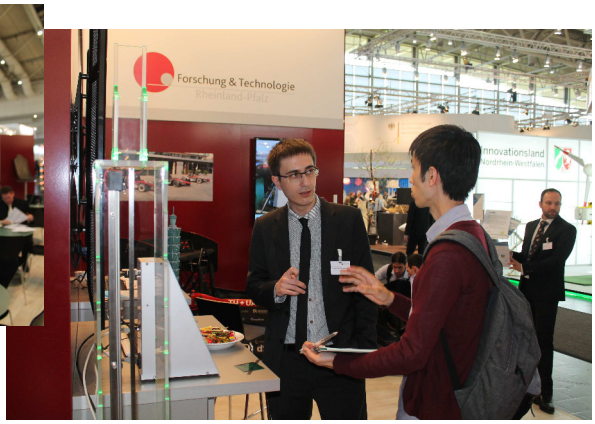

InSpin report meeting, 15.04.2015

Group excursion, 21.07.2015

Ph.D. defense Dr. Peter Clausen, 22.07.2015

Schülerinnentag, 01.10.2015

Group Retreat, 12.-14.10.2015
(Greetings card to Dr. Andrii Chumak)

Prof. Dr. Burkard Hillebrands
Fachbereich Physik
Landesforschungszentrum OPTIMAS
Technische Universität Kaiserslautern, Germany
P.O. Box 3049
67653 Kaiserslautern
Phone: +49 631 205-4228
Fax: +49 631 205-4095
hilleb@physik.uni-kl.de
www.physik.uni-kl.de/hillebrands/

TECHNISCHE UNIVERSITÄT
KAISERSLAUTERN